DEPARTMENT OF STATISTICAL PHYSICS

FACULTY OF PHYSICS
LUDWIG-MAXIMILIANS-UNIVERSITÄT MÜNCHEN

MASTER THESIS

Two Species of Self-Propelled Particles Interacting in a Snowdrift Game Scenario

- Kinetic Approach -

Author:
Johanna MAYER

Supervisor:
Prof. Dr. Erwin FREY

8. April 2021

Contents

Chapter 1

Combining Active Matter with Game Theory

In this thesis we will develop and analyze a description that combines the evolutionary dynamics of game theory with active motion. Previous studies have shown that spatial extension of a system can change the outcome of a game. Cooperators are able to survive in spatially extended systems in the prisoners dilemma scenario [37, 31], e.g. by forming clusters and thereby protecting themselves from outside defectors. Hauert et al. have shown on the other hand that spatial extension can diminish cooperator populations compared to well mixed systems in the Snowdrift game [26].

The mobility of individuals can also play a crucial role. The effects of the interplay between mobility like diffusive motion and spatial separation on the development of interacting species is one of the most interesting and complex problems in theoretical ecology [22, 25, 44]. If mobility is low, locally interacting particles can exhibit spatio-temporal patterns and spatial segregation that can promote the coexistence of species [25]. High mobility on the other hand leads to well mixed systems where spatial patterns no longer form and the system adopts a spatially uniform state [22, 44].

Previous studies on systems of different interacting species have shed light on a variety of particle interactions and on different ways of mobility. However, to our knowledge there exist no studies about the influence of *active* and *directed* motion on systems of interacting particle species. There are a number of natural systems that can be understood in the language of game theory and exhibit active or collective motion. Examples include different types of microorganisms [14, 12, 15, 16] that can self-organise into patterns or collective motion while competing with other microbes for space or nutrition. In the next chapters we will develop a simple model of self-propelled particles that interact in a Snowdrift game scenario. We suspect that the self-propulsion of particles in a spatially extended system will have an effect on the outcome of the game. The aim of this thesis is to find answers to the following questions:

1. Does the self-propulsion of particles change the outcome of the game? If it does, what are the effects?
2. How does the game interaction change the properties of a self-propelled particle system?

Before we start to develop a description of self-propelled particles with interaction rules inspired from evolutionary game theory, we will give a short general introduction to the fields of active matter and game theory in the next two chapters.

Chapter 2

Introduction to Active Matter

2.1 What is Active Matter?

Systems consisting of many particles have typically been described by the field of statistical physics. Methods for systems in thermal equilibrium allow the calculation of macroscopic average quantities such as particle number or energy, as well as average fluctuations about these quantities. Concepts of statistical physics can even be extended to a class of non-equilibrium systems by assuming that they are locally in thermal equilibrium. These methods permit predictions of pattern formation on large length- and time scales.

However, a description of biological systems often needs to take a different path. Living systems are characterized by the constant consumption and conversion of energy, which happens locally for every constituent and brings the system out of equilibrium at all scales. If the particles of a system convert this absorbed energy into systematic movement, they are called *active particles* [43, 32, 55].

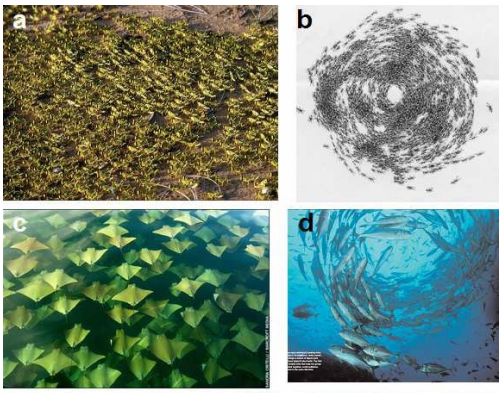

FIGURE 2.1: Examples for collective behavior in living systems. (a) Wingless Locusts marching in the field. (b) A rotating colony of army ants. (c) A three-dimensional array of golden rays. (d) A school of fish producing a vortex. Figures from [55].

The interaction of active particles with each other and with the medium they live in can give rise to highly correlated collective motion [32]. An important example of active matter are *self-propelled particles*. The direction of self-propulsion can be set by an inherent polarity of each particle, given e.g. by the long axis of elongated objects with distinct front and rear.

Collective phenomena of self-propelled particles are typically the result of a competition between decorrelation via local noise and correlation buildup due to collisions or other interactions between particles. Despite many differences, there are some patterns of collective motion that seem to apply to different systems ranging from microscopic objects as cells to groups of mammals, suggesting universal organizing

principles [55]. Theoretical models on all levels of description take these similarities typically as an inspiration to find the minimal ingredients that are necessary to understand the spontaneous emergence of collective behaviour.

Examples of living systems exhibiting collective motion include flocks of birds [27, 5], schools of fish [28, 56], colonies of bacteria [20, 39, 58] or types of living cells [49, 48] (see figure 2.1). There are also examples for collective behaviour in non-living systems, such as layers of vibrated granular rods, colloidal or nanoscale particles propelled through a fluid by catalytic activity at their surface and collections of robots [32].

Over the past few decades, a growing number of attempts have been made to observe and describe collective behaviour of self-propelled particles as well as to understand the most conspicuous features in a theoretical framework [55]. These features include intriguing non-equilibrium properties, such as emergent structures with collective behavior qualitatively different from that of the individual constituents, bizarre fluctuation statistics, non-equilibrium order-disorder transitions, pattern formation on mesoscopic scales and wave propagation and sustained oscillations even in the absence of inertia [32].

2.2 Models of Active Matter

In the field of active matter there is a distinction between so called *dry active matter* and *wet active matter* [43]. The latter means systems in which the fluid or gas surrounding the propelled particles can not be neglected. A description of wet active matter systems has to incorporate a description of the fluid. In these systems momentum is conserved. In dry active matter systems on the other hand the dynamics of the surrounding medium play a negligible role in the level of description. Here, momentum is not conserved. In this thesis we will treat a case of dry active matter. More precisely, our system consists of many self-propelled particles with an inherent polarity. The medium through which the particles move is treated as an inert substrate.

There are different strategies to describe systems of many self-propelled particles. Historically, the first theoretical approaches were agent-based models [54]. A very seminal agent-based approach to collective motion was introduced 1995 by Vicsek et al., which is referred to as *Vicsek-model*. The ingredients are simple: All particles have the same speed, are subject to a noise that changes their direction of motion at certain time steps and align their orientations with the average of all particles' orientations within a defined spatial range. The main result of the Vicsek-model is that propelled particle systems with "polar alignment" interactions and noise can give rise to a long-range ordered, broken-symmetry state of coherently moving particles [54, 11, 43].

Motivated by the Vicsek model, many agent-based simulations [13, 11, 10] have been performed to study propelled particle systems numerically. Important observations are phenomena of polar flocking and the formation of spatial patterns like traveling polar waves close to the onset of polar order [11].

In terms of analytic approaches there is in general the following fundamental problem of many-particle systems. Let us assume we know all microscopic properties

that define each particle and each interaction of the system and we have the equations that describe the time evolution for a given set of properties. We would still not be able to get a meaningful description of the system. The shear number of particles in a typical system size makes it impossible to manage the equations. Fortunately, in most situations we are interested in the macroscopic properties of the system rather than the dynamics of every single particle. To get to a macroscopic, "*hydrodynamic*" description one needs to find appropriate tools to coarsen the system. In this process the exact description is given up in favor of an approximation of the system which is analytically feasible. The first question to ask in order to coarse grain is, which level of description (length scale) makes sense? Which ones are the properties and parameters of the system that are relevant on the time and length scales we are interested in? Once these essential ("slow") variables of the system are identified, it is possible to construct the hydrodynamic equations governing the time evolution of the slow variables based on conservation laws and symmetry arguments [1, 51, 52, 53]. Toner and Tu developed the first hydrodynamic model following this argumentation. They showed that a system of self-propelled particles can exhibit a true, long-range ordered, spontaneously broken symmetry state. A disadvantage of an approach based on symmetry arguments is that the coefficients contained in the hydrodynamic equations are unknown.

An alternative analytic approach to derive a hydrodynamic description is to use a kinetic approach, rooted in the direct coarse-graining of the microscopic dynamics [3, 8, 7, 2, 42, 6]. In the coarse graining process one has to neglect higher order correlations in the system to get analytically feasible equations. The advantage over an approach based on symmetry and conservation arguments is the fact that all coefficients in the equations can be calculated as functions of microscopic parameters. A kinetic approach offers therefore better overall control [40]. It provides a link between macroscopic quantities used in hydrodynamic theories and the underlying microscopic rules.

As was explained in the first chapter, the goal of this thesis is to describe a system that combines active matter with elements of evolutionary game theory. We will consider a system of self-propelled particles that are subdivided into two different "species". Interactions between members of the same species are governed by alignment rules and lead collective behaviour. Both species compete against each other following interaction rules coming from *game theory*. The analytic description of this system follows a kinetic approach, called the *Boltzmann equation for active matter*. It governs the time-evolution of the one-particle density functions $\alpha(\mathbf{r}, \theta, t)$ and $\beta(\mathbf{r}, \theta, t)$, which describe the probability densities for particles of the two species of being at position $\mathbf{r}$ with a direction of velocity θ at time t. We will use a truncation scheme to derive a hydrodynamic description from the Boltzmann equations. These hydrodynamic equations will be analyzed analytically and numerically and the results will be compared to an agent-based simulation of the system.

Before we start with the description of our propelled particle system, we will give an introduction to the basics of game theory in the next section.

Chapter 3

The Game Theoretical Model

3.1 Strategic games

Classical game theory describes the behaviour of rational players [36]. It studies mathematical models for the strategic interactions of decision-makers. The choices of one player influence the success of others in the game.

An example for a very simple type of game are *cooperator-defector games*. In this type of game there are two players that can either choose to cooperate ($\mathcal{C}$) or to defect ($\mathcal{D}$). If both players choose to cooperate, they each get a *reward* $\mathcal{R}$. In the case that both choose to defect, they receive a *punishment* $\mathcal{P}$. If, on the other hand, one player defects while the other one cooperates, the defector gains the *temptation* $\mathcal{T}$, whereas the cooperator only gets the *suckers payoff* $\mathcal{S}$. These interactions can be summarized by the following payoff matrix:

Player \ Opponent	$\mathcal{C}$	$\mathcal{D}$
$\mathcal{C}$	$\mathcal{R}$	$\mathcal{S}$
$\mathcal{D}$	$\mathcal{T}$	$\mathcal{P}$

FIGURE 3.1: Payoff matrix for the cooperator-defector game

Depending on the relative values of $\mathcal{R}, \mathcal{P}, \mathcal{S}$ and $\mathcal{T}$ we can distinguish between four different kinds of games. A very well-known version, the so-called *prisoner's dilemma*, arises when the temptation to defect $\mathcal{T}$ is bigger than the reward $\mathcal{R}$ and the punishment $\mathcal{P}$ is bigger than the suckers payoff $\mathcal{S}$. In this case it is always strategically favourable to defect, no matter which strategy the opponent chooses to play. A social dilemma arises if $\mathcal{R} > \mathcal{P}$ and both players would get overall better payouts for cooperation. However, since we assume that players act rationally and defect, they will both get the punishment $\mathcal{P}$ and are worse off compared to universal cooperation. There are several ideas on how this unfortunate outcome of the game could be avoided (e.g. spatial separation, concepts of reciprocity or social control mechanisms [4, 23, 17]), but in its basic form the prisoner's dilemma illustrates the fundamental problem of achieving cooperation and is often viewed as a kind of *public goods game* [22].

The opposite scenario with $\mathcal{R} > \mathcal{T}$ and $\mathcal{S} > \mathcal{P}$ will consequently lead to both players cooperating. It is called *harmony* game.

A third possibility is the combination of $\mathcal{T} > \mathcal{R}$ and $\mathcal{S} > \mathcal{P}$. This scenario is called *snowdrift game*. It gets its name from the story of two people travelling in their cars that get trapped behind a snowdrift. If at least one of the two drivers gets out of the car and clears the way, both can continue their journey. In this scenario the best strategy for each driver is to do the opposite of the other person. If person 1 starts digging, person 2 will prefer to stay in the car ($\mathcal{T}$) instead of cooperating and helping to clear the way ($\mathcal{R}$) . If on the other hand person 1 stays in the car, it is better for person 2 to get out and dig himself, since paying the cost of digging in the cold ($\mathcal{S}$) is still better than staying in the car and not being able to continue the journey ($\mathcal{P}$).

Finally, the last possible scenario is called *coordination game*, which is characterized by payoff values $\mathcal{T} < \mathcal{R}$ and $\mathcal{S} < \mathcal{P}$. Hence, mutual agreement is the preferred strategy (either both players cooperate or both defect).

3.2 Evolutionary Game Theory

Classical game theory can be a useful concept for economic [24, 35] or social settings [17]. The central assumption is that players act rationally and choose the strategy that benefits them the most. Evolutionary game theory follows a fundamentally different path of argumentation [47]. It was developed to extend game theoretical concepts to biological systems. Since rational behaviour is not a meaningful concept in biological systems, evolutionary game theory considers fixed strategies for every individual that are handed down to the next generation. One typically considers a population composed of individuals following different strategies (different "*species*") that interact in a game situation over many generations. The species with the best strategy survives or has an advantage when replicating, which will lead to a dominance of the strategy after a large enough number of generations. The interactions are usually described by deterministic rules or stochastic processes, depending on the particular system [22].

Evolutionary game theory is a rich field of ongoing research. It can describe how successful strategies spread and thereby create new conditions which can alter the basis of their success. It tries to capture natural selection in mathematical terms and to understand the strategic foundations of the endless chronicle of invasions and extinctions which punctuate evolution [29]. In short, evolutionary game theory can be used to model ecosystems and the evolution of different species using methods of non-linear dynamics.

We will apply the concept of evolutionary game theory to the cooperator-defector game. Instead of two players, we will now consider a cooperator and a defector "species", whose populations either grow or shrink in time.

3.2.1 Replicator equation for the cooperator-defector game

Replicator equations describe the evolution of the frequencies of strategies in a population [29]. They are a frequently used method in evolutionary game theory to describe the time evolution of a system composed of different *species* (strategies) and to understand the mechanisms that lead to the spreading and decline or even extinction of species.

We consider a system with fixed population size N and two different competing species. Let N_A and $N_B = N - N_A$ be the number of individuals with strategy A (cooperators) and strategy B (defectors). We introduce the parameters a and b for the density of cooperators and defectors, respectively

$$a = \frac{N_A}{N}, \qquad b = \frac{N_B}{N} = \frac{N - N_A}{N} = 1 - a. \tag{3.1}$$

For simplicity, we assume that N is a large number such that a and b are continuous, and stochastic fluctuations do not matter. As a next step we introduce the concept of "*fitness*" f_A and f_B of a particular strategy A and B. This concept is often used in the mathematical literature of game theory [29, 22]. We define a background fitness set to 1 and add the average payoff given by matrix 3.1

$$\begin{aligned} f_A &= 1 + a\mathcal{R} + b\mathcal{S} \\ f_B &= 1 + a\mathcal{T} + b\mathcal{P}. \end{aligned} \tag{3.2}$$

We assume that the population of the species with the higher fitness grows in time while the population size of the species with the lower fitness shrinks. This growth (shrinking) rate is proportional to the difference of the fitness parameters f_A and f_B as well as the population densities a and b

$$\begin{aligned} \partial_t a &= (f_A - f_B) a\, b \\ \partial_t b &= (f_B - f_A) a\, b. \end{aligned} \tag{3.3}$$

Note that both equations are equivalent since $b = 1 - a$. Plugging the expressions for fitness f_A and f_B into the dynamic equations 3.3, we see that they do not depend on all four payoff values $\mathcal{R}, \mathcal{P}, \mathcal{T}$ and $\mathcal{S}$ but only on the differences $\mathcal{S} - \mathcal{P}$ and $\mathcal{T} - \mathcal{R}$. Thus we define the parameters $\tau_A := \mathcal{S} - \mathcal{P}$ and $\tau_B := \mathcal{T} - \mathcal{R}$ and get for the dynamic equations

$$\begin{aligned} \partial_t a &= (\tau_A b - \tau_B a) a\, b \\ \partial_t b &= (\tau_B a - \tau_A b) a\, b. \end{aligned} \tag{3.4}$$

τ_A can be interpreted as the advantage to be A rather than B if one encounters a member of B, whereas τ_B is the relative benefit of playing strategy B over A. Hence, the term $\tau_A b - \tau_B a$ compares the virtues of both species: if it is greater than zero, it is overall advantageous to be A; for values less than zero, it is advantageous to be B. The growth of one species is counteracted by a decrease of the other species by an equal amount. The system is therefore fully described by just one of the two equations. Plugging in $b = 1 - a$ in the dynamic equation for a we get

$$\partial_t a = (f_A - f_B)(1 - a)a = [\tau_A - (\tau_A + \tau_B)a]\,(1 - a)a. \tag{3.5}$$

The four different types of games introduced in the last chapter correspond to the four possibilities of either

$\tau_A < 0,\ \tau_B > 0$	Prisoners Dilemma
$\tau_A > 0,\ \tau_B < 0$	Harmony
$\tau_A, \tau_B > 0$	Snowdrift
$\tau_A, \tau_B < 0$	Coordination Game

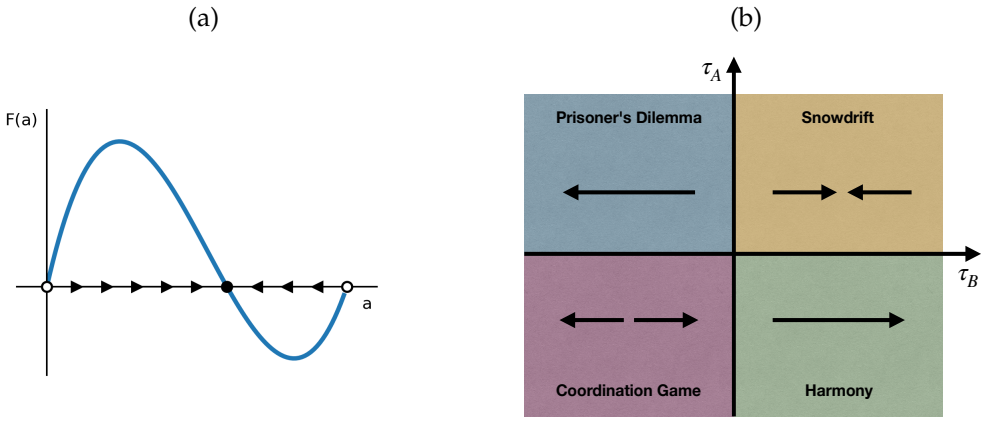

FIGURE 3.2: (a) Graphical solution for the Snowdrift replicator equation. If $F(a) > 0$ the flow (indicated by the black arrow heads) is to the right, if $F(a) < 0$ the flow is to the left. Black dots indicate fixed points (with filling: stable fixed point; without filling: unstable fixed point). (b) Overview of the dynamics of the four different games. Black arrows indicate the flow of a.

Instead of solving 3.5 exactly, we will use methods of nonlinear dynamics to study the flow and fixed points of the equation graphically. For a dynamic equation $\partial_t a = F(a)$, we know that a grows in time if $F(a) > 0$ (one says, the *flow* is to the right) and gets smaller for $F(a) < 0$ (the *flow* is to the left). At the values of a where $F(a) = 0$, there is no flow and a will stay at that particular value for all times (*fixed point*). Whether the flow is towards or away from a fixed point determines its stability.

Looking at equation 3.5, we can see that it is solved by the fixed points $a = 0$ and $a = 1$. If τ_A and τ_B have the same sign (in the case of Snowdrift or Coordination game) there is a third fixed point, $a = \frac{\tau_A}{\tau_A + \tau_B}$. Figure 3.2 shows the fixed points and flow of the Snowdrift game and gives an overview of the dynamics of the four different games depending on the game parameters τ_A and τ_B. Prisoner's dilemma, Harmony and Coordination game lead to the extinction of one of the species. Only the Snowdrift game leads to a stable coexistence state.

3.2.2 Spatially extended games

Spatial distribution of individuals, as well as their mobility, are common features of real ecosystems. Population habitats are spatially extended on all scales and individuals interact locally within their neighbourhood [34]. We want to study the dynamics and behaviour of our two-species system in a spatially extended volume V. Instead of overall particle numbers that determine the particle densities, we assume that at every point in space there is a certain overall density $\rho(\mathbf{r}) = a(\mathbf{r}, t) + b(\mathbf{r}, \mathbf{t})$ that gives the particle number N when integrated over the whole space

$$N = \int_V d\mathbf{r}\, \rho(\mathbf{r}). \tag{3.6}$$

Note that ρ is not a function of time since the replicator equation is a zero-sum game: Whatever a gains, b looses and vice versa at every point in space . This will change in the next sections when we let the individuals of both species move in space. The

replicator equation is now

$$\partial_t a = (\tau_A b - \tau_B a) a\, b = [\tau_A \rho - (\tau_A + \tau_B) a]\, (\rho - a) a \tag{3.7}$$

with the solutions $a = 0$, $a = \rho$ and (for Snowdrift and Coordination game) $a = \frac{\tau_A}{\tau_A + \tau_B}\rho$. Hence, the solutions depend on space $\mathbf{r}$, since ρ could have different values everywhere. The flow leads to these fixed points at every point in space.

In the next section we will develop a description that combines the evolutionary dynamics of game theory with a theory of self-propelled particles. Out of four different cooperator-defector games we choose the Snowdrift game to study the influence of self-propelled motion on the outcome of the game. We anticipate that it includes nontrivial populations of both species whereas other games have a kind of fixating character, leading to the extinction of one of the species in the long run. In the following we will therefore only consider the Snowdrift game type.

Chapter 4

Kinetic Boltzmann approach to Active Matter with Game Theory

The kinetic Boltzmann equation has been proposed to describe many-particle systems on a mesoscopic length-scale. Instead of describing the dynamics of each particle, the Boltzmann equation governs the evolution of a system in terms of one-particle distribution functions. Systematic coarse-graining leads to hydrodynamic equations for the macroscopic, slow variables of the system [7, 8, 40, 3, 57]. The Boltzmann approach can thereby provide a link between macroscopic quantities and the underlying microscopic rules.

Bertin et al. [7, 8] were the first to investigate systems of self-propelled, polar, point-like particles using the Boltzmann approach as a mathematical framework. The derived equations for the macroscopic variables of the system resemble the hydrodynamic equations proposed by Toner and Tu using symmetry arguments [52, 51, 53]. The advantage of the Boltzmann approach over an approach based on symmetry is the fact that all coefficients in the equations can be calculated as functions of microscopic parameters. The equations indicate a transition to a state of collective motion that happens spontaneously for high enough particle densities. Close to the transition to order, instabilities against long-wavelength perturbations indicate the formation of traveling wave patterns. Agent-based simulations have confirmed the existence of a state, where the dynamic is dominated by propagating bands of high density and high order in a low-density, disordered background [32, 11]. Away from the transition to order, a homogeneous, ordered phase is found in accordance with the continuous description [32, 8].

Since its first implementation, the Boltzmann approach has successfully been used to study different active systems, ranging from point-particles to curved polymers [30, 18, 40, 50, 57] and proven to be a very useful and reliable tool to derive minimal, well-behaved hydrodynamic descriptions of active matter [40].

In the following we will first define a microscopic model of self-propelled particles with noisy and local interaction rules tending to align the velocities of the particles. Afterwards we will outline a coarse-graining process leading to the Boltzmann equation for active matter following the work of Bertin et al. [7]. In a next step we extend the microscopic model in order to include different kinds of particles ("*species*") and game interactions between them. This extension leads us in a last step to an extended version of two Boltzmann equations that are coupled through game interactions.

4.1 Microscopic Model

The underlying microscopic model contains N point-like, active particles in continuous 2-dimensional space. The fluid or substrate on which the particles move acts as a momentum sink. Hence, overall momentum conservation (momentum of particles and fluid) is not a concern and we can neglect long-ranged interactions between particles caused by the surrounding fluid. Such a system is called *dry* [43].

The particles are driven by a force with fixed magnitude. As a result, all particles move with the same constant speed $|\mathbf{v}_i| = v_0$ with $i \in 1, ..., N$. Since the speed is fixed, the system is completely described by the positions $\mathbf{r}_i$ of all particles and their directions of motion θ_i ($i \in 1, ..., N$) at every instant of time. The positions are updated according to

$$\mathbf{r}_i(t + \Delta t) = \mathbf{r}_i(t) + v_0\, \mathbf{e}(\theta_i)\, \Delta t \tag{4.1}$$

where $\mathbf{e}(\theta)$ denotes the unit vector pointing in direction θ. Due to a noisy background or noisy propelling mechanism, this ballistic motion is interrupted by stochastic *self-diffusion* events: The particles change their orientation θ by a small angle at a rate λ per unit time to

$$\theta' = \theta + \eta_0 \tag{4.2}$$

where η_0 is a noise with Gaussian distribution $P_0(\eta)$ with standard deviation σ_0. Hence, the particles move in a run-and-tumble-like motion with a mean time between tumble events of λ^{-1}. On a large scale this leads to diffusive behaviour.

Particles interact via *collisions*: When two particles collide, they align. We look at the system in a dilute limit, meaning that we do not consider collisions of more than two particles. At our coarse-grained level of description, such collisions will be modeled in the form of simple collision rules. These collision rules map the particles' pre- to the post-collision orientations and are simple means to model the (possibly) complex interactions between particles in real systems. We also restrict our discussion to polar half-angle alignment: Two colliding particles with orientations θ_1 and θ_2 align in the direction of their average angle $\bar{\theta} = \frac{\theta_1+\theta_2}{2}$. To account for stochastic mistakes happening during the collision event, we add noise terms η_1 and η_2 drawn from a Gaussian distribution $P(\eta)$ with standard deviation σ

$$\theta_1' = \frac{\theta_1 + \theta_2}{2} + \eta_1, \qquad \theta_2' = \frac{\theta_1 + \theta_2}{2} + \eta_2. \tag{4.3}$$

The two stochastic events of self-diffusion and collision are illustrated schematically in figure 4.1.

The emergence of collective motion in this model system can be understood as a competition between the alignment of particles and the randomness of particle motion imposed by the noise terms of alignment and self-diffusion. Since alignment is more frequent for higher particle numbers and more precise for small noise values, it is plausible that high densities and low noise values are beneficial for the formation of collective behaviour.

The microscopic model is of course just one out of many possibilities to describe active systems. We study the case of polar particles (the particles have a "head" and a "tail") with ferromagnetic alignment (particles align according to their polarity). The symmetries of the particles and the interaction rule can be varied. Other classes of active particles that arise are polar particles that align by a nematic interaction

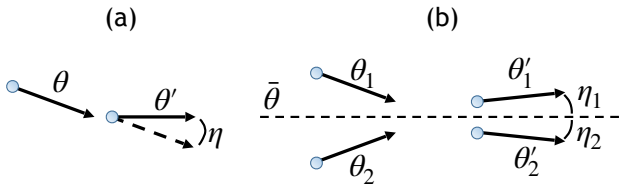

FIGURE 4.1: (a) Ballistic motion of particles is interrupted by stochastic *self-diffusion* events, where a particle changes its orientation θ by a small angle η to its new direction of motion θ'. This self-diffusion event happens at a rate λ. (b) Collision and half-angle alignment of two particles. To account for stochastic mistakes happening during the collision event, we add noise terms η_1 and η_2.

rule or head-tail symmetric apolar particles that align nematically [32]. Another possibility to model collisions could change the half-angle alignment of our example to a different alignment rule [40]. Particles could align metric-free with their nearest neighbours instead of aligning with particles that are in a certain range of distance [40]. However, the microscopic model described above is one of the simplest version of a variety of models for active matter. There have been any studies using this model [7, 8, 40] and it is therefore a good starting point for adding a game theoretical extension. For the scope of this thesis we will stick to this version for the microscopic model of active motion.

4.2 Boltzmann equation for Active Matter

The microscopic model illustrated in the last section can be described in the framework of a kinetic theory. For this purpose we introduce a generalized Boltzmann equation. The equation describes the dynamics of the one-particle probability distribution function $f(\mathbf{r}, \mathbf{p}, t)$. To be more precise, $f(\mathbf{r}, \mathbf{p}, t)$ is defined as the probability that there is a particle in a small region of space $\mathrm{d}^2\mathbf{r}$ centered at position $\mathbf{r}$, and has momentum nearly equal to $\mathbf{p}$ (thus occupying a very small region of momentum space $\mathrm{d}^2\mathbf{p}$) at a time t. Then $f(\mathbf{r}, \mathbf{p}, t)\, \mathrm{d}^2\mathbf{r}\mathrm{d}^2\mathbf{p}$ is the number of particles $\mathrm{d}N$ in an infinitesimal phase space volume $\mathrm{d}^2\mathbf{r}\mathrm{d}^2\mathbf{p}$. Integration over the whole phase space gives the total number of particles N

$$N = \int d^2\mathbf{r} \int d^2\mathbf{p}\, f(\mathbf{r}, \mathbf{p}, t)\,. \tag{4.4}$$

The Boltzmann approach relies on the approximation of *binary collisions* and the *molecular chaos* hypothesis (velocities of colliding particles are uncorrelated). These approximations are, to a certain extent, justifiable in low density systems [40].

In our model, particles all move with the same speed v_0. Fixing the speed means that the momentum of every particle is completely characterized by its direction of motion described by the angle θ

$$\mathbf{p} = \begin{pmatrix} p_x \\ p_y \end{pmatrix} = v_0 \begin{pmatrix} cos(\theta) \\ sin(\theta) \end{pmatrix}.$$

This reduces the phase space to 3 dimensions and the one-particle density $f(\mathbf{r}, \theta, t)$ is now a function of the spatial coordinates $\mathbf{r}$, the orientation θ and time t. For a

system with volume V we choose the normalization

$$\rho = \frac{1}{V}\int_V d^2\mathbf{r}\int_{-\pi}^{\pi} d\theta\, f(\mathbf{r},\theta,t)\,. \tag{4.5}$$

with ρ the mean density of the system. Let us for a moment consider a system without diffusion and collisions. Suppose there is a certain probability $f(\mathbf{r},\theta,t)\,d^2\mathbf{r}d\theta$ for a particle to be at position $\mathbf{r}$, moving in direction θ at a time t. If we wait for a small time Δt the particle will have moved to $\mathbf{r} + v_0\mathbf{e}(\theta)\,\Delta t$. The probability to find a particle is now $f(\mathbf{r} + v_0\mathbf{e}(\theta)\,\Delta t, \theta, t+\Delta t)\,d^2\mathbf{r}d\theta$. Since nothing else happened in this time interval the probabilities at t and $t+\Delta t$ have to be the same

$$0 = \left[f(\mathbf{r} + \Delta t\, v_0\mathbf{e}(\theta), \theta, t+\Delta t) - f(\mathbf{r},\theta,t)\right] d^2\mathbf{r}d\theta.$$

Dividing by Δt and taking the limit of $\Delta t \to 0$ leads to

$$\begin{aligned} 0 &= \lim_{\Delta t\to 0}\frac{1}{\Delta t}\left[f(\mathbf{r} + \Delta t\, v_0\mathbf{e}(\theta), \theta, t+\Delta t) - f(\mathbf{r},\theta,t)\right] \\ &= \frac{\partial f}{\partial t} + v_0\mathbf{e}(\theta)\cdot\nabla f(\vec{r},\theta,t). \end{aligned}$$

This is the total change of f in time due to self-propulsion and we will refer to it as *convection term*.

To account for self-diffusion and collision events we extend the equation to

$$\frac{\partial f}{\partial t} + v_0\,\mathbf{e}(\theta)\cdot\nabla f(\mathbf{r},\theta,t) = I_{diff}[f] + I_{coll}[f,f] \tag{4.6}$$

following the work of Bertin et al. [7, 8]. The diffusion and collision terms each have a gain and a loss term so that the full Boltzmann equation has the form of a Master equation. We assumed in the microscopic model that particles diffuse with probability λ, which has dimensions of inverse time. This means the loss term of the diffusion is simply

$$I_{diff}^{loss}[f] = -\lambda f(\mathbf{r},\theta,t)\,.$$

A self-diffusion event changes the direction of motion of a particle. As explained in the previous section, the change in the orientation is governed by the probability distribution $P_0(\eta)$. Hence, the gain term describes the event that particles, moving in a direction θ', self-diffuse to the direction θ

$$I_{diff}^{gain}[f] = \lambda\int_{-\pi}^{\pi} d\theta'\int_{-\infty}^{\infty} d\eta_0\left[f(\theta')\,\mathcal{P}_0(\eta_0)\,\delta_{2\pi}(\theta'+\eta_0-\theta)\right].$$

$\delta_{2\pi}(x) := \sum_{m=-\infty}^{+\infty}\delta(x+2\pi m)$ denotes the 2π-periodic δ-distribution that accounts for the periodicity of the angle. The spatial and time coordinates $\mathbf{r}, t$ are not displayed explicitly in the expression, since the diffusion only changes the angular degree of freedom.

Next we come to the collision term. Since we only consider the one-particle density, we need to restrict the model to binary collisions. This implicates that the Boltzmann equation is only valid for dilute conditions [40]. Using agent-based simulations it was shown that a model with binary collisions is legitimate to a certain degree and behaves qualitatively similar to a model with more complicated interactions [7]. To quantify the probability of collision events we need to find a measure for the rate

of particle collisions, known as the Boltzmann collision cylinder. This can be done solely by geometrical considerations (see figure 4.2). The rate is expressed by the differential cross section $\mathcal{R}(\theta_1, \theta_2)$ of a collision event between particles moving in directions θ_1 and θ_2. Let us consider two particles with diameter d, moving with constant speed v_0 in directions θ_1 and θ_2. Per definition the particles collide if their relative distance is less than d. If we go to the comoving frame of particle 1, we see particle 2 moving with velocity $\mathbf{v}_{21} := \mathbf{v}_2 - \mathbf{v}_1 = v_0 (\mathbf{e}(\theta_2) - \mathbf{e}(\theta_1))$. The two particles will collide in a time Δt if particle 2 is in an area $\mathcal{R}(\theta_1, \theta_2)\Delta t = 2d \|\mathbf{v}_{21}\| \Delta t = 2dv_0 \| (\mathbf{e}(\theta_2) - \mathbf{e}(\theta_1)) \| \Delta t$.

More complex forms of $\mathcal{R}(\theta_1, \theta_2)$ could be used to describe anisotropic interaction ranges, for example for elongated objects instead of point-like particles. However, it was demonstrated that such a change in the particle geometry in the framework of the Boltzmann equation introduces only minor quantitative effects [57].

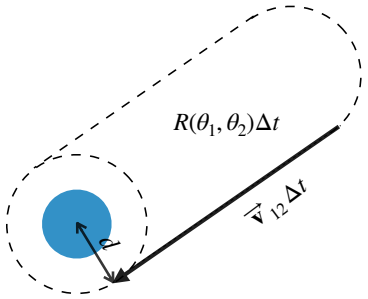

FIGURE 4.2: Differential cross section for the collision of two particles. The blue disk indicates a particle with diameter d and orientation θ_1. The particle will collide with a second particle moving in direction θ_2 during a time Δt, if the second particle is close by, in an area $\mathcal{R}(\theta_1, \theta_2)\,\Delta t = 2d \|\mathbf{v}_{21}\| \Delta t = 2dv_0 \| (\mathbf{e}(\theta_2) - \mathbf{e}(\theta_1)) \| \Delta t$ (indicated by the area inside the dashed line).

The interactions of two particles are described by an integral that takes the probability density of both particles and the differential cross section of a collision event $\mathcal{R}(\theta_1, \theta_2)$ into account. The probability density distribution required for this integral is actually the two-particle probability density $f^{(2)}(\mathbf{r}, \theta_1, \theta_2, t)$ [40]. However, usually the assumption of *molecular chaos* is made [7, 8], that approximates the two-particle distribution $f^{(2)}$ as the product of two one-particle distributions

$$f^{(2)}(\mathbf{r}, \theta_1, \theta_2, t) \approx f(\mathbf{r}, \theta_1, t)\, f(\mathbf{r}, \theta_2, t)\,.$$

Using this approximation, we assume that particle correlations prior to binary collisions can be neglected. Without this approximation, equation 4.6 would have to be complemented with dynamic equations governing the time evolution of the two-particle distribution function, which could lead to an infinite hierarchy of equations. Since this is not feasible for actual calculations, the molecular chaos assumption is a key ingredient for the Boltzmann equation. However, the assumption of molecular chaos is a rather delicate issue and it is a matter of ongoing investigation to find criteria, when this assumption is justified [40].

With the assumptions of binary collisions and molecular chaos we can now formulate the collision term of 4.6. The loss term of the collision term I_{coll}^{loss} describes the collision of a particle moving in direction θ and a second particle moving in an arbitrary direction. The collision of those two will result in a change of direction for both particles and therefore a negative contribution to $f(\mathbf{r}, \theta, t)$

$$I_{coll}^{loss}[f, g] = -f(\theta) \int_{-\pi}^{\pi} d\theta' \mathcal{R}(\theta, \theta') g(\theta').$$

Note that the collision event influences - as the self-diffusion - only the angular degree of freedom. The gain term is

$$I_{coll}^{gain}[f, g] = \int_{-\pi}^{\pi} d\theta_1 \int_{-\pi}^{\pi} d\theta_2 \int_{-\infty}^{\infty} d\eta \times \left[\mathcal{R}(\theta_1, \theta_2) f(\theta_1) g(\theta_2) \mathcal{P}(\eta) \delta_{2\pi}\left(\frac{\theta_1 + \theta_2}{2} + \eta - \theta\right)\right]$$

where $\mathcal{P}(\eta)$ is the Gaussian angular distribution function of variance σ^2 mentioned before. It describes two particles with orientations θ_1 and θ_2 colliding and the new orientation $\theta = \frac{\theta_1 + \theta_2}{2} + \eta$ after the collision event.

Everything put together gives

$$\begin{aligned} I_{diff}[f] &= -\lambda f(\theta) + \lambda \int_{-\pi}^{\pi} d\theta' \int_{-\infty}^{\infty} d\eta_0 \left[f(\theta') \mathcal{P}_0(\eta_0) \delta_{2\pi}(\theta' + \eta_0 - \theta)\right] \\ I_{coll}[f, f] &= -f(\theta) \int_{-\pi}^{\pi} d\theta' \mathcal{R}(\theta, \theta') f(\theta') \\ &\quad + \int_{-\pi}^{\pi} d\theta_1 \int_{-\pi}^{\pi} d\theta_2 \int_{-\infty}^{\infty} d\eta \left[\mathcal{R}(\theta_1, \theta_2) f(\theta_1) f(\theta_2) P(\eta) \delta_{2\pi}\left(\frac{\theta_1 + \theta_2}{2} + \eta - \theta\right)\right]. \end{aligned} \tag{4.7}$$

Without loss of generality we can rescale the Boltzmann equation 4.6 to simplify expressions

$$\begin{aligned} \tilde{t} &:= t \cdot \lambda \\ \tilde{\mathbf{r}} &:= \mathbf{r} \cdot \lambda v_0^{-1} \\ \tilde{f} &:= f \cdot d v_0 \lambda^{-1}. \end{aligned} \tag{4.8}$$

Using the rescaled and dimensionless parameters $\tilde{t}, \tilde{\mathbf{r}}$ and $\tilde{f}$amounts effectively to setting λ, v_0 and d equal to one. In the following we will omit the tilde and just write $t, \mathbf{r}$ and f to not clutter up the equations.

4.3 Extension of the Microscopic Model

We will extend the microscopic model described above to include a *game interaction* between two species. Our system consists now of N active point-like particles and each particle can either belong to species A or to species B. Particles align with other particles of the same species following the collision rules outlined in the sections above. They do not, however, align with particles of the other species. Instead, if particles of different species meet, they "play" the Snowdrift game: If the density of

particles of species A is too high (higher than the game theoretical fixed point) at a particular point in space and time, there is a probability that a particle of type A will switch species to become a particle of type B and vice versa. This interaction ensures that the overall number of particles is conserved.

We assume that the game interaction is local, meaning that it only depends on particle densities at that particular position in space. We further assume that it does not depend on the orientations of particles (in contrast to the alignment rule of particles).

4.4 Extended Boltzmann equation

We describe the evolution of the two species A and B in the Boltzmann framework with two probability density functions $\alpha(\mathbf{r}, \theta, t)$ and $\beta(\mathbf{r}, \theta, t)$. The particles of each species have the same speed v_0, diameter d and self-diffuse with probability λ. As mentioned above, particles collide and align only with members of the same species. The dynamics of both species is coupled through *game interaction terms* that influences the overall increase or decrease of densities. This leads us to the general form of the two species equations

$$\begin{aligned}
\partial_t \alpha(\mathbf{r}, \theta, t) + v_0 (\mathbf{e}(\theta) \cdot \nabla) \alpha(\mathbf{r}, \theta, t) &= I_{diff}[\alpha] + I_{coll}[\alpha, \alpha] + I_{gt}^{A}[\alpha, \beta] \\
\partial_t \beta(\mathbf{r}, \theta, t) + v_0 (\mathbf{e}(\theta) \cdot \nabla) \beta(\mathbf{r}, \theta, t) &= I_{diff}[\beta] + I_{coll}[\beta, \beta] + I_{gt}^{B}[\beta, \alpha].
\end{aligned}$$

Note that there is no term of the form $I_{coll}[\alpha, \beta]$ since per assumption different species do not collide. To find an expression for the game terms, we use the replicator equations derived in chapter 3. We saw that "playing" the Snowdrift game amounts to comparing the fitness values of both species at every point in space. The assumption that the game interaction is local and does not depend on the orientations of particles means that the fitness terms depend on the densities $a(\mathbf{r}, t)$ and $b(\mathbf{r}, t)$ of species A and B defined as

$$\begin{aligned}
a(\mathbf{r}, t) &= \int_{-\pi}^{\pi} d\theta \, \alpha(\mathbf{r}, \theta, t) \\
b(\mathbf{r}, t) &= \int_{-\pi}^{\pi} d\theta \, \beta(\mathbf{r}, \theta, t).
\end{aligned}$$

Recall that the term comparing the fitness of species A, f_A, with the fitness of species B, f_B, is

$$f_A - f_B = \tau_A \, b(\mathbf{r}, t) - \tau_B \, a(\mathbf{r}, t).$$

If $f_A > f_B$ for a particular point in space and time, the probability density to find a particle of species A should grow proportionally to $|f_A - f_B|$ at that point, while the probability to find a particle B decreases by the same amount. On the other hand if $f_A < f_B$, $\alpha(\mathbf{r}, \theta, t)$ should decrease while $\beta(\mathbf{r}, \theta, t)$ grows. We also have to account for the probability that particles of species A and B meet. The probability density for a particle A to meet a particle B is $b(\mathbf{r}, t) \, \alpha(\mathbf{r}, \theta, t)$, since the direction of motion of the B-particle does not play a role by assumption. Hence, the game theory terms that couple species A and B are

$$\begin{aligned}
I_{gt}^{A}[\alpha, \beta] &= (\tau_A b - \tau_B a) \; b \, \alpha(\theta) \\
I_{gt}^{B}[\alpha, \beta] &= (\tau_B a - \tau_A b) \; a \, \beta(\theta)
\end{aligned} \tag{4.9}$$

where we did not state the dependence on $\mathbf{r}$ and t explicitly. To keep notation short we will most of the time omit the $\mathbf{r}$- and t- dependence and just write a and b meaning $a(\mathbf{r},t)$ and $b(\mathbf{r},t)$, as well as $\alpha(\theta)$ and $\beta(\theta)$ meaning $\alpha(\mathbf{r},\theta,t)$ and $\beta(\mathbf{r},\theta,t)$. The game interaction terms 4.9 could describe all of the four different games introduced in the chapter about game theory. However, in this thesis we will stick to the Snowdrift game ($\tau_A \geq 0, \tau_B \geq 0$) since it promises the most interesting results.

We perform the same rescaling as for the Boltzmann equation for active matter in the last section and set $\lambda = v_0 = d = 1$ everywhere. In the course of this rescaling we define the new dimensionless parameters

$$\begin{aligned}\tilde{\tau}_A &= \tau_A \cdot \lambda d^{-2} v_0^{-2} \\ \tilde{\tau}_B &= \tau_B \cdot \lambda d^{-2} v_0^{-2}.\end{aligned}$$

In summary, we formulated an extended version of two coupled Boltzmann equations for active particles with a game interaction. It incorporates the convection, self-diffusion and collision (polar alignment) of particles as well as a game interaction that lets particles switch between species. The two coupled differential equations for the time evolution of species A and species B are

$$\begin{aligned}\partial_t \alpha(\theta) + (\mathbf{e}(\theta)\cdot\nabla)\,\alpha(\theta) &= I_{diff}[\alpha] + I_{coll}[\alpha,\alpha] + I_{gt}^{A}[\alpha,\beta] \\ \partial_t \beta(\theta) + (\mathbf{e}(\theta)\cdot\nabla)\,\beta(\theta) &= I_{diff}[\beta] + I_{coll}[\beta,\beta] + I_{gt}^{B}[\beta,\alpha].\end{aligned} \tag{4.10}$$

The interaction terms are

$$\begin{aligned}I_{diff}[f] &= -f(\theta) + \int_{-\pi}^{\pi} d\theta' \int_{-\infty}^{\infty} d\eta_0 \left[f(\theta')\, \mathcal{P}_0(\eta_0)\, \delta_{2\pi}(\theta' + \eta_0 - \theta) \right] \\ I_{coll}[f,f] &= -f(\theta) \int_{-\pi}^{\pi} d\theta' \mathcal{R}(\theta,\theta')\, f(\theta') \\ &\quad + \int_{-\pi}^{\pi} d\theta_1 \int_{-\pi}^{\pi} d\theta_2 \int_{-\infty}^{\infty} d\eta \left[\mathcal{R}(\theta_1,\theta_2)\, f(\theta_1)\, f(\theta_2)\, \mathcal{P}(\eta)\, \delta_{2\pi}\left(\frac{\theta_1+\theta_2}{2} + \eta - \theta \right) \right] \\ I_{gt}^{A}[\alpha,\beta] &= (\tau_A b - \tau_B a)\; b\,\alpha(\theta) \\ I_{gt}^{B}[\alpha,\beta] &= (\tau_B a - \tau_A b)\; a\,\beta(\theta)\end{aligned} \tag{4.11}$$

with

$$\begin{aligned}\mathcal{R}(\theta_1,\theta_2) &= 2\|\mathbf{e}(\theta_1) - \mathbf{e}(\theta_2)\| = 4\left|\sin\left(\frac{\theta_1-\theta_2}{2}\right)\right| \\ \mathcal{P}_0(\eta_0) &= \frac{1}{\sqrt{2\pi\sigma_0^2}}\, e^{-\frac{\eta_0^2}{2\sigma_0^2}} \\ \mathcal{P}(\eta) &= \frac{1}{\sqrt{2\pi\sigma^2}}\, e^{-\frac{\eta^2}{2\sigma^2}}.\end{aligned}$$

The assumptions of this kinetic model are:

- A dilute system (binary collisions only)

- Molecular chaos, which neglects correlations between particles (particles are statistically independent)
- Game interactions are local and do not depend on the orientations of particles

The Boltzmann equations 4.10 set the mathematical framework for the investigation of our active particle system with game interaction. It is derived from a microscopic model and therefore incorporates the dynamics of the system at the level of single particles. We will use it as a starting point to derive simpler hydrodynamic equations using a popular strategy of scaling arguments and appropriate truncation schemes [8, 40].

Chapter 5

Derivation of Hydrodynamic equations

The Boltzmann equation 4.10 is a highly complex integro-differential equation which means that an analytic treatment is not feasible. Luckily we are only interested in those variables of the system that vary slowly in time and we do not need the full description of the system. We will see that the slow variables are connected with the conserved quantities of the system as well as its symmetries. In this section we will extract a minimal set of equations for the slow variables from the full description governed by equations 4.10 following a strategy commonly employed for the active Boltzmann equation for various systems; cf. [7, 40, 8, 18, 42, 41].

The general procedure to arrive at a hydrodynamic description of the system consists of two steps. In step one, we perform a Fourier series expansion in the angular variable θ. The resulting infinite set of coupled differential equations describes the time evolution of the Fourier modes. We will see that the long wavelength (small wave number) modes grow or decay slowly whereas the short wavelength (big wave number) decay fast. In step two we will use this fact to implement a truncation scheme and cut off the short wavelength modes. This procedure will lead us to a closed set of equations for the slow variables of the system.

5.1 Fourier expansion of the extended Boltzmann equations

In the following we will perform a Fourier series expansion on the dynamic equation for $\alpha(\mathbf{r}, \theta, t)$. We use the conventions

$$\begin{aligned} \alpha_k &= \mathcal{F}[\alpha(\theta)] = \int_{-\pi}^{\pi} \mathrm{d}\theta\, \alpha(\theta)\, \mathrm{e}^{\mathrm{i}k\theta} \\ \alpha(\theta) &= \mathcal{F}^{-1}[\alpha_k] = \frac{1}{2\pi} \sum_{k=-\infty}^{\infty} \alpha_k\, \mathrm{e}^{-\mathrm{i}k\theta}, \qquad \theta \in (-\pi, \pi],\, k \in \mathbb{Z} \end{aligned} \tag{5.1}$$

where we used the abbreviations $\alpha(\theta)$ and α_k to lighten notation, keeping in mind that both depend on space $\mathbf{r}$ and time t. Note that $\alpha_{-k} = \alpha_k^*$, where the star denotes complex conjugation.

We will Fourier transform each term of equation 4.10 separately. It is sufficient to concern ourselves with the dynamic equation for α, since the equation for β is completely analogous. The first term on the left hand side is the partial derivative of α with respect to time. Since we can exchange time derivative and integration, this

term becomes

$$\int_{-\pi}^{\pi} \mathrm{d}\theta\, \mathrm{e}^{\mathrm{i}k\theta}\, \partial_t \alpha(\theta) = \partial_t \int_{-\pi}^{\pi} \mathrm{d}\theta\, \mathrm{e}^{\mathrm{i}k\theta} \alpha(\theta) = \partial_t \alpha_k.$$

The second term is the convection term. In the Fourier transformation we use $\mathbf{e}(\theta) = (\cos(\theta), \sin(\theta))^{\mathrm{T}}$ and Euler's formula to get

$$\begin{aligned}
\int_{-\pi}^{\pi} \mathrm{d}\theta\, \mathrm{e}^{\mathrm{i}k\theta} \mathbf{e}(\theta) \cdot \nabla \alpha(\theta) &= \int_{-\pi}^{\pi} \mathrm{d}\theta\, \mathrm{e}^{\mathrm{i}k\theta} \left[\cos(\theta)\partial_x + \sin(\theta)\partial_y\right] \alpha(\theta) \\
&= \int_{-\pi}^{\pi} \mathrm{d}\theta\, \mathrm{e}^{\mathrm{i}k\theta} \frac{1}{2} \left[\left(\mathrm{e}^{\mathrm{i}\theta} + \mathrm{e}^{-\mathrm{i}\theta}\right) \partial_x - \mathrm{i} \left(\mathrm{e}^{\mathrm{i}\theta} - \mathrm{e}^{-\mathrm{i}\theta}\right) \partial_y \right] \alpha(\theta) \\
&= \int_{-\pi}^{\pi} \mathrm{d}\theta \frac{1}{2} \left[\left(\partial_x + \mathrm{i}\partial_y\right) \mathrm{e}^{\mathrm{i}\theta(k-1)} + \left(\partial_x - \mathrm{i}\partial_y\right) \mathrm{e}^{\mathrm{i}\theta(k+1)} \right] \alpha(\theta) \\
&= \frac{1}{2} \left(\partial_x + \mathrm{i}\partial_y\right) \alpha_{k-1} + \frac{1}{2} \left(\partial_x - \mathrm{i}\partial_y\right) \alpha_{k+1} \\
&= \frac{1}{2} \nabla \alpha_{k-1} + \frac{1}{2} \nabla^* \alpha_{k+1}
\end{aligned}$$

where we used the abbreviations

$$\begin{aligned}
\nabla &:= \partial_x + \mathrm{i}\partial_y \\
\nabla^* &:= \partial_x - \mathrm{i}\partial_y.
\end{aligned} \tag{5.2}$$

Next we Fourier transform the right hand side of equation 4.10. The diffusion term gives

$$\begin{aligned}
&\int_{-\pi}^{\pi} \mathrm{d}\theta\, \mathrm{e}^{\mathrm{i}k\theta}\, \mathcal{I}_{diff}[\alpha] \\
&\qquad = \int_{-\pi}^{\pi} \mathrm{d}\theta\, \mathrm{e}^{\mathrm{i}k\theta} \left[-\alpha(\theta) + \int_{-\pi}^{\pi} \mathrm{d}\theta' \int_{-\infty}^{\infty} \mathrm{d}\eta_0\, \alpha(\theta') \mathcal{P}_0(\eta_0)\, \delta_{2\pi}\left(\theta' - \theta + \eta_0\right) \right] \\
&\qquad = -\alpha_k + \int_{-\pi}^{\pi} \mathrm{d}\theta' \int_{-\infty}^{\infty} \mathrm{d}\eta_0\, \mathrm{e}^{\mathrm{i}k(\theta' + \eta_0)} \alpha(\theta') \mathcal{P}_0(\eta_0) \\
&\qquad = -\alpha_k + \left[\int_{-\pi}^{\pi} \mathrm{d}\theta'\, \mathrm{e}^{\mathrm{i}k\theta'} \alpha(\theta') \right] \left[\int_{-\infty}^{\infty} \mathrm{d}\eta_0\, \mathrm{e}^{\mathrm{i}k\eta_0} \mathcal{P}_0(\eta_0) \right] \\
&\qquad = -\alpha_k + \alpha_k\, \mathcal{P}_{0,k} \\
&\qquad = \left(\mathcal{P}_{0,k} - 1\right) \alpha_k.
\end{aligned}$$

$\mathcal{P}_{0,k}$ is the Fourier transform of the self-diffusion noise probability $\mathcal{P}_0(\eta_0)$. As the probability is a Gaussian distribution with standard deviation σ_0, its Fourier transform is as well a Gaussian with standard deviation σ_0^{-1}.

The Fourier transform of the collision term is a little bit more involved. We start with the loss term 4.2 by decomposing $\alpha(\theta)$ into its Fourier modes

$$\begin{aligned}
&\int_{-\pi}^{\pi} \mathrm{d}\theta\, \mathrm{e}^{\mathrm{i}k\theta}\, \mathcal{I}_{coll}^{loss}\left[\alpha,\alpha\right] \\
&\quad = \int_{-\pi}^{\pi} \mathrm{d}\theta\, \mathrm{e}^{\mathrm{i}k\theta} \left[-\alpha(\theta) \int_{-\pi}^{\pi} \mathrm{d}\theta' \mathcal{R}\left(\theta,\theta'\right) \alpha\left(\theta'\right)\right] \\
&\quad = -\int_{-\pi}^{\pi} \mathrm{d}\theta\, \mathrm{e}^{\mathrm{i}k\theta} \frac{1}{2\pi} \sum_{q'=-\infty}^{\infty} \alpha_{q'} \mathrm{e}^{-\mathrm{i}q'\theta} \int_{-\pi}^{\pi} \mathrm{d}\theta' \mathcal{R}\left(\theta,\theta'\right) \frac{1}{2\pi} \sum_{q=-\infty}^{\infty} \alpha_q \mathrm{e}^{-\mathrm{i}q\theta'} \\
&\quad = -\frac{1}{(2\pi)^2} \sum_{q,q'=-\infty}^{\infty} \alpha_{q'}\alpha_q \int_{-\pi}^{\pi} \mathrm{d}\theta \int_{-\pi}^{\pi} \mathrm{d}\theta' \mathrm{e}^{\mathrm{i}k\theta} \mathrm{e}^{-\mathrm{i}q'\theta} \mathrm{e}^{-\mathrm{i}q\theta'} \mathcal{R}\left(\theta,\theta'\right)
\end{aligned}$$

As a next step we make a substitution of variables by defining $\psi := \theta - \theta'$ and replacing θ' everywhere with $\theta - \psi$. The bounds of integration stay the same since we integrate over all angles. We also make use of the fact that the differential cross section only depends on the difference of the two angles, $\mathcal{R}\left(\theta,\theta'\right) = \mathcal{R}\left(|\theta-\theta'|\right) = \mathcal{R}\left(|\psi|\right)$.

$$\begin{aligned}
&\int_{-\pi}^{\pi} \mathrm{d}\theta\, \mathrm{e}^{\mathrm{i}k\theta}\, \mathcal{I}_{coll}^{loss}\left[\alpha,\alpha\right] \\
&\quad = -\frac{1}{(2\pi)^2} \sum_{q,q'=-\infty}^{\infty} \alpha_q\alpha_{q'} \int_{-\pi}^{\pi} \mathrm{d}\theta\, \mathrm{e}^{\mathrm{i}\theta(k-q'-q)} \int_{-\pi}^{\pi} \mathrm{d}\psi\, \mathrm{e}^{\mathrm{i}q\psi} R(|\psi|) \\
&\quad = -\frac{1}{2\pi} \sum_{q=-\infty}^{\infty} \alpha_q\alpha_{k-q} \int_{-\pi}^{\pi} \mathrm{d}\psi\, \mathrm{e}^{\mathrm{i}q\psi} \mathcal{R}(|\psi|) \\
&\quad = -\frac{1}{2\pi} \sum_{q=-\infty}^{\infty} \alpha_q\hat{\alpha_{k-q}} \int_{-\pi}^{\pi} \mathrm{d}\psi \cos(q\psi) \mathcal{R}(|\psi|)
\end{aligned}$$

where we have used the identity $\int_{-\pi}^{\pi} \mathrm{d}\theta\, \mathrm{e}^{\mathrm{i}\theta(k-q'-q)} = 2\pi\delta_{k-q'-q}$ in the first step and the fact that only the symmetric part of $\mathrm{e}^{\mathrm{i}q\psi}$ contributes to the integral because $\mathcal{R}(|\psi|)$ is an even function in the second step. The Fourier transformation of the gain term of the collision term follows similar steps. First, we decompose $\alpha(\theta)$ into its Fourier modes and perform the integration over the delta-distribution

$$\begin{aligned}
&\int_{-\pi}^{\pi} \mathrm{d}\theta\, \mathrm{e}^{\mathrm{i}k\theta}\, \mathcal{I}_{coll}^{gain}\left[\alpha,\alpha\right] \\
&\quad = \int_{-\pi}^{\pi} \mathrm{d}\theta\, \mathrm{e}^{\mathrm{i}k\theta} \int_{-\pi}^{\pi} d\theta_1 \int_{-\pi}^{\pi} d\theta_2 \int_{-\infty}^{\infty} d\eta \times \\
&\qquad \left[\mathcal{R}\left(\theta_1,\theta_2\right) \alpha\left(\theta_1\right) \alpha\left(\theta_2\right) \mathcal{P}\left(\eta\right) \delta_{2\pi}\left(\frac{\theta_1+\theta_2}{2} + \eta - \theta\right)\right] \\
&\quad = \frac{1}{(2\pi)^2} \sum_{q,q'=-\infty}^{\infty} \alpha_{q'}\alpha_q \int_{-\pi}^{\pi} d\theta_1 \int_{-\pi}^{\pi} d\theta_2 \int_{-\infty}^{\infty} d\eta \times \\
&\qquad \left[\mathrm{e}^{\mathrm{i}k\left(\frac{\theta_1+\theta_2}{2}+\eta\right)} \mathrm{e}^{-\mathrm{i}q'\theta_1} \mathrm{e}^{-\mathrm{i}q\theta_2} \mathcal{R}\left(\theta_1,\theta_2\right) \mathcal{P}\left(\eta\right)\right] \\
&\quad = \frac{1}{(2\pi)^2} \sum_{q,q'=-\infty}^{\infty} \alpha_{q'}\alpha_q \int_{-\pi}^{\pi} d\theta_1 \int_{-\pi}^{\pi} d\theta_2 \left[\mathrm{e}^{\mathrm{i}k\left(\frac{\theta_1+\theta_2}{2}\right)} \mathrm{e}^{-\mathrm{i}q'\theta_1} \mathrm{e}^{-\mathrm{i}q\theta_2} \mathcal{R}\left(\theta_1,\theta_2\right)\right] \times \\
&\qquad \int_{-\infty}^{\infty} d\eta\, \mathrm{e}^{\mathrm{i}k\eta} \mathcal{P}\left(\eta\right).
\end{aligned}$$

The last factor is the Fourier transformation of the collision noise probability, $\mathcal{P}_k$. As for the loss term, we make a substitution, $\psi := \theta_1 - \theta_2$, and use $\int_{-\pi}^{\pi} d\theta_1 \, \mathrm{e}^{\mathrm{i}\theta_1(k-q'-q)} = 2\pi\delta_{k-q'-q}$ as well as the symmetry of $\mathcal{R}(\theta_1, \theta_2)$ to get

$$\begin{aligned}
&\int_{-\pi}^{\pi} \mathrm{d}\theta \, \mathrm{e}^{\mathrm{i}k\theta} \, \mathcal{I}_{coll}^{gain} \left[\alpha, \alpha\right] \\
&\qquad = \frac{1}{(2\pi)^2} \sum_{q,q'=-\infty}^{\infty} \alpha_{q'} \alpha_q \int_{-\pi}^{\pi} d\theta_1 \, \mathrm{e}^{\mathrm{i}\theta_1(k-q'-q)} \int_{-\pi}^{\pi} d\psi \, \mathrm{e}^{\mathrm{i}\psi(q-\frac{k}{2})} \mathcal{R}\left(|\psi|\right) \mathcal{P}_k \\
&\qquad = \frac{1}{2\pi} \sum_{q=-\infty}^{\infty} \alpha_{k-q} \alpha_q \int_{-\pi}^{\pi} d\psi \, \mathrm{e}^{\mathrm{i}\psi(q-\frac{k}{2})} \mathcal{R}\left(|\psi|\right) \mathcal{P}_k \\
&\qquad = \frac{1}{2\pi} \sum_{q=-\infty}^{\infty} \alpha_{k-q} \alpha_q \int_{-\pi}^{\pi} d\psi \cos(\psi(q-\frac{k}{2})) \mathcal{R}\left(|\psi|\right) \mathcal{P}_k .
\end{aligned}$$

As a last step we Fourier transform the game interaction term. The series expansion of $\mathcal{I}_{gt}^{A}$ is easy, since the densities a and b do not depend on the angular variable θ

$$\int_{-\pi}^{\pi} \mathrm{d}\theta \, \mathrm{e}^{\mathrm{i}k\theta} \, \mathcal{I}_{gt}^{A} \left[\alpha, \beta\right] = \left(\tau_A b - \tau_B a\right) \, b \int_{-\pi}^{\pi} \mathrm{d}\theta \, \mathrm{e}^{\mathrm{i}k\theta} \, \alpha\left(\theta\right) = \left(\tau_A b - \tau_B a\right) \, b \, \alpha_k .$$

Putting everything together and performing the same steps for the dynamic equation for β gives us the Fourier expansion of the extended Boltzmann equations

$$\begin{aligned}
&\partial_t \alpha_k + \frac{1}{2} \left(\nabla \alpha_{k-1} + \nabla^* \alpha_{k+1}\right) \\
&\qquad = \left(\mathcal{P}_{0,k} - 1\right) \alpha_k + \sum_{n=-\infty}^{\infty} C_{n,k} \, \alpha_{n-k} \, \alpha_n + \left(\tau_A b - \tau_B a\right) \, b \, \alpha_k
\end{aligned} \tag{5.3a}$$

$$\begin{aligned}
&\partial_t \beta_k + \frac{1}{2} \left(\nabla \beta_{k-1} + \nabla^* \beta_{k+1}\right) \\
&\qquad = \left(\mathcal{P}_{0,k} - 1\right) \beta_k + \sum_{n=-\infty}^{\infty} C_{n,k} \, \beta_{n-k} \, \beta_n - \left(\tau_A b - \tau_B a\right) \, a \, \beta_k
\end{aligned} \tag{5.3b}$$

with

$$\begin{aligned}
\nabla &:= \partial_x + \partial_y, \quad \nabla^* := \partial_x - \partial_y \\
\mathcal{P}_{0,k} &:= \int_{-\infty}^{\infty} d\eta \, e^{ik\eta_0} \, \mathcal{P}_0(\eta_0) = e^{-\frac{\sigma_0^2 k^2}{2}} \\
\mathcal{P}_k &:= \int_{-\infty}^{\infty} d\eta \, e^{ik\eta} \, \mathcal{P}(\eta) = e^{-\frac{\sigma^2 k^2}{2}} \\
C_{n,k} &:= \int_{-\pi}^{\pi} d\psi \, \mathcal{R}(|\psi|) \, \left[\mathcal{P}_k cos((n - k/2)\psi) - cos(n\psi)\right] .
\end{aligned} \tag{5.4}$$

5.2 Hydrodynamic variables

The Fourier expansion of the Boltzmann equation is an infinite set of coupled partial differential equations. It is fully equivalent to the original set of equations 4.10. For an analytic treatment to be feasible we need to find a reasonable cut off. Our goal is to reduce the infinite set of equations 5.3 to a minimal set of equations for the relevant fields. This can be achieved by defining a hierarchy of modes and keeping only the ones of interest. The standard approach is to look for independent, so called

slow or *hydrodynamic variables*. We will briefly introduce the notion of slow variables and apply the concept afterwards to our system.

Slow variables vary on macroscopic time scales, meaning that long wavelength excitation relax on time scales that are very large compared to the microscopic time scales of the system such as collision time or mean free time. To identify these variables for a system, one uses the fact that slow variables are in general connected to conservation laws and symmetries [33]. This claim can be explained by the following argument [51]: Assume there is a slow variable X, that is not constrained by conservation laws or symmetries. Then the dynamic equation of X will have the general form

$$\partial_t X = -\frac{X}{\tau_{mic}} + F(X, \mathbf{Y}) \tag{5.5}$$

with τ_{mic} a microscopic time scale and F a function of X and all other slow variables $\mathbf{Y}$ of the system, since nothing forbids a term of the form $-\frac{X}{\tau_{mic}}$. Then $\partial_t X \ll -\frac{X}{\tau_{mic}}$, since τ_{mic} is by assumption much smaller than the dynamics of X. We can therefore set $\partial_t X \approx 0$ in equation 5.5 and solve for X as a function of $\mathbf{Y}$. Hence, X is not an independent variable of the system, as it can be expressed by the slow variables $\mathbf{Y}$.

This argument shows that we only have to consider variables X whose equations can not contain terms of the form $-\frac{X}{\tau_{mic}}$. The two mechanisms constraining a system are conservation laws and symmetries. As far as our system is concerned, we have two constraints given by

1. Particle conservation
2. Rotational symmetry.

Particle conservation forbids a decay of the overall *density* and makes it therefore a slow variable of our system. Rotational symmetry forbids the decay of uniform rotational perturbations: If all orientation vectors are rotated by the same angle, the state of the system has effectively not changed and does not decay back to its original configuration. The corresponding hydrodynamic variables are the *momentum fields* or *polar order fields*.

As a next step we will see how the slow hydrodynamic variables are connected with the long-wavelength Fourier modes of our system of equations. From the definition of the Fourier series expansion it follows that the 0-th Fourier mode is just the density function of the respective species, since

$$\alpha_0(\mathbf{r}, t) = \int_{-\pi}^{\pi} \mathrm{d}\theta \, e^{ik\cdot 0} \alpha(\mathbf{r}, \theta, t) = \int_{-\pi}^{\pi} \mathrm{d}\theta \, \alpha(\mathbf{r}, \theta, t) = a(\mathbf{r}, t).$$

Hence, the equations of the 0-th Fourier modes, α_0 and β_0, give the evolution of the density fields a and b. It is easy to check that $(P_{0,0} - 1) = 0$ and $C_{n,0} = 0$, so the dynamic equations 5.3 for $k = 0$ become

$$\partial_t a + \frac{1}{2} \left(\nabla \alpha_{-1} + \nabla^* \alpha_1 \right) = \left(\tau_A b - \tau_B a \right) \, a \, b \tag{5.6a}$$

$$\partial_t b + \frac{1}{2} \left(\nabla \beta_{-1} + \nabla^* \beta_1 \right) = - \left(\tau_A b - \tau_B a \right) \, a \, b. \tag{5.6b}$$

where we plugged in $\alpha_0 = a$ and $\beta_0 = b$. Next, we investigate the equations for the 1st mode, $k = 1$. The definition of the Fourier series gives

$$\alpha_1(\mathbf{r}, t) = \int_{-\pi}^{\pi} d\theta \, e^{i\theta} \alpha(\mathbf{r}, \theta, t)$$
$$\beta_1(\mathbf{r}, t) = \int_{-\pi}^{\pi} d\theta \, e^{i\theta} \beta(\mathbf{r}, \theta, t).$$

We saw before, that the slow variables of the system are connected (among other things) with its symmetries. Rotational invariance holds for the dynamic equations for both species. The related slow variables are the polar order fields $\mathbf{P}_a$ and $\mathbf{P}_b$

$$\mathbf{P}_a(\mathbf{r}, t) := \frac{1}{a\,(\mathbf{r}, t)} \int_{-\pi}^{\pi} d\theta \, \mathbf{e}(\theta) \alpha(\mathbf{r}, \theta, t)$$
$$\mathbf{P}_b(\mathbf{r}, t) := \frac{1}{b\,(\mathbf{r}, t)} \int_{-\pi}^{\pi} d\theta \, \mathbf{e}(\theta) \beta(\mathbf{r}, \theta, t)$$

where $\mathbf{e}(\theta)$ denotes the unit vector. We can relate the polar order fields $\mathbf{P}_a(\mathbf{r}, t)$ and $\mathbf{P}_b(\mathbf{r}, t)$ to the first Fourier modes $\alpha_1(\mathbf{r}, t)$ and $\beta_1(\mathbf{r}, t)$ using the correspondence of complex numbers to 2-dimensional vectors in real space $e^{i\theta} \cong (\cos(\theta), \sin(\theta))^{\mathrm{T}} = \mathbf{e}(\theta)$. We also rename $w(\mathbf{r}, t) := \alpha_1(\mathbf{r}, t)$ and $u(\mathbf{r}, t) := \beta_1(\mathbf{r}, t)$ for later convenience

$$w(\mathbf{r}, t) = \alpha_1(\mathbf{r}, t) = \int_{-\pi}^{\pi} d\theta \, e^{i\theta} \alpha(\mathbf{r}, \theta, t) \cong a\,(\mathbf{r}, t)\, \mathbf{P}_a(\mathbf{r}, t) \tag{5.9a}$$
$$u(\mathbf{r}, t) = \beta_1(\mathbf{r}, t) = \int_{-\pi}^{\pi} d\theta \, e^{i\theta} \beta(\mathbf{r}, \theta, t) \cong b\,(\mathbf{r}, t)\, \mathbf{P}_b(\mathbf{r}, t). \tag{5.9b}$$

The slow variable related to the conservation of particles is the local density

$$\rho\,(\mathbf{r}, t) = a\,(\mathbf{r}, t) + b\,(\mathbf{r}, t)\,.$$

Using 5.6 and $\alpha_{-1} = \alpha_1^*, \beta_{-1} = \beta_1^*$ we get for the time evolution of ρ

$$\begin{aligned} \partial_t \rho &= \partial_t a + \partial_t b \\ &= -\frac{1}{2} \left(\nabla \alpha_1^* - \nabla^* \alpha_1 + \nabla \beta_1^* + \nabla^* \beta_1 \right). \end{aligned} \tag{5.10}$$

Plugging the definition of the polar order fields into 5.10 and using once again the correspondence of complex numbers to 2-dimensional vectors in real space gives

$$\partial_t \rho = -\nabla (w + u) \cong -\nabla \left(a \cdot \mathbf{P}_a + b \cdot \mathbf{P}_b \right) \tag{5.11}$$

which is a continuity equation with the overall flux of particles $(a \cdot \mathbf{P}_a + b \cdot \mathbf{P}_b)$. This reflects the fact that the total number of particles is conserved. In the remainder of this thesis w and u will be referred to as polar order fields.

In the next section we will argue why it is reasonable to truncate the equations after the first few modes. This procedure will lead to a closed set of differential equations for the densities and polar order fields.

5.3 Hierarchy of modes

We can get one solution of the full Boltzmann equation 5.3 quite easily since we know that $(P_{0,k} - 1) = 0$ and $C_{n,k} = 0$ for $k = 0$. When we assume spatial homogeneity ($\nabla\alpha_k = \nabla\beta_k = 0$), the Boltzmann equations become for $k = 0$

$$\begin{aligned}\partial_t a &= (\tau_A b - \tau_B a)\ a\, b \\ \partial_t b &= -(\tau_A b - \tau_B a)\ a\, b.\end{aligned}$$

Next we plug in $b = \rho - a$ to get

$$\partial_t a = (\tau_A \rho - (\tau_A + \tau_B)a)\ (\rho - a)\, a.$$

This is our well-known replicator equation from chapter 3. It has the three fixed points

$$\begin{aligned}a_0 &= 0, \\ a_0 &= \rho, \\ a_0 &= \frac{\tau_A}{\tau_A + \tau_B}\rho =: g_a \rho.\end{aligned}$$

a_0 is completely fixed by τ_A, τ_B and ρ. These are the three independent *control parameters* of the system. The fixed points of the density b_0 are given by $b_0 = \rho - a_0$:

$$\begin{aligned}b_0 &= \rho, \\ b_0 &= 0, \\ b_0 &= \frac{\tau_B}{\tau_A + \tau_B}\rho =: g_b \rho.\end{aligned}$$

Recall that only the third fixed point is stable. A solution for the full Boltzmann equations is therefor $a = a_0$, $b = b_0$ and $\alpha_k = \beta_k = 0$ for all $k > 0$. We are free to choose arbitrary values for τ_A, τ_B and ρ, which will lead to solutions for a_0 and b_0 between 0 and ρ.

This solution describes a system with spatially homogeneous densities, that are constant in time. The values of the densities a and b are given by the game theoretical fixed points. All other modes (including the polar order fields, $w = u = 0$) are zero, $\alpha_k = \beta_k = 0\,(k > 0)$, which means that the system exhibits no macroscopic order.

It is not possible to find other exact solutions for 5.3 analytically or numerically. The standard approach is instead to linearize the equations homogeneously around the solution to find out which modes will grow in time after a small perturbation. This yields for $k > 0$

$$\begin{aligned}\partial_t \delta\alpha_k &= [(\mathcal{P}_{0,k} - 1) + (\mathcal{C}_{0,k} + \mathcal{C}_{k,k})\, a_0]\, \delta\alpha_k + \mathcal{O}(\delta^2) \\ &= \lambda_k(a_0)\, \delta\alpha_k + \mathcal{O}(\delta^2)\end{aligned} \tag{5.14a}$$

$$\begin{aligned}\partial_t \delta\beta_k &= [(\mathcal{P}_{0,k} - 1) + (\mathcal{C}_{0,k} + \mathcal{C}_{k,k})\, b_0]\, \delta\beta_k + \mathcal{O}(\delta^2) \\ &= \lambda_k(b_0)\, \delta\beta_k + \mathcal{O}(\delta^2)\end{aligned} \tag{5.14b}$$

where $\mathcal{O}(\delta^2)$ stands representative for all terms that are at least quadratic in the perturbation. We defined $\lambda_k(x) := (\mathcal{P}_{0,k} - 1) + (\mathcal{C}_{0,k} + \mathcal{C}_{k,k})\, x$, which is a linear function

of $x \in \{a_0, b_0\}$ with slope $(\mathcal{C}_{0,k} + \mathcal{C}_{k,k})$ and interception point $(\mathcal{P}_{0,k} - 1)$ (note that the interception point is always negative since $\mathcal{P}_{0,k} \leq 1$). The sign of λ_k governs the linear stability of the modes α_k: If λ_k is positive, the corresponding Fourier mode grows in time and if λ_k is negative the mode decays.

The expression for λ_k shows the two main mechanisms that characterize the dynamics of the Boltzmann description of active matter: The interception point is a measure for the strength of diffusion and the slope comes from the alignment (collision) of the particles.

Calculating the slope $(\mathcal{C}_{0,k} + \mathcal{C}_{k,k})$ for different values of $k > 0$ shows that it is positive for $k = 1$ (for collision noise values $\sigma < 1$) and negative for all $k > 1$. Hence, $\lambda_1(x)$ is the only coefficient that can become positive for x high enough. All other λ_k are negative and perturbations in all modes α_k, β_k for $k > 1$ will decay. Perturbations in the polar order α_1 (β_1) grow when the order parameters ρ, τ_A, τ_B are such that a_0 (b_0) is big enough and λ_1 becomes positive. This result suggests that polar order can emerge in the dynamics of species A and B in a certain parameter regime.

5.4 Scaling ansatz

In the last section we learned that the polar order fields $\alpha_1 = w, \beta_1 = u$ are the only modes that can become unstable in a certain parameter regime. We use this fact to obtain a scaling ansatz close to the instability threshold of the polar order fields. We assume that close to this threshold, the polar order fields and the deviation from the density fixed points are of the order of a small parameter ϵ, while all higher modes are of higher orders in ϵ:

$$\begin{aligned} &a(\mathbf{r}, t) - a_0 \sim \epsilon, \\ &w(\mathbf{r}, t) \sim \epsilon, \\ &\alpha_k(\mathbf{r}, t) \sim \epsilon^{|k|}, \quad k > 0 \end{aligned} \tag{5.15}$$

and the corresponding relations for species B. Note that this scaling ansatz is consistent with the relation $\alpha_{-k} = \alpha_k^*$. Since we are interested in the long-wavelength and long-timescale dynamics, space and time derivatives are small as well

$$\nabla \sim \partial_t \sim \epsilon. \tag{5.16}$$

For further justification of this scaling ansatz we refer to the work of Bertin et al. [7]. We will use this scaling assumption in the next section to get rid of terms that are of high orders in ϵ.

5.5 Truncation and closure

Now that we have established a hierarchy of modes we can truncate the equations (meaning that we only keep terms up to a certain order in ϵ). It turns out that the lowest possible order to truncate and close the equations and get non-trivial results

is ϵ^3. The Boltzmann equations up to 3rd order in ϵ are for species A

$$\partial_t a + \frac{1}{2}\left(\nabla w^* + \nabla^* w\right) = \left(\tau_A b - \tau_B a\right)\, b\, a \tag{5.17a}$$

$$\begin{aligned}\partial_t w + \frac{1}{2}\left(\nabla a + \nabla^* \alpha_2\right) = &\left(\hat{P}_{0,1} - 1\right) w + \mathcal{C}_{-1,1} w^* \alpha_2 + \mathcal{C}_{0,1} a\, w \\ &+ \mathcal{C}_{1,1} w\, a + \mathcal{C}_{2,1} \alpha_2 w^* + \left(\tau_A b - \tau_B a\right)\, b\, w\end{aligned} \tag{5.17b}$$

$$\partial_t \alpha_2 + \frac{1}{2}\nabla w = \left(\hat{P}_{0,2} - 1\right) \alpha_2 + \mathcal{C}_{0,2} a\, \alpha_2 + \mathcal{C}_{1,2} w\, w + \mathcal{C}_{2,2} \alpha_2\, a \tag{5.17c}$$

where we used the relation $\alpha_{-1} = \alpha_1^* = w^*$. The only modes appearing in the equations are a, w and α_2 because all terms with modes α_k, $k > 2$, are of higher order in ϵ. Our final goal is a closed set of equations for the slow variables (densities and polar order fields).

Equation 5.17a for the density a already only contains the densities, a and b, and the polar order w. Note that it is an exact equation and does therefore not depend on the truncation scheme. The equation for the polar order w (equation 5.17b) on the other hand couples the modes a and w to the higher order mode α_2 via nonlinear coupling terms originating from the collision term of the Boltzmann equations.

We now turn our attention to equation 5.17c governing the dynamics of α_2. Rewriting the equation using the definition of $\lambda_k(x)$ from section 5.3 gives

$$\partial_t \alpha_2 + \frac{1}{2}\nabla w = \lambda_2(a)\, \alpha_2 + \mathcal{C}_{1,2} w^2.$$

The time derivative $\partial_t \alpha_2$ decays fast since $\lambda_2 < 0$ and $|\partial_t \alpha_2| \ll |\lambda_2 \alpha_2|$. Thus, the time derivative is negligible compared to the other terms and we can set $\partial_t \alpha_2 \approx 0$. Then we can solve for α_2 in equation 5.17c and get

$$\alpha_2 = \frac{\frac{1}{2}\nabla w - \mathcal{C}_{1,2} w^2}{\hat{P}_{0,2} - 1 + \left(\mathcal{C}_{2,2} + \mathcal{C}_{0,2}\right) a}. \tag{5.18}$$

We rewrite 5.17b

$$\begin{aligned}\partial_t w = &\left[\left(\hat{P}_{0,1} - 1\right) + \left(\mathcal{C}_{0,1} + \mathcal{C}_{1,1}\right) a + \left(\tau_A b - \tau_B a\right)\, b\right] w \\ &-\frac{1}{2}\nabla a + \left[-\frac{1}{2}\nabla^* + \left(\mathcal{C}_{-1,1} + \mathcal{C}_{2,1}\right) w^*\right] \alpha_2\end{aligned}$$

and plug 5.18 in the expression. Since we only keep track of terms of the order ϵ^3 terms like $w\nabla\rho$ and $\nabla w \nabla \rho$ can be neglected and we get the final hydrodynamic equations

$$\begin{aligned}\partial_t a &= -\frac{1}{2}\left(\nabla w^* + \nabla^* w\right) + \left(\tau_A b - \tau_B a\right)\, b\, a \\ \partial_t w &= \left(\mu_a - \xi \|w\|^2\right) w + \nu\, \nabla^* \nabla w - \gamma\, w \nabla^* w - \kappa\, w^* \nabla w - \frac{1}{2}\nabla a\end{aligned}$$

with the parameters

$$\begin{aligned}
\mu_a(a,b) &= (\mathcal{P}_{0,1}-1) + (\mathcal{C}_{0,1}+\mathcal{C}_{1,1})\,a + (\tau_A b - \tau_B a)\;b \\
&=: -\mu_0 + \mu_1 a + (\tau_A b - \tau_B a)\;b \\
\nu(a) &= -\frac{1}{4}\left[(\mathcal{P}_{0,2}-1) + (\mathcal{C}_{0,2}+\mathcal{C}_{2,2})\,a\right]^{-1} \\
\gamma(a) &= 4\,\nu(a)\,\mathcal{C}_{1,2} \\
\xi(a) &= -4\,\nu(a)\,(\mathcal{C}_{2,1}+\mathcal{C}_{-1,1})\,\mathcal{C}_{1,2} \\
\kappa(a) &= 2\,\nu(a)\,(\mathcal{C}_{2,1}+\mathcal{C}_{-1,1})\,.
\end{aligned} \tag{5.20}$$

Following the same steps for the equations for β_k (recall that $\beta_0 = b, \beta_1 = u$) we get the final set of hydrodynamic equations

$$\partial_t a = -\frac{1}{2}\left(\nabla w^* + \nabla^* w\right) + (\tau_A b - \tau_B a)\;b\,a \tag{5.21a}$$

$$\partial_t b = -\frac{1}{2}\left(\nabla u^* + \nabla^* u\right) + (\tau_B a - \tau_A b)\;a\,b \tag{5.21b}$$

$$\begin{aligned}
\partial_t w = &\left(\mu_a(a,b) - \xi(a)\|w\|^2\right) w \\
&+ \nu(a)\,\nabla^*\nabla w - \gamma(a)\,w\nabla^* w - \kappa(a)\,w^*\nabla w - \frac{1}{2}\nabla a
\end{aligned} \tag{5.21c}$$

$$\begin{aligned}
\partial_t u = &\left(\mu_b(a,b) - \xi(b)\|u\|^2\right) u \\
&+ \nu(b)\,\nabla^*\nabla u - \gamma(b)\,u\nabla^* u - \kappa(b)\,u^*\nabla u - \frac{1}{2}\nabla b.
\end{aligned} \tag{5.21d}$$

The new parameter $\mu_b(a,b)$ is - equivalent to $\mu_a(a,b)$ - defined as

$$\begin{aligned}
\mu_b(a,b) &= (\mathcal{P}_{0,1}-1) + (\mathcal{C}_{0,1}+\mathcal{C}_{1,1})\,b + (\tau_B a - \tau_A b)\;a \\
&=: -\mu_0 + \mu_1 b - (\tau_A b - \tau_B a)\;a.
\end{aligned}$$

The set of coupled partial differential equations 5.21 describes the evolution of the two densities and the corresponding polar order fields. If we set the game parameters $\tau_A = \tau_B = 0$, we recover (for each species) the well-known hydrodynamic equations for active matter [8].

A non-zero game interaction couples the densities of both species and exerts a "force" towards the game theoretical fixed point that acts on a and b. The polar order fields are coupled to the density of the respective other species through the parameters μ_a, μ_b. Note that if species A and B are precisely at the stable game fixed point ($a = a_0 = g_a\rho, b = b_0 = g_b\rho$), this coupling vanishes since then $(\tau_A b_0 - \tau_B a_0) = 0$.

5.6 Hydrodynamic equations in real space

In this section we will rewrite the complex hydrodynamic equations in real space to get more intuitive insights about the meaning and role of different terms in the equation. We will showcase the calculation only for species A, since species B is completely analogous.

Defining $w =: w_x + iw_y$ with $w_x = \mathrm{Re}(w)$ and $w_y = \mathrm{Im}(w)$, we can rewrite the equations in real space using the correspondence

$$w = w_x + iw_y \cong \begin{pmatrix} w_x \\ w_y \end{pmatrix} =: \mathbf{w}$$
$$\nabla := \partial_x + i\partial_y \cong \begin{pmatrix} \partial_x \\ \partial_y \end{pmatrix} =: \nabla.$$

With this mapping between complex numbers and vectors it is easy to rewrite the terms

$$\begin{aligned} \frac{1}{2}\left(\nabla w * + \nabla^* w\right) &\cong \nabla \cdot \mathbf{w} \\ \left(\mu_a - \xi\|w\|^2\right) w &\cong \left(\mu_a - \xi\|\mathbf{w}\|^2\right) \mathbf{w} \\ \nu\, \nabla^* \nabla w &\cong \nu\, \Delta \mathbf{w}. \end{aligned}$$

The γ and κ terms are a little bit more work. Since they have a similar structure it is convenient to examine the combination of both terms

$$\begin{aligned} &-\gamma\, w\nabla^* w - \kappa\, w^* \nabla w \\ &\quad = -\gamma\left[(w_x\partial_x + w_y\partial_y) + i(-w_x\partial_y + w_y\partial_x)\right] w \\ &\qquad\quad - \kappa\left[(w_x\partial_x + w_y\partial_y) + i(w_x\partial_y - w_y\partial_x)\right] w \\ &\quad = -(\gamma+\kappa)\,(w_x\partial_x + w_y\partial_y)w - i(\gamma-\kappa)\,(-w_x\partial_y + w_y\partial_x)w \\ &\quad \cong -(\gamma+\kappa)\,(w_x\partial_x + w_y\partial_y)\begin{pmatrix} w_x \\ w_y \end{pmatrix} + (\gamma-\kappa)\,(-w_x\partial_y + w_y\partial_x)\begin{pmatrix} w_y \\ -w_x \end{pmatrix} \\ &\quad = -(\gamma+\kappa)(\mathbf{w}\cdot\nabla)\mathbf{w} - (\gamma-\kappa)\begin{pmatrix} w_x\partial_y w_y - w_y\partial_x w_y \\ -w_x\partial_y w_x + w_y\partial_x w_x \end{pmatrix}. \end{aligned}$$

We add a zero vector $\vec{0} = \begin{pmatrix} w_x\partial_x w_x - w_x\partial_x w_x \\ w_y\partial_y w_y + w_y\partial_y w_y \end{pmatrix}$ to the second term and rearrange to get

$$\begin{aligned} &-\gamma\, w\nabla^* w - \kappa\, w^* \nabla w \\ &\quad = -(\gamma+\kappa)(\mathbf{w}\cdot\nabla)\mathbf{w} - (\gamma-\kappa)\begin{pmatrix} w_x\partial_y w_y + w_x\partial_x w_x \\ w_y\partial_x w_x + w_y\partial_y w_y \end{pmatrix} \\ &\qquad + (\gamma-\kappa)\begin{pmatrix} w_x\partial_x w_x + w_y\partial_x w_y \\ w_x\partial_y w_x + w_y\partial_y w_y \end{pmatrix} \\ &\quad = -(\gamma+\kappa)(\mathbf{w}\cdot\nabla)\mathbf{w} - (\gamma-\kappa)\mathbf{w}\,(\nabla\cdot\mathbf{w}) + (\gamma-\kappa)\frac{1}{2}\nabla\|\mathbf{w}\|^2. \end{aligned}$$

We can follow the same steps to rewrite the equations for b and u in real space. Taking everything together and defining the new parameters $\tilde{\gamma} := \gamma + \kappa$ and $\tilde{\kappa} :=$

$\gamma - \kappa$ we get the hydrodynamic equations for species A in real space

$$\partial_t a = -\nabla \cdot \mathbf{w} + (\tau_A b - \tau_B a)\, b\, a \tag{5.22a}$$

$$\partial_t b = -\nabla \cdot \mathbf{u} - (\tau_A b - \tau_B a)\, b\, a \tag{5.22b}$$

$$\begin{aligned} \partial_t \mathbf{w} + \tilde{\gamma}\,(\mathbf{w}\cdot\nabla)\,\mathbf{w} = {} & \left(\mu_a - \xi\|\mathbf{w}\|^2\right)\mathbf{w} + \nu\,\Delta\mathbf{w} \\ & - \tilde{\kappa}\,\mathbf{w}\,(\nabla\cdot\mathbf{w}) + \frac{\tilde{\kappa}}{2}\nabla\|\mathbf{w}\|^2 - \frac{1}{2}\nabla a \end{aligned} \tag{5.22c}$$

$$\begin{aligned} \partial_t \mathbf{u} + \tilde{\gamma}\,(\mathbf{u}\cdot\nabla)\,\mathbf{u} = {} & \left(\mu_b - \xi\|\mathbf{u}\|^2\right)\mathbf{u} + \nu\,\Delta\mathbf{u} \\ & - \tilde{\kappa}\,\mathbf{u}\,(\nabla\cdot\mathbf{u}) + \frac{\tilde{\kappa}}{2}\nabla\|\mathbf{u}\|^2 - \frac{1}{2}\nabla b. \end{aligned} \tag{5.22d}$$

The continuous rotational symmetry of the system can be seen explicitly in the hydrodynamic equations in real space: All terms in the polar order equations transform like vectors and the equations are therefore invariant under rotations.

There are two main differences of equations 5.22 compared to the hydrodynamic equations for one-species active matter derived by Bertin et al [8]. One new feature is that the individual densities are not conserved. Equations 5.22a and 5.22b for the dynamics of densities a and b are continuity equations with source or sink terms, depending on the local values of a and b. The conserved quantity of the system is the average of the overall density $\rho = a + b$. The second new property is that the momentum fields are not only coupled to their corresponding density fields but to the densities of both species. Fluctuations in one of the densities can therefore lead to an instability in the momentum fields of both species as we will see in the next chapter.

It is instructive to compare equations 5.22c and 5.22d with the Navier-Stokes equation for a simple fluid. The $\tilde{\gamma}$-term on the left hand side is an advection term. There is a similar term in the Navier-Stokes equation called the material derivative. The difference is that for a fluid, the coefficient is equal to one, $\tilde{\gamma} = 1$. If this is the case, the left hand side is invariant under Galileo transformations. The fact that $\tilde{\gamma} \neq 1$ for active matter reflects that particles are moving relative to a substrate and do therefore not posses Galilean invariance [32].

The second term on the right hand side is a diffusive viscosity that smoothens out distortions [43]. We can interpret the third term on the right as a sort of "crunch-anxiety": Since $\tilde{\kappa}$ is positive it leads particles to speed up (or rather to increase their order) if neighbours in front are crunched together. The fourth and fifth terms can be rewritten as the gradient of a "pressure" term $-\nabla P$, with the pressure $P(a, \|\mathbf{w}\|) = \frac{1}{2}a - \frac{\tilde{\kappa}}{2}\|\mathbf{w}\|$ in equation 5.22c and a corresponding term for equation 5.22d. This highlights the parallels and the contrast with the Navier-Stokes equation: In the latter, the pressure is determined by an equation of state in terms of the density and temperature and not the velocity (or order) field [32].

There is no analogue in the Navier-Stokes equation for the first term on the right hand side. It is responsible for the spontaneous breaking of rotational symmetry as $\mu_{a/b}$ becomes positive and determines a preferred magnitude of average velocity of the flock. When $\mathbf{w}$ and $\mathbf{u}$ are regarded as orientations rather than velocities, we can see similarities to the XY-model of spin configurations: The first term on the right could be interpreted as the derivative of a free-energy functional with a minimum

at 0 or $\sqrt{\frac{\mu_{a/b}}{\xi}}$ (depending on the sign of $\mu_{a/b}$), that tries to orient spins in the same direction.

Chapter 6

Homogeneous Solution and Stability Analysis

In this chapter we will analyze the hydrodynamic equations derived in the last chapter. The hydrodynamic equations are easier to handle than the full Boltzmann equations, but it is still a difficult task to find solutions for the full set of equations. Instead, we will start by solving the equations for a homogeneous case. Afterwards we will perturb this solution with spatially inhomogeneous perturbations in order to find the perturbations that grow in time and indicate spatial pattern formation.

6.1 Homogeneous solution

When we consider a spatially homogeneous system, all spatial derivatives are equal to zero and the density equations 5.21a and 5.21b become

$$\begin{aligned}\partial_t a &= (\tau_A b - \tau_B a)\; a\, b \\ \partial_t b &= (\tau_B a - \tau_A b)\; b\, a.\end{aligned}$$

We will assume in the following sections that $\tau_A \geqslant \tau_B$, which we can do without loss of generality, since the equations are completely symmetric with regard to interchanging A and B. It is also convenient to perform a change of variables

$$\begin{aligned}\tau_A &= \tau \\ \tau_B &= \tau * \lambda.\end{aligned} \tag{6.2}$$

In the Snowdrift game the domain of the game parameters is $\tau_A \geq 0$ and $\tau_B \geq 0$. Hence, τ and λ have a parameter range of $\tau \geq 0$ and $0 \leq \lambda \leq 1$ (since $\lambda = \frac{\tau_B}{\tau_A}$ which is smaller than one by assumption). In terms of the new variables the homogeneous density equations are

$$\partial_t a = \tau(b - \lambda a) a\, b \tag{6.3a}$$

$$\partial_t b = \tau(\lambda a - b) a\, b. \tag{6.3b}$$

Thus we can interpret τ as the strength of the game interaction (or in other words the probability that two particles will 'play' when they meet) and λ as the relative strength of B compared to A. Equations 6.3 are independent of the polar order fields

and can thus be solved separately. Adding the two equations gives

$$\partial_t a + \partial_t b = \partial_t \rho = 0 \tag{6.4}$$

indicating that ρ is constant in space and time. We can thus choose an arbitrary constant $\rho = \rho_0$ that plays the role of a control parameter for the system. Plugging in $b = \rho_0 - a$ we get

$$\partial_t a = \tau \left(\rho_0 - (1+\lambda)a\right) \left(\rho_0 - a\right) a \tag{6.5}$$

with three stationary solutions already familiar from chapter 3

$$a_0 = g_a \rho_0, \qquad g_a \in \{1, 0, \frac{1}{1+\lambda}\}. \tag{6.6}$$

We can plug the solutions in $b = \rho_0 - a$ and get the corresponding solutions for b

$$b_0 = g_b \rho_0, \qquad g_b \in \{0, 1, \frac{\lambda}{1+\lambda}\}. \tag{6.7}$$

Recall from chapter 3 that - for the Snowdrift game - only the third solution $a_0 = g_a\rho_0 = \frac{1}{1+\lambda}\rho_0$ and $b_0 = g_b\rho_0 = \frac{\lambda}{1+\lambda}\rho_0$ is stable. Note that the homogeneous solutions do not depend on the overall game interaction strength τ but only on the relative strength λ.

For a homogeneous system the hydrodynamic equations of the polar order fields, 5.21c and 5.21d, are given by

$$\partial_t w = \left(\mu_a - \xi \|w\|^2\right) w \tag{6.8a}$$

$$\partial_t u = \left(\mu_b - \xi \|u\|^2\right) u. \tag{6.8b}$$

Hence, $w = 0, u = 0$ is always a trivial solution. When we plug the homogeneous solutions for the densities in 6.8 the parameters μ_a, μ_b are given by

$$\begin{aligned}\mu_a\left(a_0, b_0\right) &= -\left(1 - \mathcal{P}_{0,1}\right) + \left(\mathcal{C}_{0,1} + \mathcal{C}_{1,1}\right) g_a \rho_0 = -\mu_0 + \mu_1 g_a \rho_0 \\ \mu_b\left(a_0, b_0\right) &= -\left(1 - \mathcal{P}_{0,1}\right) + \left(\mathcal{C}_{0,1} + \mathcal{C}_{1,1}\right) g_b \rho_0 = -\mu_0 + \mu_1 g_b \rho_0.\end{aligned}$$

Since $\mu_0, \mu_1, g_{a/b} > 0$ (see section 5.3), we know that μ_a and μ_b are negative for small ρ_0, and change sign at transition densities $\rho_{t,a}$ and $\rho_{t,b}$ defined as

$$\rho_{t,a} = \frac{1 - \mathcal{P}_{0,1}}{(\mathcal{C}_{0,1} + \mathcal{C}_{1,1}) g_a} = \frac{\mu_0}{\mu_1 g_a} \tag{6.9a}$$

$$\rho_{t,b} = \frac{1 - \mathcal{P}_{0,1}}{(\mathcal{C}_{0,1} + \mathcal{C}_{1,1}) g_b} = \frac{\mu_0}{\mu_1 g_b}. \tag{6.9b}$$

For overall densities smaller than the transition densities, $w = u = 0$ is the only stationary solution. It is stable against linear homogeneous perturbations (see figure 6.1(a)).

One can check that parameter ξ in equations 6.8 is positive for the parameter regimes that concern us. Note that $\xi > 0$ has to be the case if we want the system to be well-behaved.

When we increase the densities such that e.g. $\rho_0 \geq \rho_{t,a}$, μ_a becomes positive and $w = 0$ becomes unstable. Instead, a new homogeneously stable solution emerges with $\|w\| > 0$ (see figure 6.1(b)). The equivalent happens in the polar order field u if

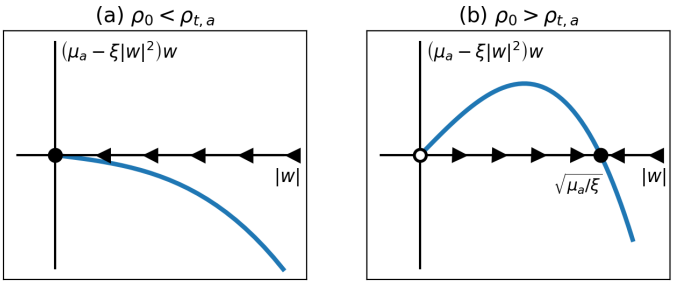

FIGURE 6.1: Flow diagrams for the homogeneous equations of the polar order field w. (a) for $\rho_0 < \rho_{t,a}$ the isotropic state ($\|w\| = 0$) is stable. (b) for $\rho_0 > \rho_{t,a}$ the isotropic solution becomes unstable and a new stable, stationary solution with $\|w\| = \sqrt{\mu_a/\xi}$ emerges. This bifurcation structure describes the spontaneous breaking of the rotational symmetry of the system.

the density reaches the transition density of species B. The new stable solutions for w and u are

$$w = \sqrt{\frac{\mu_a}{\xi}}\, e_w \qquad \text{for } \rho_0 > \rho_{t,a} \tag{6.10a}$$

$$u = \sqrt{\frac{\mu_b}{\xi}}\, e_u \qquad \text{for } \rho_0 > \rho_{t,b}. \tag{6.10b}$$

with e_w and e_u complex numbers of unit length, pointing in arbitrary directions in complex space. This result suggests, that the system is in an isotropic state ($\|w\| = 0$) for low overall densities and that order can emerge spontaneously ($\|w\| > 0$) in an arbitrary direction as soon as $\rho_0 > \rho_{t,a}$. The equivalent happens for species B as $\rho_0 > \rho_{t,b}$. From the assumption that $\lambda \leq 1$ ($\tau_B \leq \tau_A$) follows that $\rho_{t,a} \leq \rho_{t,b}$. This process describes the spontaneous breaking of the continuous rotational symmetry of the system in the polar order field of species A.

We can conclude that for a homogeneous system there are in general three distinct states, marking different regions in parameter space:

1. both species have no polar order (for $\rho_0 < \rho_{t,a}, \rho_0 < \rho_{t,b}$)
2. species A is ordered, species B has no order (for $\rho_0 \geq \rho_{t,a}, \rho_0 < \rho_{t,b}$)
3. both species show polar order (for $\rho_0 \geq \rho_{t,a}, \rho_0 \geq \rho_{t,b}$)

We will now analyze these different states and their respective regions in parameter space for the different homogeneous solutions of the densities given by 6.6 and 6.7. The first two solutions are symmetric in a and b, which means, it is sufficient to analyze one of them and transfer the results to the second one by interchanging a and b as well as w and u everywhere. Let us take $(a_0, b_0) = (\rho_0, 0)$. Since b_0 is zero at all times, there are only two distinct states: Species A is either in an isotropic, disordered state or in a homogeneously ordered state. The transition is governed by the control parameter $\rho_0 = a_0$.

However, we know that for the Snowdrift game the solution for $(a_0, b_0) = (\rho_0, 0)$ is not stable and the system will therefore not stay in this state. Instead, the densities will shift towards the stable solution $(a_0, b_0) = (\frac{1}{1+\lambda}\rho_0, \frac{\lambda}{1+\lambda}\rho_0)$. Now the transition

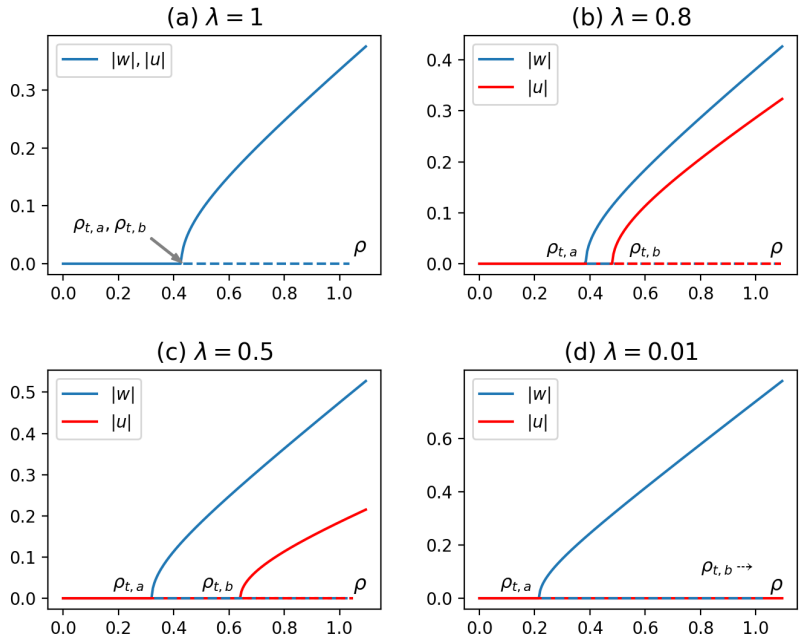

FIGURE 6.2: Bifurcation for the homogeneous equations. If $\rho_0 \geq \rho_{t,a}$ ($\rho_0 \geq \rho_{t,b}$) the isotropic solution $w = 0$ ($u = 0$) becomes unstable and a new stable solution with $\|w\| = \sqrt{\mu_a/\xi}$ ($\|u\| = \sqrt{\mu_b/\xi}$) exists and breaks the rotational symmetry of the system. The control parameter λ determines the overall density ρ_0 at which this transition takes place. The figures show the bifurcation of the polar order fields of the homogeneous system for (a) $\lambda = 1$, (b) $\lambda = 0.8$, (c) $\lambda = 0.5$, (d) $\lambda = 0.01$. Noise parameters are set to $\sigma = \sigma_0 = 1/2$.

between isotropic and ordered states for both species depends on the two control parameters ρ_0 and λ.

Let us fix the game parameter λ and see what happens for different values of ρ_0 (see figure 6.2). If both species are equally strong ($\lambda = 1$) then $\rho_{t,a} = \rho_{t,b} = \frac{2\mu_0}{\mu_1}$. and order emerges simultaneously in both species. If species A is stronger than species B ($\lambda < 1$), the density threshold for order in A, $\rho_{t,a} = \frac{\mu_0(1+\lambda)}{\mu_1}$, is smaller than the transition density for B $\rho_{t,a} = \frac{\mu_0(1+\lambda)}{\mu_1\lambda}$. Hence, order emerges in species A for smaller overall densities than for species B. For the limit of $\lambda \to 0$, $g_a = \frac{1}{1+\lambda} \to 1$ and $g_b = \frac{\lambda}{1+\lambda} \to 0$ and the onset of order for species A goes to $\rho_{t,a} \to \frac{\mu_0}{\mu_1}$ (which is the transition density for a one-species system) while order will never occur in B.

6.2 Interlude: Role of the noise

An aspect we have not considered so far is that the system depends not only on three but on five free parameters: Besides the two game parameters and the density, the two noise parameters σ and σ_0 also play the role of control parameters. Plugging the expressions for $\mathcal{P}_{0,1}, \mathcal{C}_{0,1}$ and $\mathcal{C}_{1,1}$ in 6.9a, we can find an expression for the transition

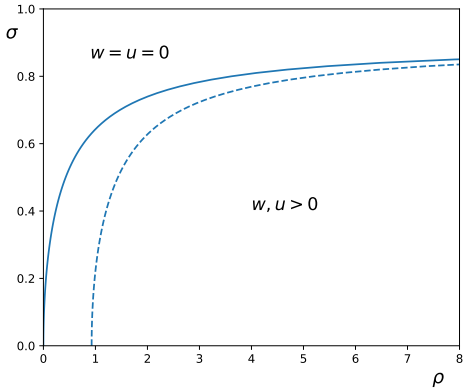

FIGURE 6.3: Phase diagram of the model in the (ρ, σ)-plane for $\lambda = 1$. In this case $\rho_{t,a} = \rho_{t,b}$. For high noise σ or low density ρ, the homogeneous system is in an isotropic state with no order ($w = u = 0$). When the noise is turned down or the density is turned up, the isotropic state becomes unstable, indicated by the transition lines in the graph (full line: $\sigma_0 = \sigma$; dashed line: $\sigma_0 = 1$).

density $\rho_{t,j}$, where $j \in \{a, b\}$, as a function of the noise σ_0 and σ

$$\rho_{t,j} = \frac{\pi \left(1 - e^{-\sigma_0^2/2}\right)}{8 \left(e^{-\sigma^2/2} - \frac{2}{3}\right) g_j} \tag{6.11}$$

The transition density increases for increasing noise (see figure 6.3). We will always keep the diffusive noise tied to the alignment noise, $\sigma = \sigma_0$, which is the convention used by Bertin et al. [8]. For systems with $\sigma = \sigma_0 = 0$ the transition density is zero, which means that the alignment of particles will always lead to ordered motion. Changing the two noise intensities relative to each other results in a shift of the transition line. For high densities, the noise at which a transition occurs saturates to a value $\sigma = \sqrt{2 \ln \frac{3}{2}} \approx 0.9$, above which order will never occur.

The mechanism responsible for the disorder-order transition lies in the interplay between diffusion which drives the system towards isotropy and particle alignment, which promotes the formation of order. Instead of considering the transition as a function of the density, we could also look for the transition by varying the noises at given fixed densities [8]. However, in this thesis we choose to use the density as free control parameter and we will keep the noise parameters at fixed values

$$\sigma_0 = \sigma = \frac{1}{2} \tag{6.12}$$

in order not to get too many free parameters. Choosing other values for the noise would change our results quantitatively but would not lead to qualitatively different results.

6.3 Stability against inhomogeneous perturbations

So far we have seen that the minimal set of hydrodynamic equations for the system 5.21 has a homogeneous solution that is stable against homogeneous perturbations.

The main feature of this solution is that it suggests a transition from an isotropic state to a broken symmetry state with macroscopic order in A (for $\lambda \leq 1$) and a second transition to a state in which both species show macroscopic order. However, so far we have only tested the solution against homogeneous perturbations (i.e. perturbations with infinite wavelength). We do not know how inhomogeneities influence the dynamics of the system. In fact, experiments of self-propelled particle systems [46, 45, 9] show that inhomogeneities become important at the transition to macroscopic order and can lead to spatial patterns.

In this section we will test the homogeneous solutions against perturbations with a finite wavelength. Similar to one-species active matter systems we will find that there are instabilities close to both transitions to macroscopic order for long wavelength perturbations.

The main difficulties in solving 5.21 are the non-linearities of the equations. We will perturb the homogeneous solutions of the equations with inhomogeneous perturbations that are small enough to neglect all terms of non-linear order in the perturbation

$$\begin{aligned} a(\mathbf{r},t) &= a_0 + \delta a(\mathbf{r},t), \quad w(\mathbf{r},t) = w_0 + \delta w(\mathbf{r},t) \\ b(\mathbf{r},t) &= b_0 + \delta b(\mathbf{r},t), \quad u(\mathbf{r},t) = u_0 + \delta u(\mathbf{r},t). \end{aligned} \tag{6.13}$$

If we plug this into the full hydrodynamic equations 5.21 and only keep terms up to linear order in the perturbation we get for the equations for a and w

$$\begin{aligned} \partial_t \delta a =& -\frac{1}{2}\left(\nabla^* \delta w + \nabla \delta w^*\right) + \tau(b_0 - 2\lambda a_0) b_0\, \delta a + \tau(2b_0 - \lambda a_0) a_0\, \delta b \\ \partial_t \delta w =& \mu_a \delta w - \xi\left(w_0^2 \delta w^* + 2\left|w_0\right|^2 \delta w\right) + \left(\frac{\partial \mu_a}{\partial a} - \frac{\partial \xi}{\partial a}\|w_0\|^2\right) w_0 \delta a \\ &+ \left(\frac{\partial \mu_a}{\partial b} - \frac{\partial \xi}{\partial b}\|w_0\|^2\right) w_0 \delta b - \kappa w_0^* \nabla \delta w - \gamma w_0 \nabla^* \delta w - \frac{1}{2}\nabla \delta a + \nu \nabla^* \nabla \delta w \end{aligned} \tag{6.14}$$

and the two corresponding equations for b and u. Note that we have to differentiate between perturbations δw and its complex conjugate δw^*. In a next step we expand the perturbations in Fourier space

$$\begin{aligned} \delta a(\mathbf{r},t) &= \frac{1}{2\pi}\int_{-\infty}^{\infty} \mathrm{d}\mathbf{q}\, \mathrm{e}^{\mathrm{i}\mathbf{q}\cdot\mathbf{r}} \delta a_{\mathbf{q}}(t) \\ \delta w(\mathbf{r},t) &= \frac{1}{2\pi}\int_{-\infty}^{\infty} \mathrm{d}\mathbf{q}\, \mathrm{e}^{\mathrm{i}\mathbf{q}\cdot\mathbf{r}} \delta w_{\mathbf{q}}(t) \\ \delta w^*(\mathbf{r},t) &= \frac{1}{2\pi}\int_{-\infty}^{\infty} \mathrm{d}\mathbf{q}\, \mathrm{e}^{-\mathrm{i}\mathbf{q}\cdot\mathbf{r}} \delta w^*_{\mathbf{q}}(t). \end{aligned} \tag{6.15}$$

and equivalently for $\delta b_{\mathbf{q}}, \delta u_{\mathbf{q}}, \delta u^*_{\mathbf{q}}$. Our task is now to find out which modes $\delta a_{\mathbf{q}}, \delta b_{\mathbf{q}}$, $\delta w_{\mathbf{q}}, \delta w^*_{\mathbf{q}}, \delta u_{\mathbf{q}}, \delta u^*_{\mathbf{q}}$ as functions of $\mathbf{q}$ grow in time. To this end we plug the Fourier expansion of the perturbations in the linearised equations 6.14. We can now perform the spatial derivatives since only the exponential depends on $\mathbf{r}$. Afterwards we multiply by $\mathrm{e}^{i\mathbf{q}'\cdot\mathbf{r}}$ and integrate over $\mathbf{r}$. Overall this results in the replacement of the derivatives by the following replacement rules

$$\begin{aligned} \nabla &= \partial_x + \mathrm{i}\partial_y \to \mathrm{i}q_x - q_y \\ \nabla^* &= \partial_x - \mathrm{i}\partial_y \to \mathrm{i}q_x + q_y. \end{aligned} \tag{6.16}$$

We plug this replacement rule in the equations and omit the subscript $\mathbf{q}$ for better legibility and get

$$
\begin{aligned}
\partial_t \delta a =& \tau(b_0 - 2\lambda a_0) b_0\, \delta a + \tau(2b_0 - \lambda a_0) a_0\, \delta b - \frac{1}{2}(\mathrm{i}q_x + q_y)\delta w - \frac{1}{2}(\mathrm{i}q_x - q_y)\delta w^* \\
\partial_t \delta b =& \tau(-b_0 + 2\lambda a_0) b_0\, \delta a + \tau(-2b_0 + \lambda a_0) a_0\, \delta b - \frac{1}{2}(\mathrm{i}q_x + q_y)\delta u - \frac{1}{2}(\mathrm{i}q_x - q_y)\delta u^* \\
\partial_t \delta w =& \left[\left(\frac{\partial \mu_a}{\partial a} - \frac{\partial \xi}{\partial a}\|w_0\|^2\right) w_0 - \frac{1}{2}(\mathrm{i}q_x - q_y)\right] \delta a + \left[\frac{\partial \mu_a}{\partial b} w_0\right] \delta b \\
&+ \left[-\xi\|w_0\|^2 - \kappa(\mathrm{i}q_x - q_y) w_0^* - \gamma(\mathrm{i}q_x + q_y) w_0 - \nu(q_x^2 + q_y^2)\right] \delta w \\
&- \xi w_0^2 \delta w^* \\
\partial_t \delta w^* =& \left[\left(\frac{\partial \mu_a}{\partial a} - \frac{\partial \xi}{\partial a}\|w_0\|^2\right) w_0^* - \frac{1}{2}(\mathrm{i}q_x + q_y)\right] \delta a + \left[\frac{\partial \mu_a}{\partial b} w_0^*\right] \delta b \\
&- \xi (w_0^*)^2 \delta w \\
&+ \left[-\xi\|w_0\|^2 - \kappa(\mathrm{i}q_x + q_y) w_0 - \gamma(\mathrm{i}q_x - q_y) w_0^* - \nu(q_x^2 + q_y^2)\right] \delta w^* \\
\partial_t \delta u =& \left[\frac{\partial \mu_b}{\partial a} u_0\right] \delta a + \left[\left(\frac{\partial \mu_b}{\partial b} - \frac{\partial \xi}{\partial b}\|u_0\|^2\right) u_0 - \frac{1}{2}(\mathrm{i}q_x - q_y)\right] \delta b \\
&+ \left[-\xi\|u_0\|^2 - \kappa(\mathrm{i}q_x - q_y) u_0^* - \gamma(\mathrm{i}q_x + q_y) u_0 - \nu(q_x^2 + q_y^2)\right] \delta u \\
&- \xi u_0^2 \delta u^* \\
\partial_t \delta u^* =& \left[\frac{\partial \mu_b}{\partial a} u_0^*\right] \delta a + \left[\left(\frac{\partial \mu_b}{\partial b} - \frac{\partial \xi}{\partial b}\|u_0\|^2\right) u_0^* - \frac{1}{2}(\mathrm{i}q_x + q_y)\right] \delta b \\
&- \xi (u_0^*)^2 \delta u \\
&+ \left[-\xi\|u_0\|^2 - \kappa(\mathrm{i}q_x + q_y) u_0 - \gamma(\mathrm{i}q_x - q_y) u_0^* - \nu(q_x^2 + q_y^2)\right] \delta u^*
\end{aligned}
\tag{6.17}
$$

Overall we get a system of six linear equations that we can summarize in the form

$$
\partial_t \begin{pmatrix} \delta a \\ \delta b \\ \delta w \\ \delta w^* \\ \delta u \\ \delta u^* \end{pmatrix} = \mathbf{J} \begin{pmatrix} \delta a \\ \delta b \\ \delta w \\ \delta w^* \\ \delta u \\ \delta u^* \end{pmatrix} \tag{6.18}
$$

where $\mathbf{J}$ is the Jacobian of the system. It is a 6×6 matrix depending on $\mathbf{q}$ and the homogeneous solution (a_0, b_0, w_0, u_0). Its components can be read off from equations 6.17. Compared to one-species active matter systems we get several new terms. The time evolution of perturbations in the densities depends not only on fluctuations of the corresponding order parameter but also on fluctuations of both densities. These terms have a smoothing effect on perturbations that deviate from the game theoretical fixed point. A second difference to one-species active matter systems is that fluctuations in the order parameter fields depend not only on their respective density fields but also on perturbations in the density of the other species. This implies that a fluctuation in density a (b) could lead to a growing instability in the polar order field u (w), even if species B (A) is in a homogeneous state.

Finding the regions of parameter space for which the modes grow in time is equivalent to finding the parameters for which there are positive eigenvalues, $s(\mathbf{q}) > 0$, of $\mathbf{J}$. The eigenvectors corresponding to positive eigenvalues point in the direction of the instability.

Before we show the results for the calculations of the eigenvalues and eigenvectors of the full Jacobian $\mathbf{J}$ we will briefly discuss what happens when we turn off the game.

6.4 Stability without game interaction

When we turn off the game by setting $\tau = 0$, we have a system of two active species that do not interact with each other. The equations for the two species are completely equivalent and the Jacobian has therefore only three degenerate eigenvalues (instead of six).

Hence, for $\tau = 0$ we recover the well-known properties of active systems described by a Boltzmann approach [7, 8]. We used this fact to check our equations and methods. Here, we briefly summarize the main results for a stability analysis of active matter without game, to have an overview of the status quo:

- Calculations of the eigenvalues show that for $\rho < \rho_t = \rho_{t,a/b}$, the system is stable against inhomogeneous perturbations.
- When ρ reaches the onset of order with the spatially homogeneous, polarized solution w_0, the system becomes unstable with respect to longitudinal perturbations. One a priori considers vectors $\mathbf{q}$ and perturbations δw_0 that point in arbitrary directions with respect to the macroscopic order w_0. However, one can show that the real part of the eigenvalues s can only be positive for perturbations with $\mathbf{q}$ pointing along the direction of w_0 [8]. The growth rate s is maximal for perturbations δw_0 pointing as well in the direction of macroscopic order.
- The longitudinal instabilities of the homogeneously ordered state are expected to give rise to a state with a stationary wave-like spatial pattern. Bertin et al. [8] showed that the Boltzmann equation supports a solitonic wave solution. Such a wave pattern is also found in agent-based simulations of microscopic models such as the Vicsek-model [11].
- For ρ big enough, the instability vanishes again and a homogeneously ordered state emerges. This result of the hydrodynamic description is also supported by agent-based simulations [11].

To illustrate these findings, we calculate all eigenvalues for $\tau = 0$ and $\lambda = 1$, such that the two species are not coupled and the density fixed points are at $a_0 = b_0 = \rho/2$. Polar order fixed points are either $w_0 = u_0 = 0$ for $\rho < \rho_t \approx 0.43$, or $w_0 = \sqrt{\mu_a/\xi}$, $u_0 = \sqrt{\mu_b/\xi}$ for $\rho \geq \rho_t$. Plugging the parameter and fixed point values in the Jacobian defined by 6.18, we can calculate the eigenvalues as functions of $\mathbf{q}$ and ρ. As mentioned above, there are three degenerate eigenvalues. We call the biggest eigenvalue as a function of the longitudinal wave vector $s(\mathbf{q}_\parallel)$. Figure 6.4a shows $s(\mathbf{q}_\parallel)$ for different values of the control parameter ρ. For small ρ (exemplary in the figure for $\rho = 0.3$), the eigenvalue is smaller or equal to zero for all values of $\mathbf{q}_\parallel$. If $\rho \geq \rho_t$, s becomes positive for a band of long-wavelength, longitudinal

perturbations $\mathbf{q}_\parallel$. In figure 6.4a this is demonstrated for the values $\rho = 0.5$ and $\rho = 0.8$. The instability vanishes again for ρ bigger than a transition density to homogeneous order, which we call $\rho_{dh} \approx 0.98$. Figure 6.4a shows this effect for $\rho = 1.0$.

We summarize the behaviour of $s(\mathbf{q}_\parallel)$ for increasing overall density ρ in figure 6.4b. It shows the maximal value of s, which we call s_{max}, as a function of ρ. A value of $s_{max} \leq 0$ means that the system is stable against inhomogeneous perturbations for the corresponding value of ρ. If $s_{max} > 0$, perturbations grow in time.

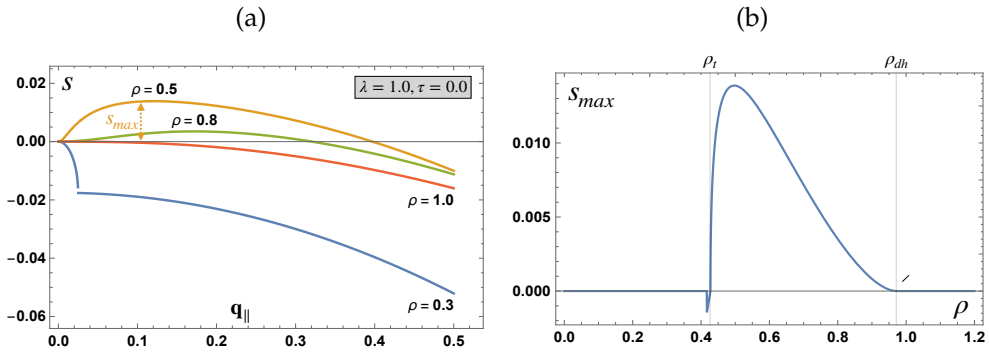

FIGURE 6.4: (a) Biggest eigenvalue s of the Jacobian as a function of the wavevector $\mathbf{q}_\parallel$ pointing in direction of macroscopic order for a system with no game interaction ($\tau = 0$). For $\rho < \rho_t \approx 0.43$ all eigenvalues are negative and the homogeneous isotropic solution is therefore stable (here, $\rho = 0.3$). As soon as the density reaches the onset of order, $\rho \geq \rho_t$, eigenvalues becomes positive, which indicates an instability of the system against inhomogeneous, longitudinal perturbations (here shown for, $\rho = 0.5, \rho = 0.8$). For high enough ρ the system stabilizes again (here shown for, $\rho = 1.0$). (b) Maximal value of s over all $\mathbf{q}_\parallel$ as a function of the overall density ρ. The system is unstable against inhomogeneous perturbations ($s_{max} > 0$) for values $\rho_t < \rho < \rho_{dh}$.

6.5 Stability with game interaction

The six eigenvalues of the Jacobian 6.18 are functions of $\mathbf{q}$ and of the control parameters (ρ, τ, λ). As fixed points for the polar order fields we set $w_0 \parallel u_0$, since we expect that the coupling of both species through inhomogeneous terms will result in the polar orders w and u always emerging in the parallel direction for sufficiently long times. This expectation will be justified through our numerical analysis of the full hydrodynamic equations and through agent-based simulations.

Similar to the case without game interaction, we find that eigenvalues are maximal for wave-like perturbations with wave vectors $\mathbf{q}_\parallel$ pointing in the direction of ordered motion w_0, u_0. Hence, as for one-species systems, instabilities are longitudinal.

Figure 6.5 shows the maximal eigenvalue s as a function of $\mathbf{q}_\parallel$ for different values of ρ, fixed $\tau = 0.5$ and $\lambda = 1$ in figure 6.5a, $\lambda = 0.5$ in figure 6.5b. For small ρ the homogeneous isotropic state of the system is stable for both values of λ. As ρ reaches the respective first transition density, $\rho_{t,a} = \rho_{t,b} \approx 0.43$ for $\lambda = 1$ and

$\rho_{t,a} \approx 0.32$ for $\lambda = 0.5$, the maximal eigenvalue s becomes positive in a range of small $\mathbf{q}_{\|}$. This indicates an instability of the system at the onset of order against long-wavelength, longitudinal perturbations. The instability persists for ρ in a parameter range that depends on λ. When ρ crosses transition values that we call $\rho_{dh,a}$ and $\rho_{dh,b}$ respectively, s becomes negative again for all $\mathbf{q}_{\|}$. This transition happens at values $\rho_{dh,a} = \rho_{dh,b} \approx 0.98$ for $\lambda = 1$ and $\rho_{dh,a} \approx 0.51$ for $\lambda = 0.5$. For $\lambda = 1$, the eigenvalues will stay negative if we further increase ρ. Note that the transition values of ρ for $\lambda = 1$ are the same as for a system without game interaction (compare the values of $\rho_{t,a/b}, \rho_{dh,a/b}$ with the ones from the last section). For $\lambda = 0.5$ on the other hand, there is a second unstable band when ρ reaches the second transition density, $\rho_{t,b} \approx 0.64$ until values of $\rho_{dh,b} \approx 1.2$ are reached.

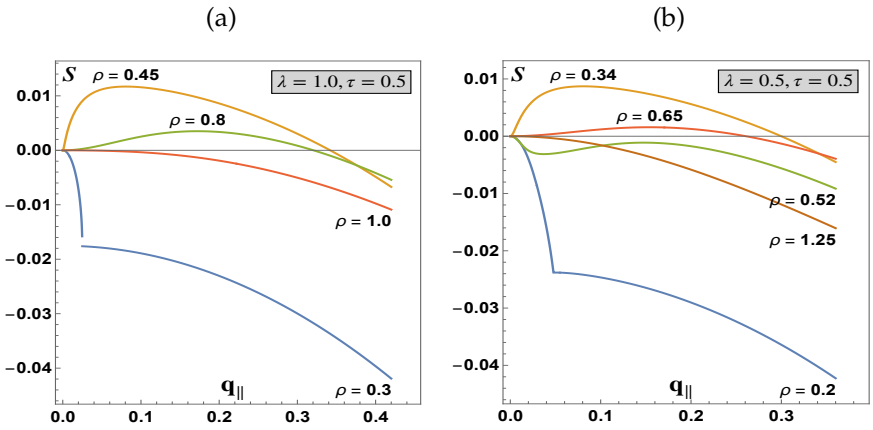

FIGURE 6.5: (a) Biggest eigenvalue s of the Jacobian as a function of the wavevector $\mathbf{q}_{\|}$ for $\tau = 0.5$ and two different values of λ. (a) $\lambda = 1$: s has a positive band for values of $\rho \in [\rho_{t,a}, \rho_{dh,a}] = [\rho_{t,b}, \rho_{dh,b}] \approx [0.43, 0.98]$ and is smaller than zero otherwise. (b) $\lambda = 0.5$: There are two unstable bands, one at each transition density: $\rho \in [\rho_{t,a}, \rho_{dh,a}] \approx [0.32, 0.51]$ and $\rho \in [\rho_{t,b}, \rho_{dh,b}] \approx [0.64, 1.2]$.

As a next step we look for the parameter regions of the unstable bands. In order to do so, we compute the real part of the maximal value of $s(\mathbf{q})$ over all $\mathbf{q}$, called s_{max}. If s_{max} is smaller or equal to zero for certain parameter values (ρ, τ, λ), perturbations will decay and the homogeneous solution is stable. If $s_{max} > 0$, perturbations grow in time and the system is unstable.

Figures 6.6 illustrate the results for the calculations of s_{max} done with Mathematica. They show the values of s_{max} in the (τ, ρ) plane for different fixed $\lambda \in \{1.0, 0.8, 0.6, 0.5, 0.4, 0.2\}$. Coloured regions indicate values in parameter space (τ, ρ) for which $s_{max} > 0$, white regions mean that $s_{max} \leq 0$.

The main results of the linear stability analysis are:

- There are no instabilities for the homogeneous isotropic state ($\rho < \rho_{t,a}, \rho < \rho_{t,b}$).
- At the onset of order for A ($\rho \geq \rho_{t,a}$) the system becomes unstable. This instability vanishes again when ρ is sufficiently larger than $\rho_{t,a}$.
- A second instability occurs at the onset of order for B ($\rho_0 \geq \rho_{t,b}$), which also stabilizes again for ρ sufficiently larger than $\rho_{t,b}$.

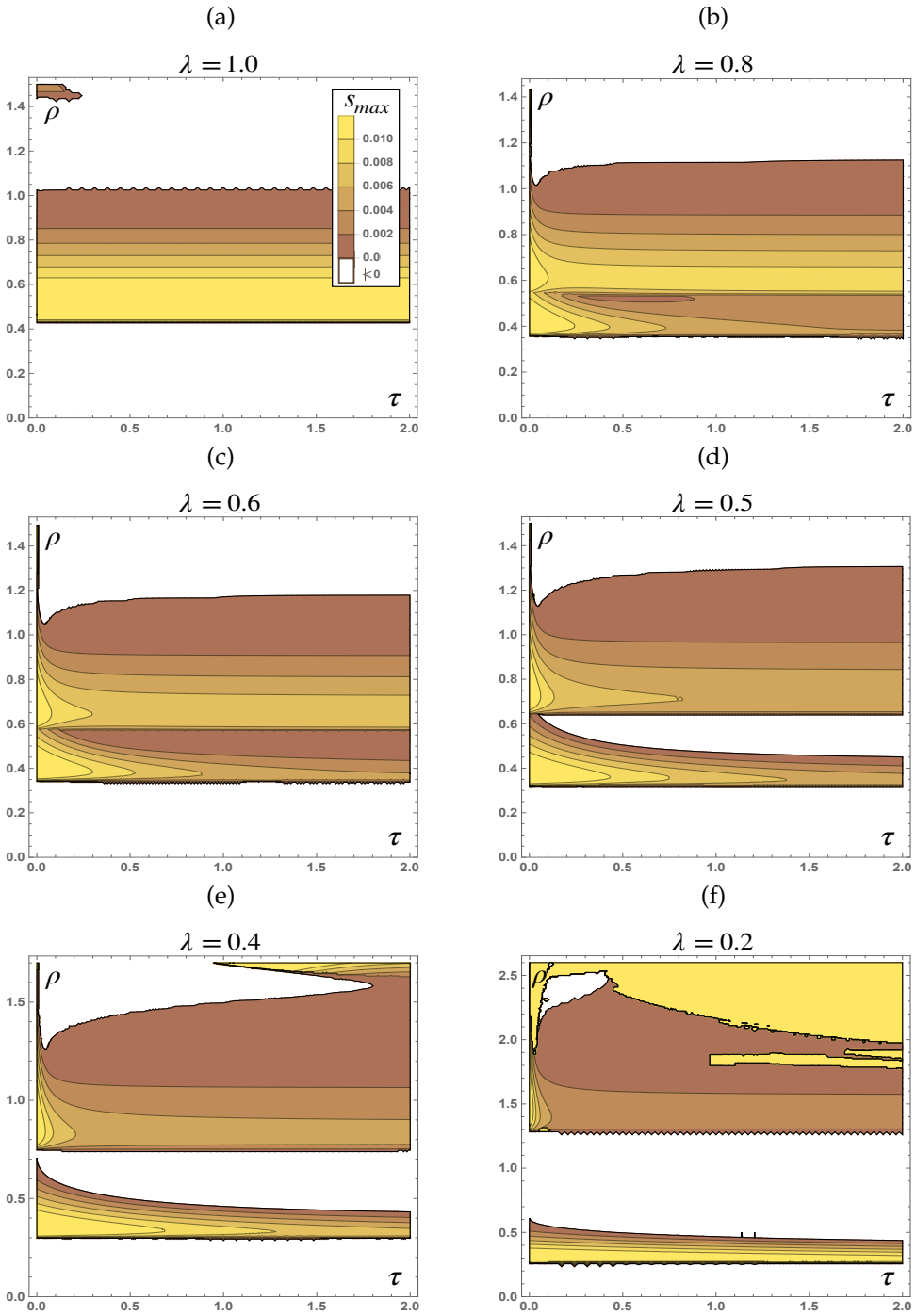

FIGURE 6.6: Contour plots of the maximum value of all eigenvalues of the Jacobian, s_{max}, in the (τ, ρ) plane for different λ. Coloured regions indicate values in parameter space (τ, ρ) for which $s_{max} > 0$. The legend in (a) is valid for all plots. (a) For $\lambda = 1$ there is a band, that is unstable against long-wavelength, longitudinal perturbations, at the onset of order, $\rho_{t,a} = \rho_{t,b} \approx 0.43$, which is independent of the game strength τ. (b)-(f) For $\lambda < 1$ we can distinguish between two different unstable bands, that emerge when ρ crosses the transition densities $\rho_{t,a}(\lambda)$ and $\rho_{t,b}(\lambda)$ respectively. The transition densities (and therefore the unstable bands) move away from each other for decreasing λ. The system stabilizes again for ρ far enough from the respective onsets of order.

The unstable bands depend on the control parameters. We summarize our findings in the following statements:

- for $\lambda = 1$ (both species are equally strong) and therefore $\rho_{t,a} = \rho_{t,b}$, there is only one parameter region in which the system is unstable. It is the same regime of ρ as the unstable band of a system with no game interaction (compare the values of the transitions for ρ with the ones from the previous section with no game). The value of the game interaction strength τ does not play a role.
- for decreasing λ (for A getting stronger than B) the transition densities differ ($\rho_{t,a} < \rho_{t,b}$) and there are two distinct parameter regions of instability. For λ close enough to 1, the regions of instability overlap (see figure 6.6b and 6.6c ($\lambda = 0.8$ and $\lambda = 0.6$)). When λ is small enough there are separate regions (see figure 6.6d,6.6e,6.6f ($\lambda = \{0.5, 0.4, 0.2\}$)).
- for $\tau \to 0$ we recover the well-known results for active matter. One can check for $\tau \to 0$, that the parameter ranges of ρ of the unstable bands correspond to the unstable regime of a system without game interaction. When the game is turned on ($\tau > 0$), the results show that the parameter region of linear instability is more narrow, hence the game has a (linearly) stabilizing effect.
- We can distinguish between not only three as in the case without game interaction [8], but up to five different regions in parameter space that suggest different phases of the system. The five different regions have the following properties:
  1. Isotropic, stable state (for $\rho < \rho_{t,a}, \rho < \rho_{t,b}$)
  2. The homogeneous solution with polar order fields $w_0 > 0, u_0 = 0$ is unstable, which indicates pattern formation (for $\rho \geq \rho_{t,a}, \rho < \rho_{t,b}$)
  3. The system stabilizes again. Homogeneous order in A ($w_0 > 0$), no order in B ($u_0 = 0$) (for ρ well above $\rho_{t,a}, \rho < \rho_{t,b}$)
  4. The homogeneous solution with polar order fields $w_0 > 0, u_0 > 0$ is unstable and indicates pattern formation (for $\rho \geq \rho_{t,a}, \rho \geq \rho_{t,b}$)
  5. The system is stable with homogeneous solution $w_0 > 0, u_0 > 0$.

In the next two sections we will take a look at the transition from an isotropic system to a system with macroscopic order and analyze the eigenvectors in the regions of instability.

6.6 Transition to order

We start in the region of parameter space with $\rho < \rho_{t,a}, \rho < \rho_{t,b}$. The system is in an isotropic, homogeneous state with the fixed point $(a_0, b_0, w_0, u_0) = (\frac{1}{1+\lambda}\rho, \frac{\lambda}{1+\lambda}\rho, 0, 0)$.

As mentioned before, the calculations show that all eigenvalues are smaller than zero for all values of $\mathbf{q}$ in this region. Thus the isotropic homogeneous state is stable against inhomogeneous perturbations.

An interesting question we can ask is, how the transition at $\rho = \rho_{t,a}$ from the isotropic state to a state with macroscopic order, $w > 0$, happens. We want to know which modes become unstable when the system crosses the border to the parameter regime

of order formation. These will be the modes that start growing and push the system out of its homogeneous, isotropic state.

We start with a homogeneous system $(a_0, b_0, w_0, u_0) = (\frac{1}{1+\lambda}\rho, \frac{\lambda}{1+\lambda}\rho, 0, 0)$ with $\rho < \rho_{t,a}$ and calculate the maximal eigenvalue s of the Jacobian at this fixed point as functions of ρ for fixed $\lambda = 0.5, \tau = 0.5$. We then turn up the density such that it becomes slightly bigger than the transition density, $\rho \gtrapprox \rho_{t,a}$.

We find that s becomes positive for a range of $\mathbf{q}$-values as expected. Since (so far) the symmetry of the system is not broken, q_x and q_y are symmetric in the equations of s and the eigenvalue is positive for an arbitrary direction of $\mathbf{q}\cdot$ The eigenvector corresponding to the instability points always in the w-direction in space that is transverse to $\mathbf{q}$, which means that the instability amplifies the polar order field perpendicular to $\mathbf{q}$.

6.7 Eigenvectors

The two unstable bands have different homogeneous fixed points. For the following discussion we choose coordinates s.t. the x-axis points in the direction of macroscopic order. For the first parameter region of instability the fixed point is then

$$\begin{aligned} a_0 &= \frac{1}{1+\lambda}\rho > \rho_{t,a}, \qquad & w_0 &= w_x + 0 \cdot i = \sqrt{\frac{\mu_a}{\xi}}, \\ b_0 &= \frac{\lambda}{1+\lambda}\rho < \rho_{t,b}, \qquad & u_0 &= 0 \end{aligned} \tag{6.19}$$

and for the second region of instability

$$\begin{aligned} a_0 &= \frac{1}{1+\lambda}\rho > \rho_{t,a}, \qquad & w_0 &= w_x + 0 \cdot i = \sqrt{\frac{\mu_a}{\xi}}, \\ b_0 &= \frac{\lambda}{1+\lambda}\rho > \rho_{t,b}, \qquad & u_0 &= u_x + 0 \cdot i = \sqrt{\frac{\mu_b}{\xi}}. \end{aligned} \tag{6.20}$$

We find that the eigenvector corresponding to both instabilities has the general form

$$\mathbf{v} = \begin{pmatrix} v_a \\ v_b \\ v_w \\ v_w \\ v_u \\ v_u \end{pmatrix}. \tag{6.21}$$

Note that the components of the vector corresponding to growth rates in δw and δw^* are equal, which means that the eigenvector has a non-zero component in x-direction, δw_x, whereas it does not point in y-direction, δw_y. The equivalent statement is true for , δu_x and δu_y. Hence, the general form of the eigenvector shows that modes $\delta a, \delta b, \delta w_x$ and δu_x are unstable (the instability points in δa- , δb-, δw_x and δu_x -direction). The instability in the polar order fields is in the direction of macroscopic order.

The values of $v_j, j \in a, b, w, u$, vary strongly with the values of the control parameters. However, components in a- and w_x-direction are always of comparable size, just as components in b- and u_x-direction.

If $\lambda = 1$ there is only one unstable region. All non-zero components of the eigenvector have values of the same order of magnitude. This means that all of the four modes $\delta a, \delta b, \delta w_x$ and δu_x will grow at a comparable speed and lead to inhomogeneities of similar sizes in the four fields.

If $\lambda < 1$ we can distinguish between the two emerging unstable regions. Let us start with the first region, $\rho \geq \rho_{t,a}, \rho < \rho_{t,b}$. The smaller the values of λ, the smaller are the components of the eigenvector pointing in b- and u_x-direction compared to the components in a- and w_x-direction ($v_a, v_w \gg v_b, v_u$ for λ well below 1). Hence, the eigenvector points mainly in δa- and δw_x-direction and perturbations in δa and δw_x will grow faster than in δb and δu_x.

Let us pause here for a second and think about what these results indicate. We are looking at the region in parameter space with $\rho > \rho_{t,a}$, meaning that order can form spontaneously in A, whereas the fixed point of B is still in the isotropic regime. We know from the Boltzmann equation without game interaction that there is a linear instability at the onset of order, so the instability pointing in a- and w_x-direction as soon as ρ crosses the threshold density $\rho_{t,a}$ is not surprising. However, the calculations show that the instability points not only in a- and w_x-direction but has also non-zero components pointing in the direction of density b and its corresponding polar order field (in the direction of macroscopic order) u_x. This is a new effect coming purely from the game coupling of the two species: The instability in A leads to an instability of the isotropic state of B.

We now turn to the second region of instability, $\rho_0 \geq \rho_{t,a}, \rho_0 \geq \rho_{t,b}$. Here, calculations show that all non-zero components of the eigenvector have the same order of magnitude. From the hydrodynamic equations without game we know, that we are in a region where (without game) we would only expect an instability in b and u_x-direction. This suggests that the observed instability in a- and w_x-direction is an effect of the coupling of both species through the game interaction.

Chapter 7

Numerical Analysis of the Hydrodynamic equations

7.1 Numerical methods

To investigate the full equations we use numerical methods, specifically a finite-difference approximation. We model our system by a 2D-grid with periodic boundary conditions and replace all spatial derivatives with their finite difference approximations. The idea is then, that if we know the state of the system (the values of the fields at every grid point) at $t = 0$, we can find the solution for $t = \Delta t, 2\Delta t, 3\Delta t, ...$ via an explicit iterative process (4th order Runge-Kutta method).

First, we recall the Taylor series expansion of a function $f(z)$

$$f(z+k) = f(z) + kf'(z) + \frac{k^2}{2}f''(z) + ... \tag{7.1}$$

with k a small number. If we truncate after the first two terms and solve for $f'(z)$ we get

$$f'(z) \approx \frac{1}{k}\left[f(z+k) - f(z)\right] \tag{7.2}$$

which is called the forward-difference approximation to the first derivative of f. We will use a slightly different approximation, which can be obtained by the Taylor series of $f(z+k) - f(z-k)$

$$f'(z) \approx \frac{1}{2k}\left[f(z+k) - f(z-k)\right] \tag{7.3}$$

and is called the central-difference method. We can use the central-difference method twice using $\frac{k}{2}$ as small parameter instead of k to obtain an approximation for the second derivative

$$f''(z) \approx \frac{1}{k}\left[f'(z+k/2) - f'(z-k/2)\right] = \frac{1}{k^2}\left[f(z+k) - 2f(z) + f(z-k)\right]. \tag{7.4}$$

These approximations are the same for partial derivatives. In our case f represents the densities or the polar order fields (then f is a complex function) and z is a space variable. To solve our equations by finite differences, we start by defining a square

grid in space with grid points

$$\begin{aligned} x_i &= ik \\ y_j &= jk, \qquad i,j \in 1,2,3,...,N. \end{aligned}$$

The fields are now time dependent $N \times N$ matrices

$$\begin{aligned} a_{i,j}(t) &:= a(t, x_i, y_j) \\ b_{i,j}(t) &:= b(t, x_i, y_j) \\ w_{i,j}(t) &:= w(t, x_i, y_j) \\ u_{i,j}(t) &:= u(t, x_i, y_j) \end{aligned}$$

with complex entries in the case of w and u. Using the approximations for spatial derivatives we get the following replacement rules for the field equations

$$\begin{aligned} a(t,x,y) &\to a_{i,j}(t) \\ \partial_x a(t,x,y) &\to \frac{1}{2k}\left[a_{i+1,j}(t) - a_{i-1,j}(t)\right] \\ \partial_y a(t,x,y) &\to \frac{1}{2k}\left[a_{i,j+1}(t) - a_{i,j-1}(t)\right] \\ \partial_x^2 a(t,x,y) &\to \frac{1}{k^2}\left[a_{i+1,j}(t) - 2a_{i,j}(t) + a_{i-1,j}(t)\right] \\ \partial_y^2 a(t,x,y) &\to \frac{1}{k^2}\left[a_{i,j+1}(t) - 2a_{i,j}(t) + a_{i,j-1}(t)\right] \end{aligned}$$

and the corresponding rules for b, w and u. Overall we now have $4N^2$ ODEs (one ODE for every entry of the four $N \times N$ matrices) of the general form

$$\partial_t a_{i,j} = G(a_{k,l}, b_{k,l}, w_{k,l}, u_{k,l}), \qquad k,l \in 1,2,3,...,N. \tag{7.5}$$

We assume now that we know the state of the system at a time $t = 0$. To iteratively solve for later times, the 4th order Runge-Kutta (RK4) method worked very well for our system. Before we apply the method to our system, we will explain the general concept of RK4 briefly. Consider the initial value problem

$$\dot{f} = F(f), \qquad f(t=0) = f_0$$

where the initial value f_0 and the function F are given. As a first step we discretise the time

$$t_n = hn, \qquad n \in 1,2,3,...,M$$

with h a small number. Hence, also the time dependent function is disctretised as $f_n := f(t_n)$. The RK4 method now states that $f_{n+1} = f(t_{n+1})$ can be approximated by

$$f_{n+1} = f_n + \frac{h}{6}\left(k_1 + 2k_2 + 2k_3 + k_4\right) \tag{7.6}$$

with

$$\begin{aligned} k_1 &= F(f_n) \\ k_2 &= F\left(f_n + \frac{k_1}{2}\right) \\ k_3 &= F\left(f_n + \frac{k_2}{2}\right) \\ k_4 &= F(f_n + k_3)\,. \end{aligned} \tag{7.7}$$

The value of the wanted function after one time step, f_{n+1}, is determined by the present value f_n plus the weighted average of four different increments. Each one of the increments is the product of the time interval h, and an estimated slope calculated from the function F.

The first increment, k_1, is based on the slope at the beginning of the time interval. k_2 and k_3 are based on the slope at the midpoint of the interval. The value of f at the midpoint is estimated by $f_n + \frac{k_1}{2}$ for k_2 and $f_n + \frac{k_2}{2}$ for k_3. The fourth increment, k_4 is based on the slope at the end of the interval, estimated using $f_n + k_3$. These four increments are averaged, whereas greater weight is given to the increments at the midpoint.

In our case, f is an array of the four relevant fields

$$f_n = \begin{pmatrix} a_{n;i,j} \\ b_{n;i,j} \\ w_{n;i,j} \\ u_{n;i,j} \end{pmatrix} := \begin{pmatrix} a_{i,j}(t_n) \\ b_{i,j}(t_n) \\ w_{i,j}(t_n) \\ u_{i,j}(t_n) \end{pmatrix} \tag{7.8}$$

and $F = F(f)$ is given by the hydrodynamic equations 5.21. We choose initial conditions $(a_{0;i,j}, b_{0;i,j}, w_{0;i,j}, u_{0;i,j})$ for the fields at every grid point (i, j) and find the solution for $t = \Delta t, 2\Delta t, 3\Delta t, ...$ via the RK4 method outlined above.

We choose periodic boundary conditions for our system. In order to discretise the fields we have to select the size of the 2D grid (the matrices) and the spacing between grid points Δx. One can show that we the time step Δt has to be $\Delta t \leq \frac{\Delta x^2}{2}$ in order for the algorithm to converge [21]. We typically chose the parameters to be

$$\text{gridsize} = 160 \times 160, \quad \Delta x = 0.4, \quad \Delta t = 0.25 * \Delta x^2 \tag{7.9}$$

and let the program run for times of the order of magnitude of $T \in [1000, 100\,000]$. The methods described here proved to work very well for our system. We typically started with a homogeneous field configuration $(a_{0;i,j}, b_{0;i,j}, w_{0;i,j}, u_{0;i,j}) = (\frac{\rho}{2}, \frac{\rho}{2}, 0, 0)$ for fixed control parameters ρ, τ, λ. We perturbed the system at all points of the grid with perturbations of random sizes of the order of magnitude 10^{-3}. This perturbation is necessary since a homogeneous configuration is an (unstable) fixed point and without perturbing the system, it could stay there forever. After setting the initial state of the system we let it evolve iteratively in time steps Δt.

In the next sections we will present our findings from the numeric calculations about the active matter system with game interaction.

7.2 Phases and spatial patterns

As we discussed in chapter 6, a linear stability analysis of the hydrodynamic equations (for $\lambda < 1$) suggests up to five distinct phases - two of which are linearly unstable. Previous work on active matter suggests the formation of traveling waves emerging in regions of linear instability. This state, characterized by spatially inhomogeneous, density-segregated moving patterns, was shown to exist in the hydrodynamic framework [8] as well as in numeric solutions of the Boltzmann equation [50]. Agent-based simulations have confirmed this traveling wave state [11].

The numerical treatment of our system confirms the existence of five distinct phases suggested by linear stability analysis. In this section we will give an overview of the phases and the emerging spatial patterns. Transitions between phases and their corresponding parameter regimes will be subject of the next section. Ordered by increasing overall density ρ, the different phases are:

1. An isotropic, homogeneous phase, in the following referred to as IHP.
2. A broken symmetry state with macroscopic order and traveling wave patterns in A and B, respectively, where waves in B are induced by A (we will explain what we mean by this statement later in this section). In the following we will refer to this phase as *traveling wave phase one* (WP1).
3. A broken symmetry state with macroscopic homogeneous order in A and an isotropic state with no macroscopic order in B, which we will refer to as *ordered phase one* (OP1).
4. A broken symmetry state with macroscopic order and traveling wave patterns in A and B, where waves in A are induced by B. We will refer to this phase as *traveling wave phase two* (WP2).
5. A broken symmetry state with macroscopic homogeneous order in A and B, which we will refer to as *ordered phase two* (OP2).

We assumed for this list that λ is sufficiently small, such that there is a clear distinction between the different phases. If we increase λ, WP1 and WP2 start to overlap until for $\lambda = 1$, OP1 is gone completely and the region of parameter space for WP1 is the same as for WP2 (compare with figures 6.6).

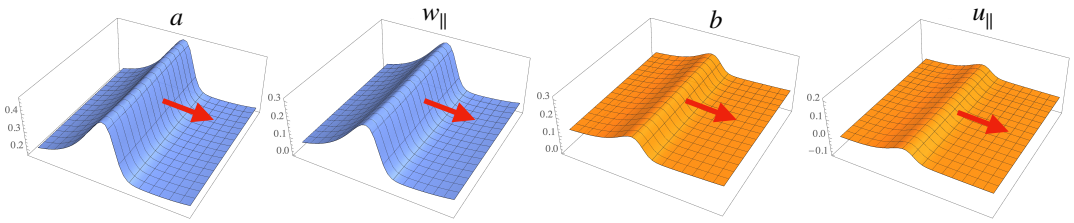

FIGURE 7.1: Wave patterns emerge in WP1 for the parameters $\rho = 0.4, \lambda = 0.5, \tau = 1$. From left to right: $a, w_{\parallel}, b, u_{\parallel}$, where $w_{\parallel}$ and $u_{\parallel}$ point in the direction of macroscopic order. The components of the polar order fields in perpendicular direction to macroscopic order are negligible: $w_{\perp} \approx 0, u_{\perp} \approx 0$. The red arrows indicate the direction of motion of the wave fronts. All plots have the same scaling for better comparability.

Figure 7.1 shows a wave pattern in our 2D system in WP1. The wave vector of the traveling wave front points in the direction of macroscopic order, as suggested by linear stability analysis. When viewed from a comoving frame, the pattern is homogeneous in the direction perpendicular to the wave vector $x_\perp$. We can therefore restrict the description of the emerging patterns to the parallel direction $x_\parallel$ along macroscopic order.

For $\lambda < 1$, we have distinct phases WP1 and WP2, which both show traveling wave patterns.

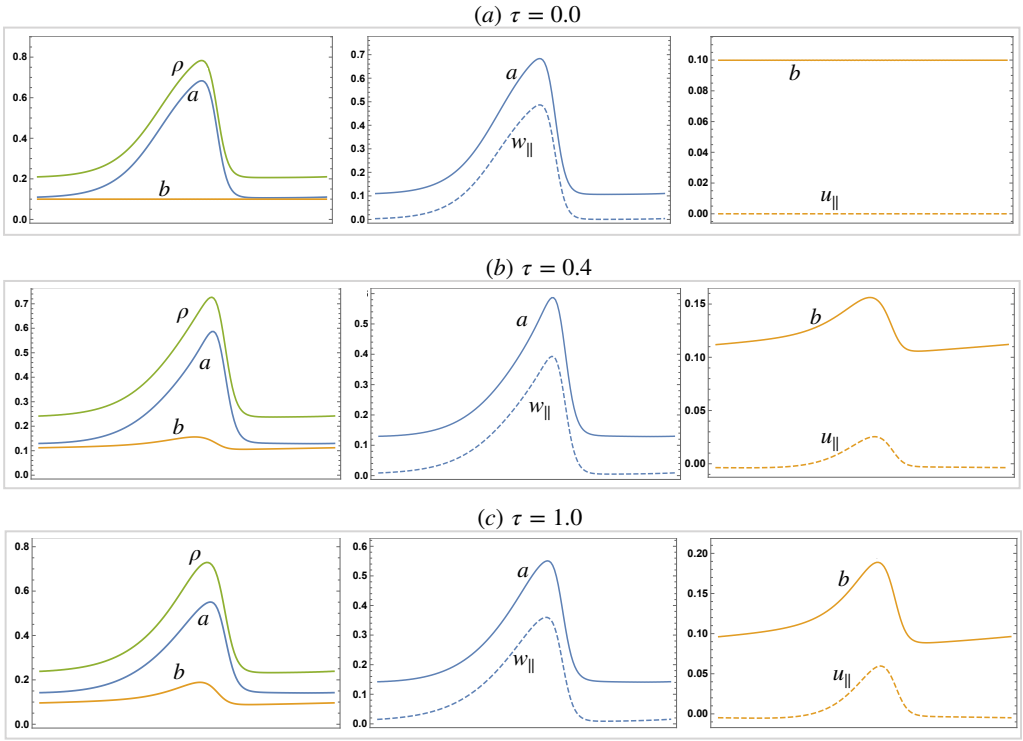

FIGURE 7.2: Wave profiles for $\rho = 0.35, \lambda = 0.4$ and different game strengths. The system is in WP1. (a) For $\tau = 0$, density a exhibits waves, while b is in an isotropic, homogeneous state. (b) For $\tau = 0.2$, the traveling wave in A induces an enslaved wave in species B through the game interaction. The stronger the game interaction, the more do the wave patterns approach each other. This is illustrated in (c), where we see an increase of wave amplitudes in b and $u_\parallel$ as well as a decrease of wave amplitudes in a and $w_\parallel$ compared to (b) for game strength $\tau = 1.0$

Figure 7.2 shows wave profiles for the system in WP1 for different values of τ. The other control parameters are $\rho = 0.35$ and $\lambda = 0.4$. For these parameters, the overall density is higher than the transition density for a, $\rho > \rho_{t,a}$, but lower than the transition density for b, $\rho < \rho_{t,b}$. Hence, if we turn off the game interaction, $\tau = 0$, but keep the average densities $\bar{a}$ and $\bar{b}$ at their respective fixed points, $\bar{a} = \frac{\rho}{1+\lambda} = 0.25, \bar{b} = \frac{\lambda\rho}{1+\lambda} = 0.1$, traveling waves emerge in species A, while species B is in an isotropic, homogeneous state. Figure 7.2a shows the wave profiles in $a, b, w_\parallel$ and $u_\parallel$ for $\tau = 0$. The spatial averages of the waves in a and $w_\parallel$ are the fixed point $\bar{a} = 0.25, \bar{w}_\parallel = \sqrt{\mu_a/\xi} \approx 0.09$. As expected, species B is in an isotropic, homogeneous state with $b = 0.1, u_\parallel = 0$, everywhere in the system.

When we now turn on the game, $\tau > 0$, we see a wave pattern forming in species B (see figures 7.2b and 7.2c)). The pattern in b follows the wave in a through the system. The wave in species B is *enslaved* to the traveling wave in species A. Recall that our results in the linear stability analysis showed a positive growth rate in b- and $u_{\parallel}$-direction in WP1, which already hinted at the formation of patterns in species B. We call this process of wave pattern formation for $\tau > 0$ in a species, that does not exhibit waves for $\tau = 0$, an *induction of waves*.

Figure 7.2 shows how the mutual influence between the species grows with the game strength: The higher τ, the higher the amplitude of the induced wave and the lower the amplitude of waves in A. This is illustrated in figure 7.2c with $\tau = 1.0$ compared to 7.2b. There is an increase of wave amplitudes in b and $u_{\parallel}$ as well as a decrease of wave amplitudes in a and $w_{\parallel}$.

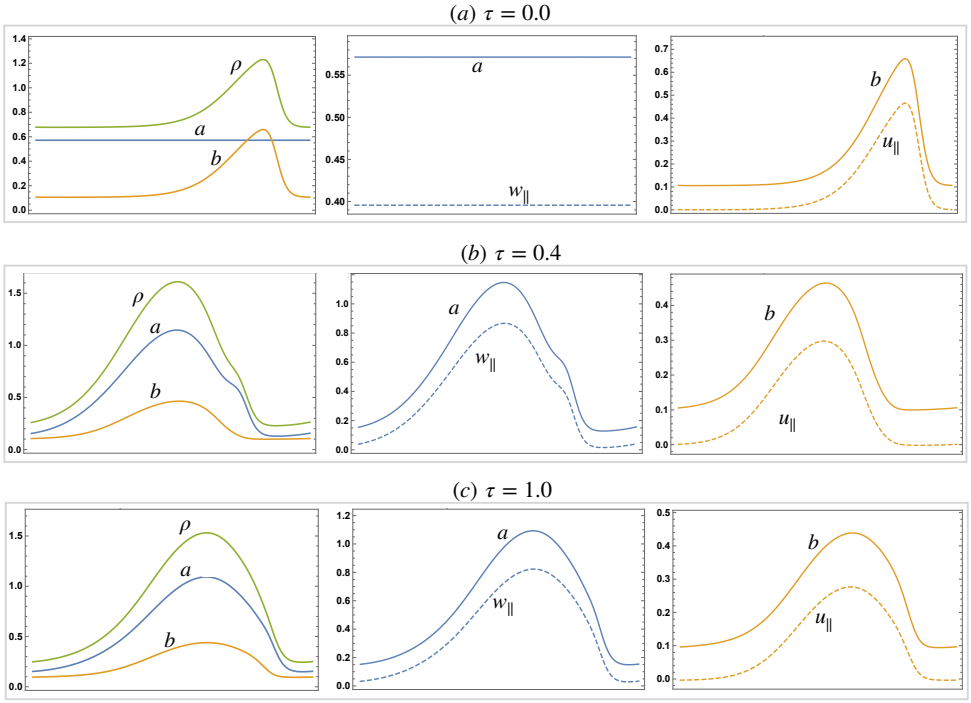

FIGURE 7.3: Wave profiles for $\rho = 0.8, \lambda = 0.4$ and different game strengths. The system is now in WP2. (a) For $\tau = 0$, species A is in a homogeneously ordered state, while species B exhibits traveling waves. (b), (c) For $\tau > 0$, the traveling wave in B induces an enslaved wave in species A through game interaction.

We now turn to the second density-segregated phase with traveling waves, WP2, with $\rho \geq \rho_{t,a}, \rho \geq \rho_{t,b}$. Exemplary for this phase we choose parameters $\rho = 0.8, \lambda = 0.4$, which leads to the homogeneous density fixed points $\bar{a} = \frac{\rho}{1+\lambda} \approx 0.57$ and $\bar{b} = \frac{\lambda\rho}{1+\lambda} \approx 0.23$. Here, the stationary state of A is - for a system without game - in a regime of homogeneous flow, $w_{\parallel} = \sqrt{\mu_a/\xi} \approx 0.39$. The stationary state for B is in the regime of wave formation with the homogeneous polar order fixed point $\bar{u}_{\parallel} = \sqrt{\mu_b/\xi} \approx 0.06$. Hence, for $\tau = 0$, we expect wave patterns in b and $u_{\parallel}$ and homogeneous ordered motion in a and $w_{\parallel}$ (see figure 7.3a).

We now turn on the game by setting $\tau > 0$. Figures 7.3b and 7.3c show, that species B induces traveling waves in species A. The induction of traveling waves leads to

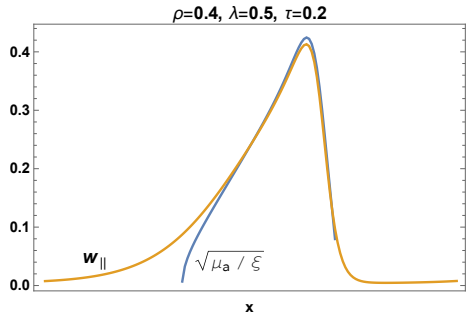

FIGURE 7.4: Density profile and polar order profile are approximately related via the homogeneous polar order fixed point $w_{\parallel} = \sqrt{\mu_a/\xi}$ everywhere.

high amplitudes even for low τ.

A general feature of the patterns is, that the wave profiles of density and polar order are related to each other via the homogeneous polar order fixed point $w_{\parallel} = \sqrt{\mu_a/\xi}$ at every point to a high degree of accuracy (see figure 7.4).

Having now established that the interplay of activity and game interaction leads to the formation of wave patterns in both species, we test how the patterns vary for different values of ρ. First, we look at the patterns when both species are equally strong, $\lambda = 1$. In this case we only have one phase that exhibits pattern formation (the parameter regime of WP1 equals the parameter regime of WP2). Figure 7.5a shows typical profiles of density a for different overall densities ρ. The wave pattern in b has (for the special case of $\lambda = 1$) the exact same shape and both waves travel synchronously through the system.

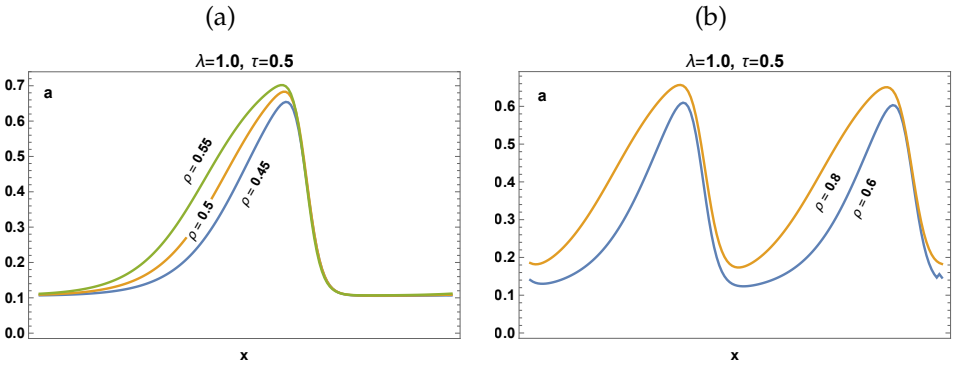

FIGURE 7.5: Typical wave profiles of density a for $\lambda = 1, \tau = 0.5$. (a) A wave pattern spontaneously emerges for $\rho > \rho_{t,a}$, segregating the system in regions of high density with macroscopic order ($w > 0$) and isotropic regions of low density ($w = 0$). The wave gets broader and higher as the overall density is increased, whereas the low density background stays unchanged. (b) For high enough densities ρ we observe two wave peaks in the size of our system.

The wave patterns have a rather steep front and fall off less steep in the back. This asymmetry has also been reported in several numerical studies of self-propelled, polar particles without game interaction [50, 11]. For densities close to the onset of

order, the waves are relatively narrow. As we increase the density, the wave profiles get broader and the asymmetry becomes more pronounced.

The pattern segregates the system in regions of high density with macroscopic order ($w > 0$) and isotropic regions of low density ($w = 0$). The high density, ordered wave moves through the system on an isotropic, low density background [50]. Note that the density level for the low density background stays approximately the same for varying overall densities. Hence, the plus in density a is solely added to the high density wave pattern when ρ is increased. Similar results have been reported for one-species active matter systems. An increasing density broadens the wave patterns, while the low density background remains approximately unchanged [50].

For high enough densities we also observe two wave peaks in the system size L (see figure 7.5b). The wave structures get broader as the overall density is further increased. Compared to wave structures with just one peak, the low density background for this state is slightly higher and increases with the overall density ρ.

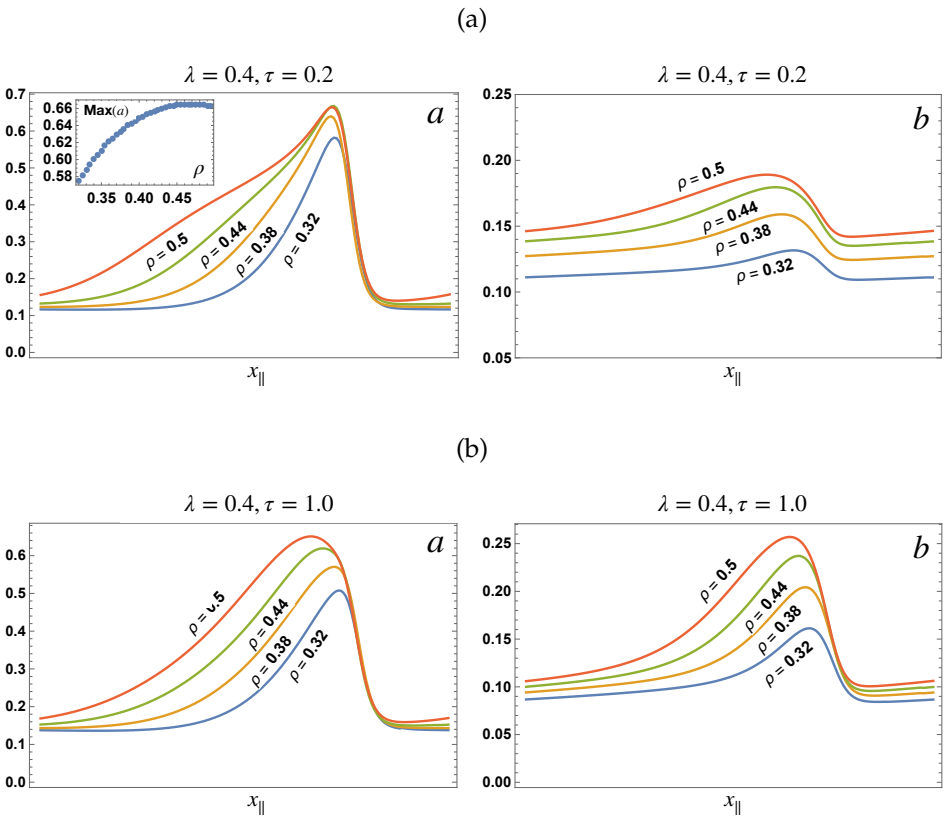

FIGURE 7.6: Wave profiles of density a and b for $\lambda = 0.4$ and (a) $\tau = 0.2$, (b) $\tau = 1.0$ for different values of the overall density, $\rho \in \{0.32, 0.38, 0.44, 0.5\}$. The wave gets broader and more asymmetric as the overall density is increased. The low density background stays roughly unchanged for density a. Inset of (a): The amplitude of the wave (Max(a)) initially grows approximately linearly with ρ and saturates for high enough densities.

When $\lambda < 1$, the wave shapes in a and b differ from each other. Figure 7.6 shows wave patterns in a and b for different values of ρ. The system is in WP1 with the parameters $\lambda = 0.4$ and $\tau = 0.2$ in figure 7.6a and $\tau = 1.0$ in figure 7.6b. Values

in ρ are $\{0.32, 0.38, 0.44, 0.5\}$. As before, the low density background stays approximately the same for the inducing species A for all densities. The background in density b increases with ρ, which shows that the wave formation is due to a different mechanism (induction through game interaction) and not due to active motion. With increasing ρ the wave shapes get broader. We also observe that the amplitudes grow initially approximately linearly with the overall density and saturate for high enough densities.

7.3 Bifurcation structure

After having seen that the system gives rise to up to 5 distinct phases, we will analyze the transitions between the different phases and the bifurcation structure in more detail. In chapter 6 we computed the regions in parameter space that are linearly unstable. This gives us a first draft for the phase diagram of our system. Using the numerical methods outlined in section 7.1 we can now check how non-linearities influence the phase diagram.

We will test the system especially for hysteresis effects, which have been reported in numerical solvers of the Boltzmann equations for one species [50], hydrodynamic descriptions [40], as well as in agent-based simulations of the Vicsek model [19].

In order to detect hysteresis effects, we numerically compute the stationary solution of the system for fixed parameters (λ, τ) and initial conditions $a = b = \rho/2, w = u = 0$ plus random perturbations at every grid point. Then we quasistatically reduce (or increase) the overall density ρ in small steps. With the term "quasistatic", we mean here that the system is given a sufficient amount of time to equilibrate in between successive adjustments in ρ.

As a measure of whether spatial patterns exist, we use parameters that we call *variation parameters* $\eta(a)$ and $\eta(b)$, which measure spatial variations in the densities a and b by taking the average of the numeric spatial derivative 7.3 over all grid points. If $\eta = 0$, the density of the corresponding species is homogeneously distributed. For $\eta > 0$ the system is in an inhomogeneous state, hence, a state with traveling wave patterns.

First, we calculate the bifurcation diagram of the variation parameter and the polar order parameter as a function of the overall density for no game interaction, $\tau = 0$ (see figure 7.7a). Since for no game interaction both species behave exactly the same, we only show $\eta(a)$ and $\|w\|$ in figure 7.7. Blue dots indicate stable fixed points of the system's dynamics and have been determined numerically. Dashed lines are drawn "by hand" and indicate the estimated position of unstable fixed points.

To get the numerical data for the bifurcation diagram, we used the following protocol. We start in an isotropic homogeneous state ($\eta(a) = 0, \bar{w} = 0$) at low densities $\rho = 0.2$, and then quasistatically increase ρ. We have indicated the path of the system for increasing ρ with black arrows in figure 7.7. At the transition density $\rho_t \approx 0.43$, wave patterns emerge spontaneously in A, which we can see by a jump of the variation and the spatial average of the order parameter $\eta(a) > 0, |\bar{w}| > 0$. The homogeneous state of the system is now unstable, indicated by the dashed line at $\eta(a) = 0, |\bar{w}| = 0$ in figure 7.7a. The system stays in the traveling wave phase as we further increase the overall density ρ up to densities well beyond the transition density to a homogeneously ordered phase, $\rho_{dh} \approx 0.9$ suggested by linear stability analysis. This transition occurs at a density $\rho_h \approx 1.1$, where the variation $\eta(a)$ jumps back to zero.

Once we have reached this point, we start to quasistatically decrease ρ again. The path of the system is now indicated by grey arrows. The system stays in a homogeneously ordered phase until ρ_{dh}, where it jumps back to a traveling wave state. As we further decrease density ρ, the system stays in the wave state until a density $\rho_i \approx 0.3$, well below ρ_t.

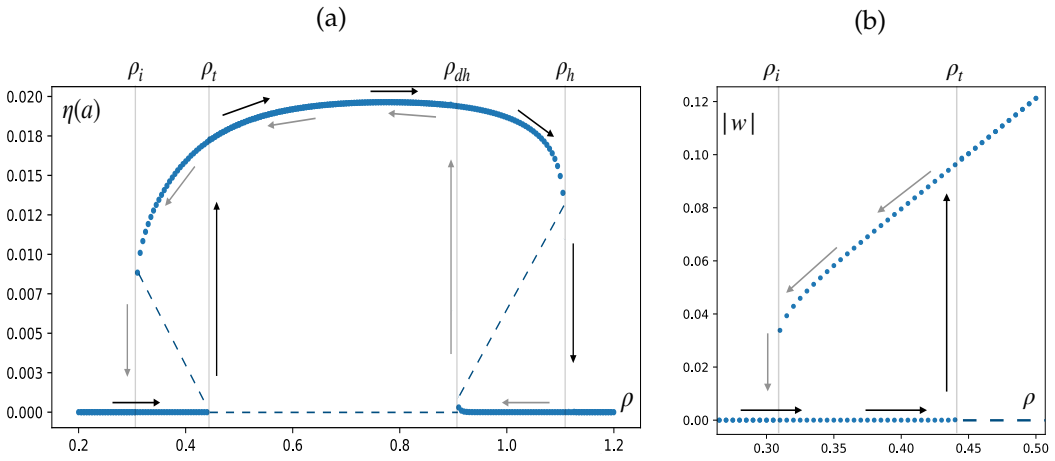

FIGURE 7.7: (a) Variation $\eta(a)$ and (b) average of the polar order parameter $|\bar{w}|$ as a function of the overall density ρ for a system without game interaction, $\tau = 0$. The variation is a measure of pattern formation. Dots indicate stable fixed points of the systems dynamics and have been determined numerically. Dashed lines are drawn "by hand" and estimate unstable fixed points. The data indicates that the bifurcation is subcritical with hysteresis effects and the transitions are first order. The arrows show the path of the system for quasistatic increase (black arrows) and decrease (grey arrows) of density ρ.

Summarizing, we can conclude that the bifurcation is subcritical and the system is bistable in the regions $\rho \in [\rho_i, \rho_t]$ and $\rho \in [\rho_{dh}, \rho_h]$, in the sense that two different stable solutions exist for the same values of the parameters. The transitions between the isotropic phase, the traveling wave phase and the homogeneously ordered phase are accompanied by hysteresis effects. This behaviour suggests first order transitions as has previously been reported for one species active matter systems [50, 40].

We can now turn the game on again. Figure 7.8 shows the variation parameters, $\eta(a)$ and $\eta(b)$, and the average polar order parameters $|\bar{w}|$ and $|\bar{u}|$ as functions of ρ for $\lambda = 0.4$, $\tau = 0.2$. It shows the bifurcation diagrams for the transitions between the phases IHP, WP1 and OP1. Blue and red dots indicate stable fixed points of A and B respectively and dashed lines indicate the approximate positions of unstable fixed points.

Following the same protocol of quasistatic increase and decrease of the overall density as described above, we get the following results: If the initial state of the system is in IHP and we quasistatically increase the overall density, the transition density to WP1 is at $\rho_{t,a} \approx 0.31$, where the variation parameters $\eta(a), \eta(b)$ and the polar order parameters $\bar{w}$ and $\bar{u}$ jump to non-zero values (see figure 7.8a for $\eta(a), \eta(b)$ and figure 7.8b for $\bar{w}$,$\bar{u}$). Non-zero values of the induced quantities $\eta(b)$ and $\bar{u}$ are much smaller than the ones of variation $\eta(a)$ and polar order $\bar{w}$, that jump to non-zero values due to the properties of active matter. The values of $\eta(b)$ and $\bar{u}$ are higher the bigger the value of the overall game strength τ is, as we have already seen in the last section. If the system is on the other hand initially in WP1 and the density is decreased, the stationary inhomogeneous state is stable down to values $\rho_{i,a} \approx 0.23$.

An equivalent effect occurs for the transition WP1 $\leftrightarrow$ OP1: Starting in WP1, the

system stays in the inhomogeneous phase up until $\rho_{h,a} \approx 0.55$. An initial state in OP1 and quasistatic decrease leads to a transition to WP1 at $\rho_{dh,a} \approx 0.52$. Figure 7.8a shows that $\eta(a)$ jumps to higher values than it had for increasing ρ during this transition. This is due to the formation of wave structures with a wavelength that fits twice in the system size L (hence, a wave structure with two wave peaks in L). We suspect that this state was suppressed for increasing ρ, since the system was already in a wave state with one peak in L when the respective values were reached. The shorter-wavelength (two-peak) state decays to the longer-wavelength (one-peak) state for low enough ρ (in figure 7.8a the system jumps from the higher values of $\eta(a)$ to the same non-zero values as for increasing ρ at a density of approximately $\rho = 0.35$). The same effect happens for species B, the effect on $\eta(b)$ is just very small compared to species A since the variation in B is much smaller than the one in A.

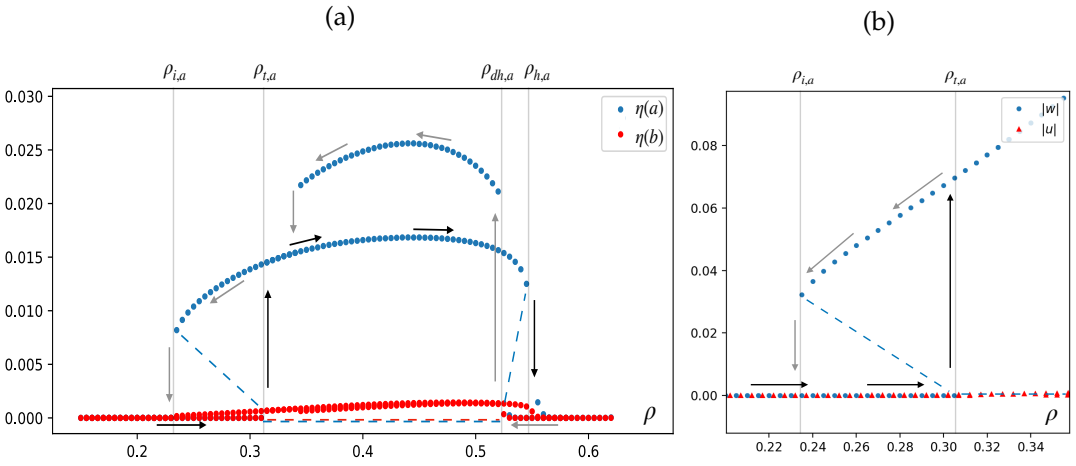

FIGURE 7.8: (a) Variation $\eta(a)$ and (b) average of the polar order parameter $|\bar{w}|$ as a function of the overall density ρ for $\lambda = 0.4, \tau = 0.2$. Dots indicate stable fixed points (calculated numerically), dashed lines indicate unstable fixed points (drawn "by hand"). The control parameter ρ sweeps over regimes of IHP, WP1 and OP1. Black and grey arrows show the path of the system for quasistatic increase and decrease of ρ respectively. The bifurcation is subcritical and exhibits hysteresis effects.

We follow the same procedure of increase and decrease in ρ for the transitions OP1 $\leftrightarrow$ WP2 and WP2 $\leftrightarrow$ OP2. The results for the whole range of overall density ρ is shown in figure 7.9. If the initial state of the system is in the inhomogeneous wave regime WP2 and we quasistatically decrease the overall density, the stationary inhomogeneous state is stable down to values $\rho_{i,b} \approx 0.63$, below the transition point $\rho_{t,b} \approx 0.77$ for the transition OP1 $\rightarrow$ WP2. The transition from WP2 to OP2 occurs at $\rho_{h,b} \approx 1.4$ and the transition from OP2 to WP2 at $\rho_{dh,b} \approx 1.2$. Figure 7.9b shows the jumps in the polar orders $|w|$ and $|u|$ at the respective transition points and the steady increase of polar order with the overall density afterwards.

As a summary we can make the following statements: Phase separated, inhomogeneous solutions are observed in parameter regions *wider* than the linear instability domains of the homogeneous states. This implies that there are *bistable regions* in the

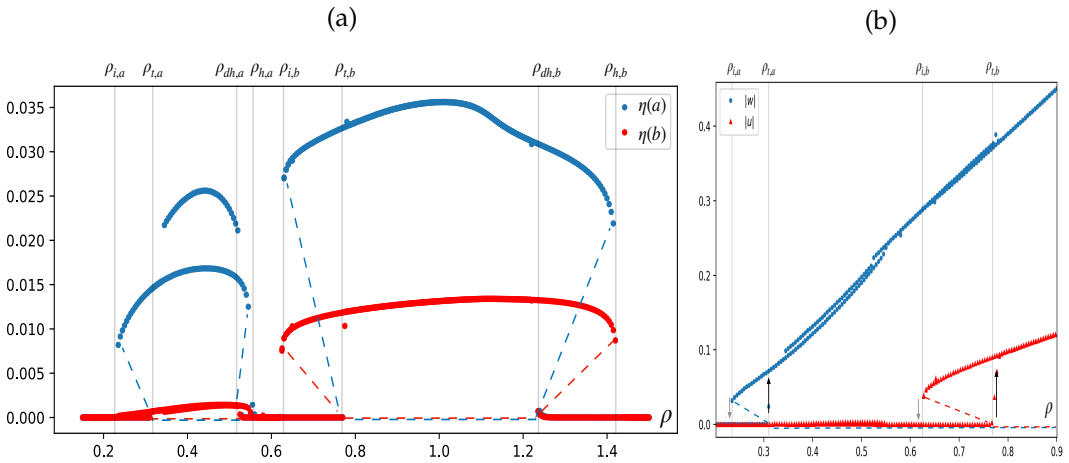

FIGURE 7.9: (a) Spatial variations $\eta(a), \eta(b)$ and (b) average of the polar order parameters $|\bar{w}|, |\bar{u}|$ as functions of the overall density ρ for $\lambda = 0.4, \tau = 0.2$. Dots indicate stable fixed points (calculated numerically), dashed lines indicate unstable fixed points (drawn "by hand"). The sweep in ρ goes over all of the five distinct phases. There are bistable regions with two coexisting phases and hysteresis effects at every transition. The system performs jumps in the variation parameters and the order parameters at the transition points, indicating first order phase transitions.

sense that two stable phases coexist in the parameter regions: For $\rho_{i,a} < \rho < \rho_{t,a}$, the system is either in IHP or WP1; for $\rho_{dh,a} < \rho < \rho_{h,a}$, it is either in WP1 or OP1; for $\rho_{i,b} < \rho < \rho_{t,b}$ in OP1 or WP2 and for $\rho_{dh,b} < \rho < \rho_{h,b}$, the system is either in WP2 or OP2. The initial conditions determine which phase is realized in each of the coexistence regions. The bifurcation is *subcritical* and there are *hysteresis effects* at every transition. A consequence of the subcritical nature of the bifurcation is that a homogeneous system in a coexistence region is stable to small perturbations but unstable to large ones that will lead to pattern formation. The system performs jumps in the variation parameters and the order parameters at the transition points, indicating first order phase transitions.

Following this procedure for fixed $\lambda = 0.4$ and increasing τ, we expect from linear stability analysis that $\rho_{dh,a}$ decreases and that the distance between $\rho_{dh,a}$ and $\rho_{t,b}$ grows (see figure 6.6). Figure 7.10 compares bifurcation diagrams for $\eta(a), \eta(b)$ for increasing values of τ and $\lambda = 0.4$. Indeed, as can be seen in figure 7.10, we measure a decrease in $\rho_{dh,a}$ as well as in $\rho_{h,a}$. However, the stable branches of the phases WP1 and WP2 do not move correspondingly farther apart. Since the value of $\rho_{i,b}$ decreases faster than $\rho_{h,a}$ for increasing τ, the distance between $\rho_{h,a}$ and $\rho_{i,b}$ actually gets smaller. Hence, the branches of the traveling wave phases approach each other until they unite to one branch ($\rho_{i,b} \approx \rho_{h,a}$) for $\tau \approx 1$ (see figure 7.10d). The structure of the bifurcation diagram is different, in the sense that now there is only one phase transition to an inhomogeneous state and one transition back to a homogeneous state (instead of two) when ρ is increased or decreased quasistatically over the whole parameter range. A state of homogeneous order in A and isotropy in B is only exhibited by the system if it is placed in this state by its initial conditions.

The transition from WP1 to WP2 is continuous for increasing or decreasing ρ. Consequently, there is only one discontinuous transition to order in $|w|$ and $|u|$. This is illustrated in figure 7.11. The system is only in OP1 if its initial conditions are restricted to this phase. In particular, OP1 is unstable for sufficiently large fluctuations in this case and is therefore not a globally stable state anymore.

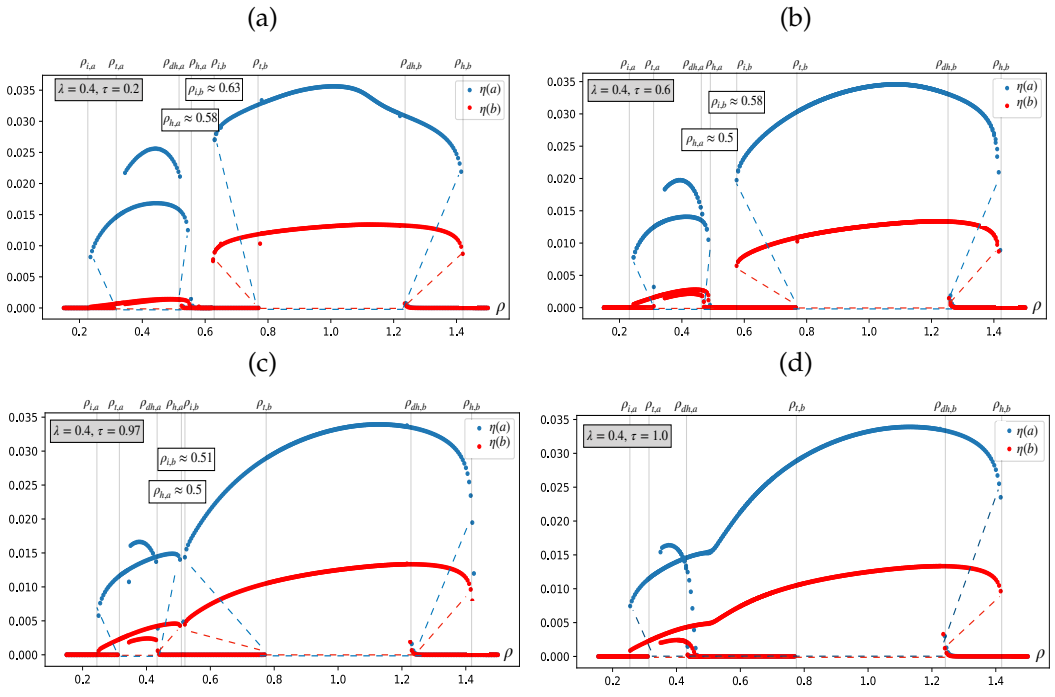

FIGURE 7.10: Variations $\eta(a)$, $\eta(b)$ for different values of $\tau \in \{0.2, 0.6, 0.97, 1.0\}$ and fixed $\lambda = 0.4$ as functions of the overall density ρ. Dots indicate stable fixed points (calculated numerically), dashed lines indicate unstable fixed points (drawn "by hand"). The value of $\rho_{i,b}$ decreases faster than $\rho_{h,a}$ for increasing τ. Hence, the branches of the traveling wave phases, WP1 and WP2, approach each other until they unite to one branch at $\tau \approx 1$. Then there is a continuous transition from WP1 to WP2 and OP1 is unstable to large fluctuations everywhere.

The bifurcation diagram has a different structure for certain parameter regimes of λ. We know from linear stability analysis that if λ is decreased, the inhomogeneous phases WP1 and WP2 move farther apart from each other in parameter space (see figure 6.6). For $\lambda < 0.4$, we find that the bifurcation diagram has qualitatively the same structure as the one for $\lambda = 0.4, \tau = 0.2$, characterized by five distinct phases and discontinuous transitions between them. The distance between the branches of the inhomogeneous states increases for decreasing λ such that the distance is too big for the branches to meet and unite in the parameter regime of $\tau \in [0, 1]$ that we have considered here. It would be subject for further investigations to explore higher values of τ to get a more complete picture of the bifurcation structure and phase diagram of the system.

If λ is increased on the other hand, we see a new effect: If τ is sufficiently small, the branches of the inhomogeneous phases do not meet at their "edges" as they did in the case of figure 7.10, instead they overlap in a parameter region of $\rho \in [\rho_{i,b}, \rho_{h,a}]$ (note that in this case $\rho_{i,b} < \rho_{h,a}$). Figure 7.12 illustrates this effect for the parameter values

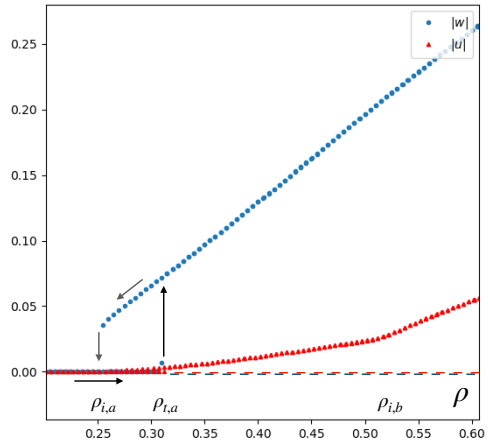

FIGURE 7.11: Averages of $|w|$ and $|u|$ as functions of ρ. Game parameters are set to $\lambda = 0.4$ and $\tau = 1.0$. The inhomogeneous phases WP1 and WP2 are united to one phase and there is consequently only one discontinuous transition to order in $|w|$ and $|u|$. The transition from WP1 to WP2 is continuous and can roughly be estimated by the kink in both curves.

$\lambda = 0.5, \tau = 0.2$. The fundamentally new feature of the bifurcation is, that there are regions in parameter space where both inhomogeneous traveling wave states are stable. Depending on the initial conditions, the system can either be in WP1 or WP2 in these regions. This property leads to the existence of tristable states (one stable homogeneous solution and two stable inhomogeneous, traveling-wave solutions).

Similar to the $\lambda = 0.4$ case described above, the branches unite to one inhomogeneous phase if τ is increased and reaches a threshold value that depends on λ. In the parameter region of ρ where both branches would have overlapped, the system is neither in WP1 nor WP2 as we defined it, since neither of the waves is purely due to the induction mechanism. Instead, both species form traveling waves, that move with approximately the same speed through the system, synchronized by the game interaction.

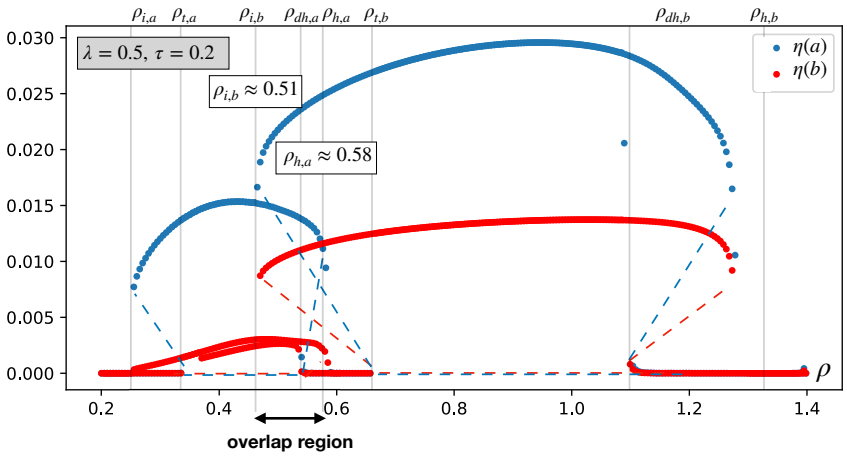

FIGURE 7.12: Bifurcation diagram of $\eta(a), \eta(b)$ for parameter values $\lambda = 0.5, \tau = 0.2$. The branches of the inhomogeneous phases overlap, which leads to regions in parameter space where both inhomogeneous traveling wave states are stable.

7.4 Wave delay

We have seen that a wave pattern in A induces waves in B and vice versa, as we turn on the game interaction. Since the waves travel through the system and the game interaction can only react within a time proportional to τ^{-1}, there is a time delay of the induced wave compared to the original wave. We can quantify this delay d in the numeric solutions and measure it as a function of the game interaction strength τ.

This was done by counting the number of spatial grid points, d, that lie between the peak of the wave in a and the peak of the wave in b. The other control parameters ρ and λ were kept constant for each τ-sweep. Figure 7.13a shows $d(\tau)$ for $\rho = 0.4, \lambda = 0.4$. The system is in WP1. For a strong game interaction,$\tau \gg 1$, the reaction time of the game is fast and the system is pulled strongly towards its fixed point everywhere. The induced wave closely follows the first wave. It is thus an intuitive result that the delay vanishes ($d(\tau) \to 0$) for $\tau \gg 1$.

Figure 7.13b shows the delay $d(\tau)$ for different values of λ. We find that the delay is bigger when λ is smaller. For $\lambda \geq 0.5$ we observe a drop in the delay when τ reaches certain values. This can be explained by the change of the bifurcation diagram of the system. As was explained in the last section, an increasing value of τ decreases the value of $\rho_{i,b}$, at which species B starts to form traveling wave bands. The drop of the delay $d(\tau)$ in figure 7.13b can be traced back to the value of τ for which $\rho_{i,b} = 0.4$, thus the smallest value of τ with traveling waves in B. Before this drop (and for the lower values of λ displayed in the figure), the system is in a state where A induces waves in B (WP1). This induction is delayed in time because of the finite reaction time of the game. After the drop in the delay for $\lambda \geq 0.5$, the system is in a state where both species form waves. In this state, both traveling waves move with approximately the same speed and are synchronized by the game interaction. Compared to an enslaved wave, the delay is thus much smaller.

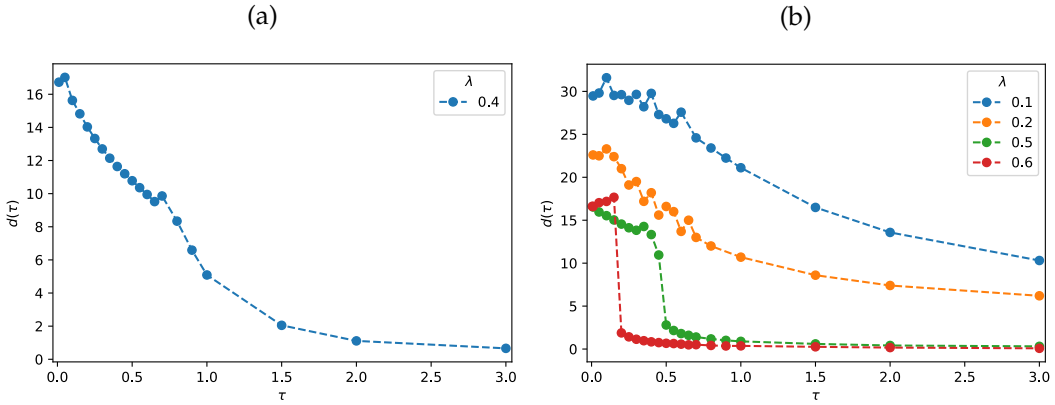

FIGURE 7.13: (a) Delay of the wave in density b compared to the wave in a as a function of τ for $\rho = 0.4, \lambda = 0.4$. The effect is higher for small τ. (b) Comparison of $d(\tau)$ for $\rho = 0.4$ and $\lambda \in \{0.1, 0.2, 0.5, 0.6\}$. The smaller λ, the bigger the delay. The drop in the delay for $\lambda = 0.5, \lambda = 0.6$ can be explained by the change of transition density $\rho_{i,b}$ for increasing τ.

7.5 Density shift

We find in the numerical calculations that the system goes to its fixed point, $(\bar{a}, \bar{b}, |\bar{w}|, |\bar{u}|) = (a_0, b_0, w_0, u_0)$, when it is in a homogeneous phase. Figure 7.14 illustrates this statement for the system in two different homogeneous phases for fixed $\lambda = 0.3$ and $\tau = 0.5$. In figure 7.14a, the value of the overall density is $\rho = 0.2$ and the system is in the isotropic ($|\bar{w}| = |\bar{u}| = 0$), homogeneous ($\eta(a) = \eta(b) = 0$) phase, IHP. For $\rho = 0.6$ in figure 7.14b, the system is in the phase of homogeneous order in species A and isotropy in species B, OP1. The different graphs show the time evolution of the spatial average of the densities, $\bar{a}$ and $\bar{b}$, the average of the polar order fields, $|\bar{w}|$ and $|\bar{u}|$, as well as the measure for spatial variation of the densities, $\eta(a)$ and $\eta(b)$. The initial state is $a = b = \frac{\rho}{2}$, $w = u = 0$ at every point on the spatial grid plus random perturbations.

Figure 7.14 shows that the densities reach their respective fixed points, $a_0 = \frac{1}{1+\lambda}\rho$, $b_0 = \frac{\lambda}{1+\lambda}\rho$ after some time and stay there. The variation of the densities goes to zero after the initial perturbation of the system, which shows the homogeneity of the final state. The values of the order parameters $|\bar{w}|$ and $|\bar{u}|$ both go to zero in the isotropic case in figure 7.14a. If the system is in OP1, as in figure 7.14b, order parameter $|\bar{w}|$ goes to its fixed point given by $|w| = \sqrt{\mu_a/\xi} \approx 0.3$ while $|\bar{u}| = 0$. Hence, the stationary state in the numerical calculations reproduces the predictions we made analytically.

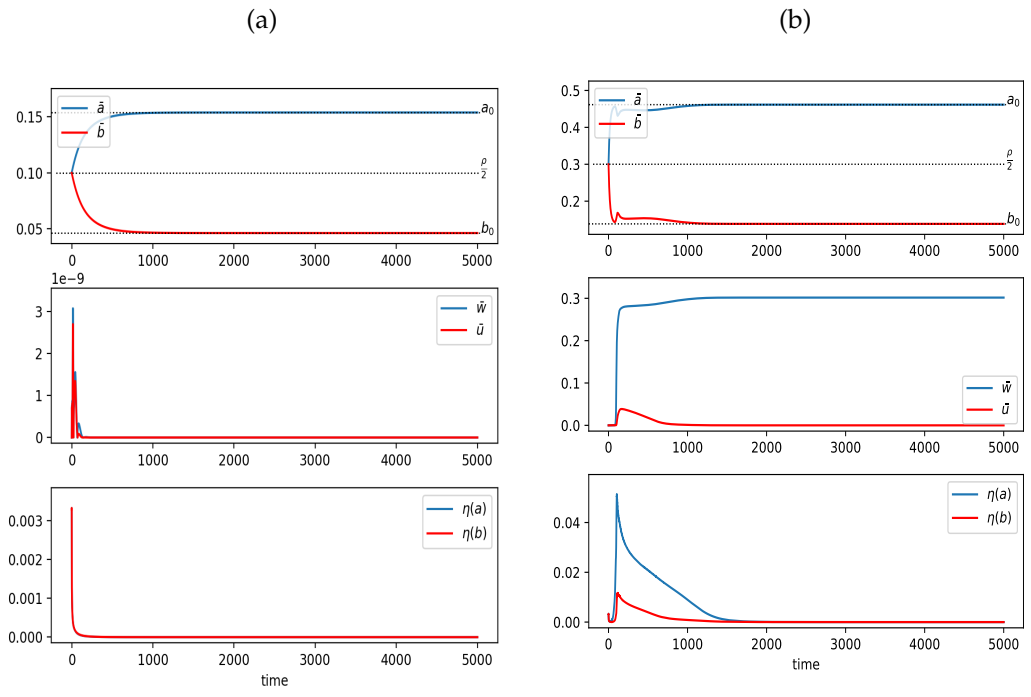

FIGURE 7.14: Spatial average of densities $\bar{a}$ and $\bar{b}$ (upper graph), polar order fields $\bar{w}$ and $\bar{u}$ (middle graph) and spatial variation of the densities $\eta(a), \eta(b)$ (lower graph) over time for $\tau = 0.5$, $\lambda = 0.3$ and (a) $\rho = 0.2$ (isotropic phase IHP) (b) $\rho = 0.6$ (homogeneously ordered phase OP1). The initial state is $a = b = \frac{\rho}{2}$, $w = u = 0$ at every grid point plus random spatial perturbations. In both cases the system goes to its homogeneous fixed point $a = \frac{1}{1+\lambda}\rho$, $b = \frac{\lambda}{1+\lambda}\rho$ and in (a) $\bar{w} = 0$, $\bar{u} = 0$, in (b) $|\bar{w}| = \sqrt{\mu_a/\xi}$, $\bar{u} = 0$.

Now we turn to systems that are in an inhomogeneous phase with traveling waves as stationary state. Figure 7.15a shows an example for the time evolution of the spatially averaged fields for the system in WP1 for parameters $\rho = 0.4, \lambda = 0.4, \tau = 0.2$. We find that in the beginning, while the system is still homogeneous, densities $\bar{a}$ and $\bar{b}$ go towards their respective fixed points $a_0 \approx 0.29, b_0 \approx 0.11$. However, as soon as wave patterns form ($\eta(a) > 0$), the densities shift away from the homogeneous fixed point, such that $\bar{a} < a_0$, $\bar{b} > b_0$. The amount by which density $\bar{a}$ decreases is the same as the increase of density $\bar{b}$, since the overall density ρ is conserved. The average values of the polar order fields are given by their respective fixed points, evaluated at the average densities, $|\bar{w}| = \sqrt{\frac{\mu_a(\bar{a},\bar{b})}{\xi}}$, $|\bar{u}| = \sqrt{\frac{\mu_b(\bar{a},\bar{b})}{\xi}}$.

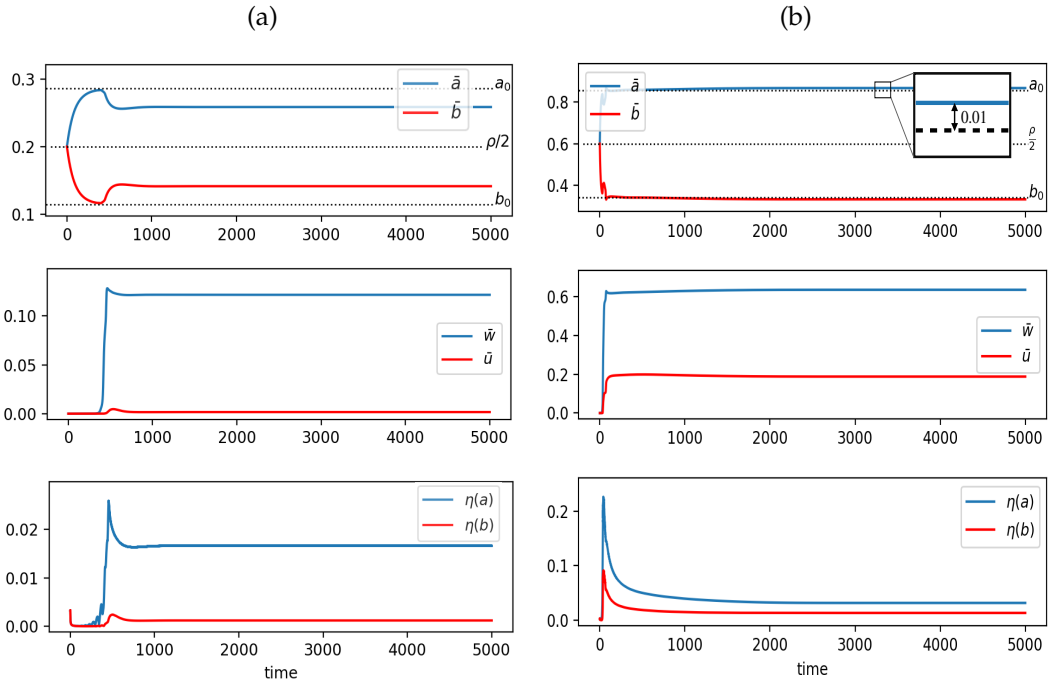

FIGURE 7.15: Spatial average of densities $\bar{a}$ and $\bar{b}$ (upper graph), polar order fields $\bar{w}$ and $\bar{u}$ (middle graph) and spatial variation of the densities $\eta(a), \eta(b)$ (lower graph) over time for $\tau = 0.2, \lambda = 0.4$ and (a) $\rho = 0.4$, (b) $\rho = 1.2$. As soon as patterns form in the system, $\eta(a) > 0$, the densities shift away from the homogeneous fixed point, such that in (a) $\bar{a} < a_0$, $\bar{b} > b_0$(the system is in WP1) and in (b) $\bar{a} > a_0$, $\bar{b} < b_0$ (the system is in WP2).

In the second region of instability, the density shift is in the opposite direction: The average density $\bar{a}$ increases while $\bar{b}$ decreases by the same amount. This is illustrated by figure 7.15b for the parameters $\tau = 0.2, \lambda = 0.4$ and $\rho = 1.2$.

We can therefore conclude that the species that induces waves in the system has a disadvantage in the game. The species that would be in a homogeneous state, if it were not for the game interaction, gains an advantage. In general, we can say that the activity of the particles changes the outcome of the game.

This phenomenon is an effect of the coupling of active matter with game theory. When the actively moving particles of one species form traveling wave patterns, the game interaction leads to a feedback mechanism that induces a traveling wave in

the second species. Since the formation of the two waves is due to different mechanisms, their shapes differ and are not just scaled versions of each other. Another feature is the time delay between both waves which we saw in the last section. These differences in shape and position of the pattern give rise to the non-linear feedback that changes the outcome of the game. We will analyze this interplay further in section 7.5.2, where we will derive an analytic expression for the mechanism of density shifts.

As a next step we fix τ and λ and look at the magnitude of the density shift as a function of ρ. Figure 7.16 shows the density shift of species A, $\bar{a} - a_0$, for the parameters $\lambda = 0.4, \tau = 0.2$. Note that we use the same values for λ and τ as in our example for the bifurcation structure in the last section. Hence, the values for all transition densities are the same and figure 7.16 can be compared with figure 7.8. The data was collected by quasistatic increase and decrease of the density.

When the system is in WP1, species A induces traveling waves in B and the average density of A is shifted towards lower values, $\bar{a} < a_0$. In figure 7.16 this can be seen in the region $\rho \in [\rho_{i,a}, \rho_{h,a}]$, where $\bar{a} - a_0 < 0$. Note that at densities, for which we have seen the coexistence of one-peak and two-peak wave solutions, we also see two different values for the density shift. The shift depends on which wave pattern is realized. When the system is in WP2, species B induces waves and species A gains an advantage. in figure 7.16 we see an increase of $\bar{a}$ in $\rho \in [\rho_{i,b}, \rho_{h,b}]$.

Since the system undergoes hysteresis at the transitions between homogeneous and inhomogeneous stationary states, the density shift also exhibits coexistence regions. Note that the density shift of species B, which is not shown here, has the same values as the shift of A with opposite sign, $\bar{b} - b_0 = -(\bar{a} - a_0)$, since the overall density ρ is conserved.

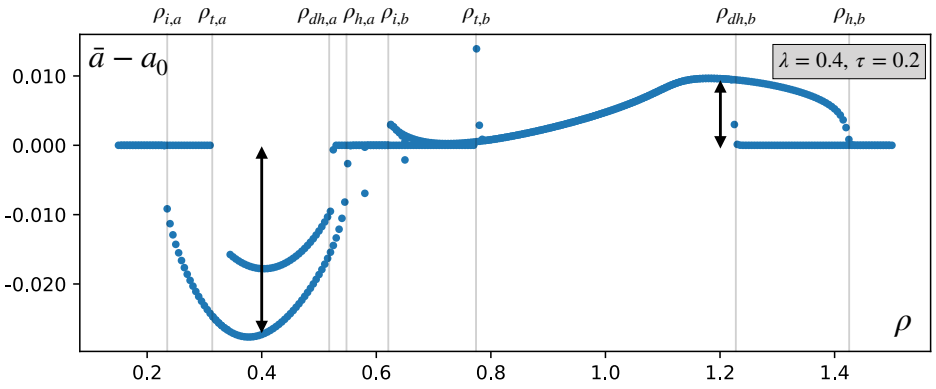

FIGURE 7.16: Bifurcation diagram of the density shift of species A for the parameters $\lambda = 0.4, \tau = 0.2$. In WP1, density $\bar{a}$ decreases due to the shift. In WP2 we see an increase in $\bar{a}$. Since the system undergoes hysteresis at the transitions between homogeneous and inhomogeneous stationary states, the density shift also exhibits coexistence regions. The grey arrows mark the density shifts at $\rho = 0.4$ and $\rho = 1.2$ corresponding to figures 7.15a and 7.15b respectively.

The density shift does not only depend on ρ but on all control parameters. Figure 7.17a shows the absolute value of the the shift of species A, $|\bar{a} - a_0|$, in WP1 as a function of τ for different values of λ and fixed $\rho = 0.4$. The magnitude of the shift

is higher for $\tau \ll 1$ and goes to zero for large τ. This behaviour is quite intuitive: If τ is big, game interactions happen fast, the waves have similar positions and shapes, and the system does not deviate largely from its fixed point. For small τ on the other hand, the species are weakly coupled, thus the delay between waves is high and their shapes differ significantly. This leads to a larger effect in the density shift. For the extreme case of $\tau \ll 1$ the induced waves in b are so small that $b(x) \approx \bar{b} =$ constant. The deviations of the values of $a(x)$ from the fixed point a_0 are maximal in this case.

Figure 7.17 shows that the shift grows with increasing λ. We can explain this fact intuitively when we think about what a small or big value of λ means for the system. A small relative game strength λ implicates that density $\bar{a}$ is much bigger than density $\bar{b}$. Since there are factors of $a(\mathbf{x}, t)$ and $b(\mathbf{x}, t)$ in the game term of the hydrodynamic equations, the game interaction has a weaker effect when the value of one of the densities is small. Hence, the density shift increases for increasing values of λ.

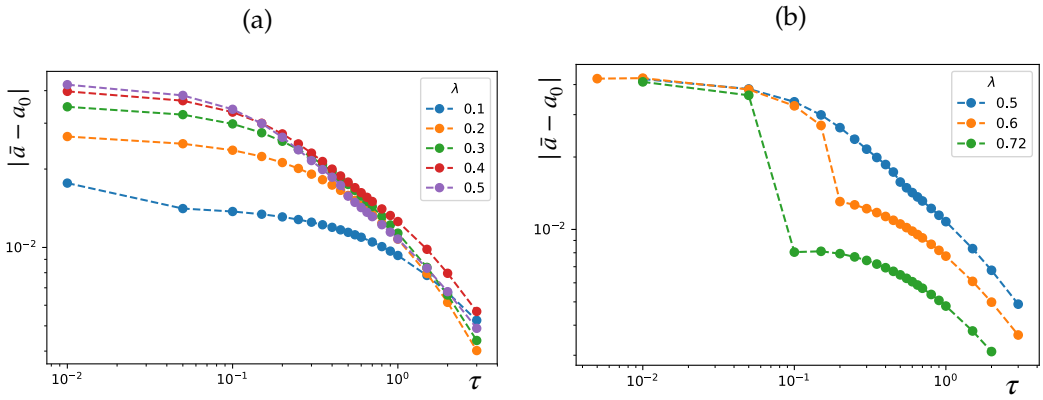

FIGURE 7.17: (a) Density shift compared to the fixed point, $|\bar{a} - a_0|$, as a function of τ for $\lambda \in 0.1, 0.2, 0.3, 0.4, 0.5$ and $\rho = 0.4$ in logarithmic scale. The magnitude of the shift is higher for small τ and high λ. (b) For $\lambda \geq 0.5$ there is a drop in the density shift as τ is increased. This effect can be explained by changes in the bifurcation diagrams.

For $\lambda \geq 0.5$ we encounter the same effect that is responsible for a jump in the delay function $d(\tau)$ from the last section: The transition density $\rho_{i,b}$ decreases for increasing values of τ and the branches of the inhomogeneous phases overlap. As long as $\rho_{i,b} > 0.4$, species A induces waves in species B and the average density $\bar{a}$ is shifted to lower values by a non-linear feedback mechanism that is due to deviations from the fixed point because of the formation of traveling spatial patterns. When the parameters λ and τ are such that $\rho_{i,b} = 0.4$ (which is the value of ρ in figure 7.17), B starts to form wave patterns on its own and the density shift jumps to lower values (see figure 7.17b for $\lambda = \{0.6, 0.72\}$). The system is then in a regime in which both A and B form traveling waves moving with similar speed, $w/a \approx u/b$, through the system. Compared to induced waves in WP1, which have small amplitudes, the separation in low and high density regions of the wave in b is more extreme when species B forms waves on its own. Since the wave pattern travels simultaneously with the wave in density a, the system is then closer to its fixed point values at every point in space. The mechanism responsible for the density shift is therefore weaker.

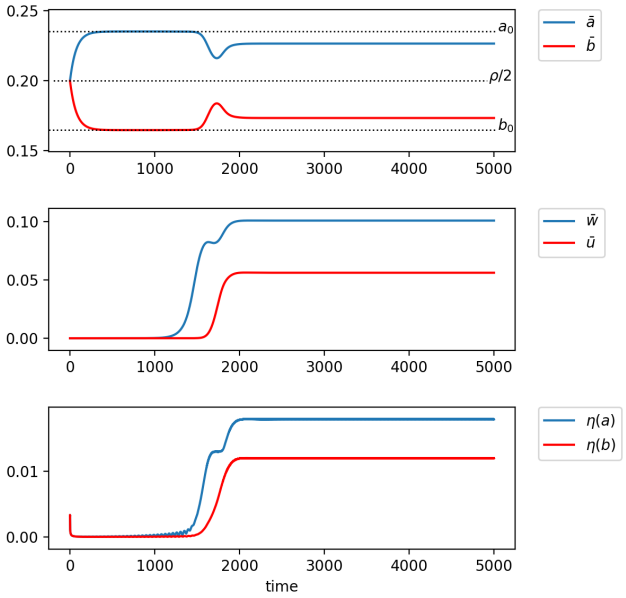

FIGURE 7.18: Time evolution of the system in WP1 for $\rho > \rho_{i,b}$. Parameters are set to $\rho = 0.4, \lambda = 0.7, \tau = 0.2$. When species A starts to form wave patterns ($\eta(a) > 0$), $\bar{a}$ ($\bar{b}$) is shifted to lower (higher) values. As soon as $\eta(b) > 0$, this effect gets damped and $\bar{a}$ ($\bar{b}$) shifts back to higher (lower) values.

This process over time is illustrated in figure 7.18 for $\rho = 0.4, \lambda = 0.7, \tau = 0.2$. First (as long as the system is still homogeneous) the average densities $\bar{a}$ and $\bar{b}$ go towards their respective fixed points. As soon as inhomogeneities start to form in species A ($\eta(a) > 0$), the mechanism of the density shift kicks in and starts to shift $\bar{a}$ ($\bar{b}$) to lower (higher) values. Then also species B starts to form wave patterns ($\eta(b) > 0$) and the effect of the density shift gets damped.

Convenient parameters to quantify the density shift for varying λ and τ are $g_b = \frac{\lambda}{1+\lambda}$ and $\tau_{total} := \tau_A + \tau_B = \tau(1+\lambda)$. Figure 7.19 shows the average density $\bar{a}$ as a function of g_b for $\rho = 0.4$ and $\tau_{total} \in \{0.01, 0.1, 0.5\}$. In the new coordinates, the fixed point a_0 follows a straight line from $a_0 = \rho$ at $g_b = 0$ to $a_0 = 0$ at $g_b = 1$. The parameters are chosen such that the system is in WP1. For $g_b = 1/2$, both species are equally strong and the density shift vanishes ($\bar{a} = a_0$). If species A is stronger than B ($g_b < 1/2$), we know that $\bar{a} < a_0$. Since the system is symmetric with respect to switching A and B, we know that the curve of $\bar{a}$ has to be symmetric about $g_b = 1/2$ (for $g_b > 1/2$, species B is stronger than A). We see in figure 7.19 that the deviation of the density from the fixed point is small for values of g_b close to zero or one, gets bigger as g_b approaches $\frac{1}{2}$ and decreases again to zero as $g_b = \frac{1}{2}$. The density shift is, as we have seen before, higher for low τ_{total}.

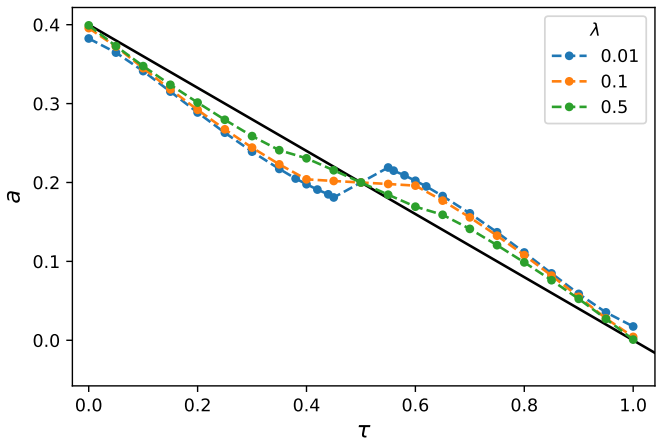

FIGURE 7.19: average density a as a function of $g_b = \frac{\lambda}{1+\lambda}$. The solid black line shows the fixed point of a (parameters: $\rho = 0.4, \tau_{total} = \tau(1+\sigma) = 0.01$). The deviation from the fixed point is maximal for values of g_b close to $\frac{1}{2}$.

7.5.1 Inversion of the game

We have seen that the activity of the particles changes the outcome of the game through a mechanism we called *density shift*. In some parameter regimes the density shift can even lead to an inversion of the game outcome. This happens when the fixed points of the densities lie relatively close to each other and the parameters are such that shift is large. Figure 7.20 shows an example of this phenomenon for the parameters $\rho = 0.4, \lambda = 0.72, \tau = 0.006$. Both species start out at $a = b = \rho/2$. In the beginning, density $\bar{a}$ increases towards its fixed point until it crosses the transition density for pattern formation. At that point waves start to form in A ($\eta(a) > 0$) and induce a wave pattern in B ($\eta(b) > 0$). Note that the wave pattern in b is almost negligible ($\eta(b) \approx 0$) since the game strength τ is small. The density shift kicks in and $\bar{a}$ decreases. In figure 7.20 this decrease (and respective increase in $\bar{b}$) is big enough such that eventually $\bar{a}$ becomes bigger than $\bar{b}$.

In the example above, the density of species A entered the regime of pattern formation and induced waves in B. After $\bar{a}$ has decreased below $\bar{b}$, the traveling wave pattern in A is still intact because of hysteresis effects. Species B on the other hand is still below the threshold density for pattern formation and is therefore enslaved to the waves of species A. We can check this claim in 7.20 when we take a look at the variations of the densities $\eta(a)$ and $\eta(b)$. The variation in the density of A, $\eta(a)$, shows that there are traveling waves in a, whereas the variation in the density of B, $\eta(b)$, is close to zero. This indicates that waves in B are very small and are thus not formed by active matter effects but are induced by the traveling waves of species A.

However, if the increase in $\bar{b}$ is big enough such that $\bar{b}$ crosses the transition threshold for pattern formation as a consequence of the density shift, we observe a new kind of state in the system (see figure 7.21): B starts forming wave patterns on its own while the traveling waves of A still persist. The density shift will now push $\bar{b}$ down to lower values and A has the upper hand again. Figure 7.21b shows snapshots of the wave profiles for different times of the system in figure 7.21. Since the wave fronts have different speeds, the faster wave of species A will pass the slower wave

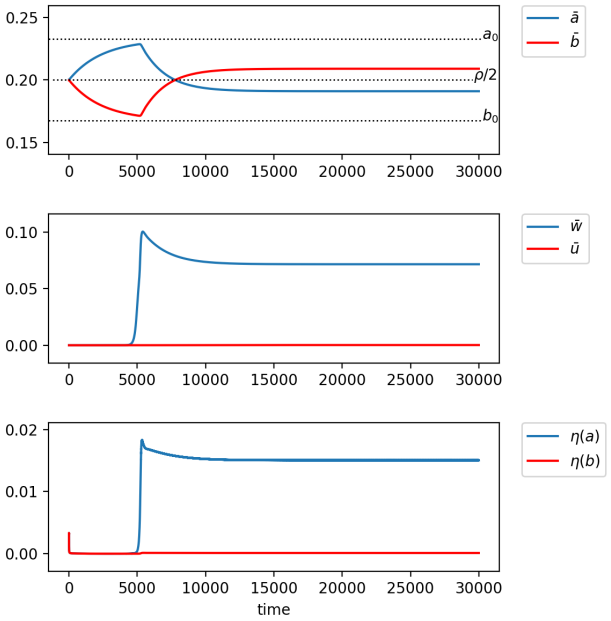

FIGURE 7.20: Spatial average of densities $\bar{a}$ and $\bar{b}$ (upper graph), polar order fields $\bar{w}$ and $\bar{u}$ (middle graph) and spatial variation of the densities $\eta(a), \eta(b)$ (lower graph) as functions of time for the parameters $\rho = 0.4, \lambda = 0.72, \tau = 0.006$. After $\bar{a}$ crosses the transition density for pattern formation ($\eta(a) > 0$), the density shift leads to a decrease (increase) of $\bar{a}$ ($\bar{b}$). This decrease (increase) is big enough to eventually invert the outcome of the game.

of species B from time to time. The non-linear feedback mechanisms during this process give rise to the oscillations in densities and polar orders we see in figure 7.21.

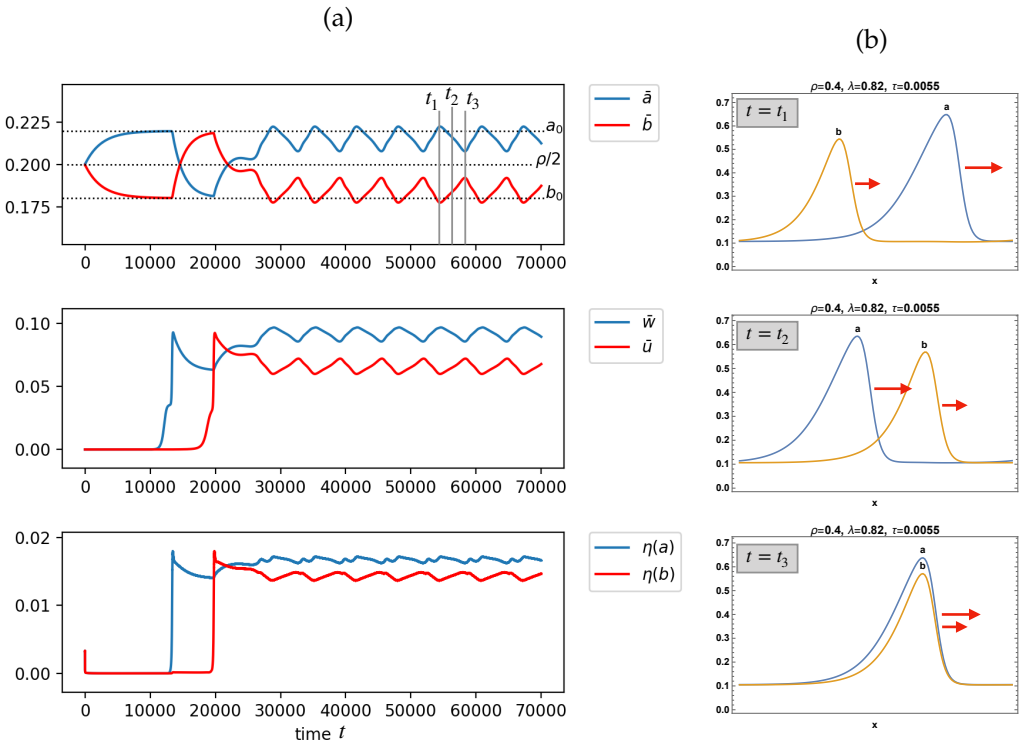

FIGURE 7.21: (a) Traveling waves in $\bar{a}$ and the subsequent density shift lead to an increase in $\bar{b}$. This increase is high enough such that $\bar{b}$ forms a wave pattern on its own and shifted back to lower values. Traveling waves in $\bar{a}$ are faster than in $\bar{b}$. The passing of wave patterns gives rise to the oscillations in densities and polar order fields. The parameters are set to $\rho = 0.4, \lambda = 0.82, \tau = 0.0055$. (b) Snapshots of wave profiles of densities a and b at consecutive times. Red arrows indicate the speed of the wave fronts. The faster wave in a passes the slower wave in b from time to time.

7.5.2 Analytic explanation of density shift

To explain the phenomenon of the density shift analytically we use the condition

$$0 = \frac{1}{V} \int d\mathbf{r}\, (\tau_A b - \tau_B a) a\, b \tag{7.10}$$

meaning that the overall game interaction integrated over all space points should cancel out. Note that this is an exact condition if the pattern is stationary $\partial_t \int d\mathbf{r}\, a = 0$, which is true for long enough times. We assume that the wave pattern is in x-direction and that it is independent of the y-direction in a system of size $L \times L$. Next, we assume that we know the shape of the wave profiles in a and b. We define the shape of the waves $s_a(x)$ and $s_b(x)$ s.t.

$$\int_0^L dx\, s_a(x) = 0, \qquad \int_0^L dx\, s_b(x) = 0, \tag{7.11}$$

Then

$$a(x) = \bar{a} + s_a(x), \qquad b(x) = \bar{b} + s_b(x) = \rho - \bar{a} + s_b(x) \tag{7.12}$$

with $\bar{a}, \bar{b}$ the average densities. Our goal is to find $\bar{a}$ (and therefore $\bar{b}$) as a function of the control parameters and the shapes of the wave profile. Note that $s_a(x)$ and $s_b(x)$ are actually determined by the control parameters, but we do not have the means to calculate that functionality. We can now use condition 7.10 to find $\bar{a}$

$$\begin{aligned} 0 &= \frac{1}{L} \int_0^L dx\, (\tau_A b(x) - \tau_B a(x)) a(x)\, b(x) \\ &= \frac{1}{L} \int_0^L dx\, (\tau_A \bar{b} - \tau_B \bar{a} + \tau_A s_b(x) - \tau_B s_a(x))(\bar{b} + s_b(x))(\bar{a} + s_a(x)). \end{aligned}$$

We know that all terms linear in s_a or s_b will per definition not contribute to the integral. Hence, when we factorize the product we get

$$\begin{aligned} 0 =& (\tau_A \bar{b} - \tau_B \bar{a}) \bar{b} \bar{a} + -\tau_B \bar{b} \int_0^L \frac{dx}{L} s_a(x)^2 + \tau_A \bar{a} \int_0^L \frac{dx}{L} s_b(x)^2 \\ &+ 2(\tau_A \bar{b} - \tau_B \bar{a}) \int_0^L \frac{dx}{L}\, s_a(x)\, s_b(x) + \int_0^L \frac{dx}{L} (\tau_A s_b(x) - \tau_B s_a(x))\, s_a(x)\, s_b(x). \end{aligned}$$

As a next step we plug in $\tau_A = \tau$ and $\tau_B = \lambda\tau$. In the following we will use the abbreviation $\int_0^L \frac{dx}{L} s_{a/b}(x) = \int s_{a/b}$ to keep the notation simple

$$\begin{aligned} 0 =& \tau\, (\bar{b} - \lambda \bar{a}) \bar{b} \bar{a} + -\lambda\tau \bar{b} \int s_a^2 + \tau \bar{a} \int s_b^2 \\ &+ 2\tau(\bar{b} - \lambda \bar{a}) \int s_a\, s_b + \int \tau(s_b - \lambda s_a)\, s_a\, s_b. \end{aligned}$$

We divide by τ, plug in $\bar{b} = \rho - \bar{a}$ and bring the first term to the left hand side to get

$$\begin{aligned} (\rho - (1+\lambda)\bar{a})(\rho - \bar{a})\bar{a} = &\left[\lambda\, \rho \int s_a^2 - 2\, \rho \int s_a s_b + \int (\lambda s_a - s_b) s_a s_b\right] + \\ &\left[-\lambda \int s_a^2 - \int s_b^2 + 2\,(1+\lambda) \int s_a s_b\right] \bar{a} \end{aligned}$$

Introducing the parameters

$$\begin{aligned} k &:= \lambda\rho \int s_a^2 - 2\rho \int s_a s_b + \int (\lambda s_a - s_b) s_a s_b \\ m &:= -\lambda \int s_a^2 - \int s_b^2 + 2(1+\lambda) \int s_a s_b \end{aligned} \tag{7.13}$$

we get the final form of the equation

$$(\rho - (1+\lambda)\bar{a})(\rho - \bar{a})\bar{a} = k + m\,\bar{a}. \tag{7.14}$$

The left hand side is the familiar replicator equation from chapter 3 with roots at $\bar{a} = \{0, \rho, \frac{\rho}{1+\lambda}\}$. The right hand side is a linear equation in $\bar{a}$ where the intersection with the vertical axis and the slope depend on the shapes of the wave patterns s_a and s_b. The solution for $\bar{a}$ is the intersection of the two graphs of left and right hand side (see figure 7.22).

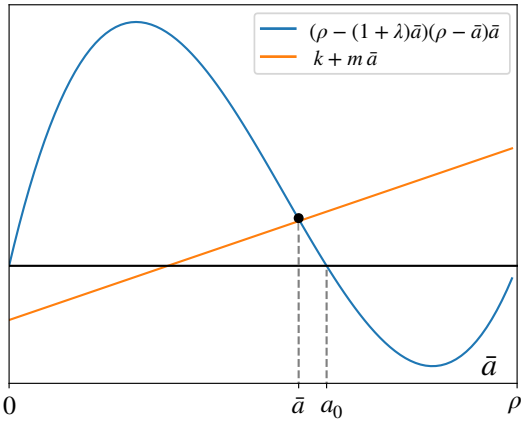

FIGURE 7.22: Graphical solution for the density shift condition. The intersection point of the two graphs is the solution for $\bar{a}$.

To check our solution, we deduce values for the wave shapes at every point of the grid from numerical calculations for different values of the control parameters and plug them into our analytic expression. The so derived solution matches perfectly the results for $\bar{a}$ coming from numerics (see figure Table 7.1). Hence, condition 7.10 provides an explanation for the underlying reasons of the density shift. For a stationary state, the game interaction has to cancel out over the whole system. Wherever $a(\mathbf{x}, t) > a_0$, the game interaction executes a "pull" to lower values and at points in space where $a(\mathbf{x}, t) < a_0$, the density is "pushed" to higher values. However, the pull towards lower values is overall stronger. This imbalance comes both from the non-linearity of the game interaction term and the asymmetric shape of the wave pattern. and leads to an effectively lowered average density.

We can now ask, under which conditions the average of the density and the fixed point match, $\bar{a} = a_0$? We plug $\bar{a} = a_0$ into 7.5.2 and use the fact that $(\tau_A b_0 - \tau_B a_0) = 0$ to get

$$0 = \int dx\, (\tau_A s_b - \tau_B s_a)(b_0 + s_b)(a_0 + s_a). \tag{7.15}$$

τ	k	m	$\bar{a}_{analytic}$	$\bar{a}_{numeric}$
0.01	0.0056	-0.014	0.224	0.224
0.2	0.0026	-0.004	0.240	0.240
0.4	0.0001	0.002	0.248	0.248
0.6	-0.0027	0.014	0.252	0.252
0.8	-0.0034	0.016	0.254	0.254
1.0	-0.0039	0.017	0.256	0.256

TABLE 7.1: Comparison of $\bar{a}$ computed analytically (with numerical input for the shape functions) vs numerically for different values of τ and $\rho = 0.4, \lambda = 0.5$. The game theoretical fixed point lies at $a_0 = 0.2\bar{6}$

This condition is obviously fulfilled for $s_a(x) = s_b(x) = 0$, which corresponds to a homogeneous system with no patterns. A second solution is

$$s_b(x) = \frac{\tau_B}{\tau_A} s_a(x) = \lambda s_a(x). \tag{7.16}$$

This corresponds to a wave in B that is the game theoretical fraction of the wave in A. If this relation holds, A and B are at the fixed point at every point in space. This result is intuitive, since if A and B are at the fixed point everywhere, the game interaction is zero everywhere.

We know that relation 7.16 can only hold if the the densities go to the fixed point at every point in space much faster than all other interactions of the system happen, hence, for $\tau \gg 1$. We will use this fact to get some general results about the average density from equation 7.14. In general the game interaction is not fast enough to bring the system to its fixed point everywhere. Instead, the wave induced in species B is delayed (as explained in the previous sections) and its amplitude is smaller than λ times the amplitude of the wave in species A. Relation 7.16 is the limiting case for big τ, so we know that

$$\begin{aligned} \int s_b^2 &\leq \lambda^2 \int s_a^2 \quad \text{and} \\ \int s_a s_b &\leq \lambda \int s_a^2. \end{aligned} \tag{7.17}$$

We will now use these relations on the right hand side of equation 7.14 for the region $\bar{a} \leq a_0 = \frac{\rho}{1+\lambda}$

$$\begin{aligned} k + m\bar{a} &= \lambda(\rho - \bar{a}) \int s_a^2 - \bar{a} \int s_b^2 - 2(\rho - (1+\lambda)\bar{a}) \int s_a s_b + \int (\lambda s_a - s_b) s_a s_b \\ &\geq \lambda(\rho - \bar{a}) \int s_a^2 - \bar{a}\lambda^2 \int s_a^2 - 2(\rho - (1+\lambda)\bar{a})\lambda \int s_a^2 \\ &= \lambda[-\rho + (1+\lambda)\bar{a}] \int s_a^2 \end{aligned} \tag{7.18}$$

where we have used in the second line that $\int dx\,(\lambda s_a - s_b) s_a s_b \geq 0$. The linear equation on the right hand side of the inequality is $k + m\bar{a}$ in the limit of big τ. Its

intersection point with the y-axis is at $-\lambda\rho\int s_a^2 < 0$ and it becomes positive at the game theoretical fixed point $\bar{a} = a_0 = \frac{\rho}{1+\lambda}$. Hence, the intersection with the left hand side of equation 7.14 is precisely at the fixed point.

The inequality 7.18 tells us, that the values of $k + m\bar{a}$ are always bigger or equal than the line leading to the fixed point solution. Hence, the intersection with the left hand side of equation 7.14 will always be at lower values of $\bar{a}$ (see figure 7.23). This shows that the unstable species, inducing the wave pattern (in our case species A), will always experience a decrease in its density (and never an increase).

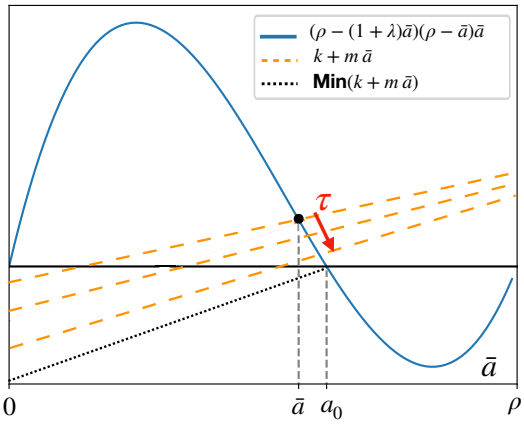

FIGURE 7.23: Graphical solution for the density shift condition. For the limit of $\tau \gg 1$, the graph of $k + m\bar{a}$ intersects the graph of the replicator equation at the fixed point, $\bar{a} = a_0 = \frac{\rho}{1+\lambda}$. The values $k + m\bar{a}$ for all τ are always higher or equal to this limiting case in the region of $\bar{a} \leq a_0 = \frac{\rho}{1+\lambda}$. Hence, the intersection of the two graphs is always at values $\bar{a} \leq a_0$ and the density shift will therefore always lead to a decrease in the density of the wave inducing species. Note that this figure is only schematically correct since actually the left hand side (blue graph) also changes with τ.

Chapter 8

Agent-based Simulation

Our hydrodynamic description left us with interesting results. In order to validate the assumptions and approximations our equations are based on, we use an agent-based simulation as a reference tool. In this chapter we will briefly discuss how the simulation was done and compare the main results with the predictions of the hydrodynamic description. For a detailed description of the simulation and its results we refer to the Master Thesis of Michael Obermüller [38].

8.1 Microscopic agent-based Model

The agent-based model aims to reproduce the microscopic model described in section 4.1 as far as possible. We base it on a model of active matter introduced by Bertin et al. [8]. The implementation and adaptation to include game theory was done by Michael Obermüller, whose approach we will briefly describe below. A detailed explanation of how the simulation is implemented efficiently for many particle systems can be found in [38].

N particles move on a two-dimensional plane of size $L \times L$. Each particle belongs to either of the species A or B, and is characterized by its position $\mathbf{r}_i$ and its orientation θ_i. Every particle moves with the fixed speed v_0. Time is discretized in steps of dt and the position of particles follows the update rule $\mathbf{r}_i^{t+dt} = \mathbf{r}_i^t + v_0\mathbf{e}(\theta_i^t)dt$.

Self-diffusion and collisions of particles are implemented by the following update rules. We define an *active matter vicinity* $\mathcal{A}_i^t$ for every particle as a disk with radius d_0 around its position $\mathbf{r}_i$. If there are no other particles at time t in $\mathcal{A}_i^t$, the particle self-diffuses with a probability p_{diff}. Self-diffusion means that the particle changes its orientation by a value η_0, which is a stochastic variable drawn from a flat distribution of range $(-h_0\pi, h_0\pi]$, $h_0 \in [0,1]$. We can connect h_0 with the standard deviation σ_0 from the analytic description via $\sigma_0 = h_0\frac{\pi}{\sqrt{3}}$. If on the other hand there are other particles in the active matter vicinity, all of them align with the orientational average of all particles in $\mathcal{A}_i^t$. To account for mistakes during the alignment process, we add a stochastic noise η, which is given by a flat distribution in the range $(-h\pi, h\pi]$, $h \in [0,1]$ and connected to the standard deviation $\sigma = h\frac{\pi}{\sqrt{3}}$. Noises are uncorrelated in time and independently drawn for each particle. The new direction at time $t + dt$

is therefore calculated by

$$\theta_j^{t+dt} = \begin{cases} \arg\left(\sum_{k\in\mathcal{A}_j^t} e^{i\theta_k t}\right) + \eta_j^t & \text{if } \mathcal{A}_j^t \neq \{j\} \\ \theta_j^t + \eta_{0,j}^t & \text{with probability } p_{diff}dt \text{ and if } \mathcal{A}_j^t = \{j\} \\ \theta_j^t & \text{else} \end{cases} \tag{8.1}$$

Besides the active matter interaction, we also need to implement the game interaction of the Snowdrift game. Particles should switch their species if it is beneficial for them. In order to do so, we define a *game theory vicinity* $\mathcal{G}_j^t$ as a disk around particle j with radius d_{gt}. In the analytic description, the time evolution of densities a and b were proportional to the factor $\pm\tau(b - \lambda a)$. We translate this for the agent-based model in the following way. In a first step the number of particles of species A, $N_{A,j}^t$, and B, $N_{B,j}^t$, in the game theory vicinity of particle j are counted. We can then define *local densities* of species A and B as $a_j^t := \frac{N_{A,j}^t}{N_{A,j}^t + N_{B,j}^t}$ and $b_j^t := \frac{N_{B,j}^t}{N_{A,j}^t + N_{B,j}^t}$. Then particle j switches its species with probability p_j^t given by

$$p_j^t = \begin{cases} -\tau(b_j^t - \lambda a_j^t)dt & \text{if } j \text{ is of species } A \text{ and } (b_j^t - a_j^t\lambda) < 0 \\ \tau(b_j^t - \lambda a_j^t)dt & \text{if } j \text{ is of species } B \text{ and } (b_j^t - a_j^t\lambda) > 0. \end{cases} \tag{8.2}$$

If a particle switches species, it loses its directional information and flies in a random direction afterwards until it aligns with partners of its new species again. This is done to prevent directional information transfer between the two species [38].

8.2 Results and comparison with the Hydrodynamic treatment

In analogy to the analysis of the hydrodynamic equations, we use three parameters of the system as free control parameters: The overall density, which is defined as $\rho = NL^{-2}$, the relative game strength λ and the overall game strength τ, which has to be adapted by a factor to incorporate the game theory radius d_{gt} [38]. In some cases it is convenient to replace the density control parameter with the noise parameter σ, which we tie to the diffusive noise σ_0, so $\sigma_0 = \sigma$. In section 6.2 we argued that it is a matter of taste whether to use ρ or σ as free control parameter, since increasing density and decreasing noise have the same qualitative effects. All other parameters of the simulation are kept at fixed values.

In a first step we compare the simulation for turned off game interaction ($\tau = 0$) with previous agent-based models of active matter done by Bertin et al. [8]. As in previous studies, the simulation finds that the system exhibits three distinct phases: An isotropic state for low densities (high noise), a state of homogeneous motion for high densities (low noise) and in between a state with wave patterns that move through the system. Measurements of the onset of order in parameter space (ρ, σ) are in almost perfect agreement with the results of [8].

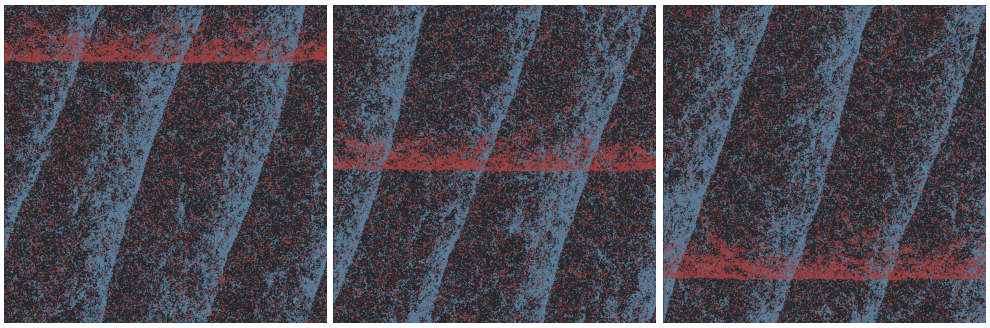

FIGURE 8.1: Snapshots of the 2D system of size $L = 512$ at successive time steps. Blue dots are particles of species A, red dots particles of species B. Parameters are set to $\rho = N/L^2 = 0.61, \sigma = \sigma_0 = 0.5$, $\tau = 0$ (the species are uncoupled) and $\lambda = 0.5$ in the sense that the densities of the two species are $a = \frac{\rho}{1+\lambda} \approx 0.41$ and $b = \frac{\lambda\rho}{1+\lambda} \approx 0.2$. Both species form wave patterns that move uncoupled through the system: The wave in A moves diagonally to the bottom right while the wave in B moves downwards. The wave pattern in A is more distinct and broader than the one in species B since density a is higher than density b.

As long as the game interaction is turned off, both species are not coupled to each other. Figure 8.1 shows snapshots of the 2D system of size $L = 512$ at successive time steps. The overall density is $\rho = N/L^2 = 0.61$ and the game parameters are set to $\tau = 0$ (both species are uncoupled) and $\lambda = 0.5$ in the sense that we initialize the densities of the two species at the fixed points given by $a_0 = \frac{\rho}{1+\lambda} \approx 0.41$ and $b_0 = \frac{\lambda\rho}{1+\lambda} \approx 0.2$. Both species form wave patterns. The wave in A is more distinct and broader than the one in species B since density a is higher than b. Since the two species are uncoupled, the wave patterns move in arbitrary directions.

In a next step we switch the game interaction on to check which predictions of the hydrodynamic equations can be verified by the simulations. As a starting point we implement that half the population size is of species A and the other half of species B. The game interaction between particles instantly leads to the switching of species until the game theoretical fixed point is (almost) reached (we will come back to why the fixed point is not reached exactly at the end of this section). We will keep λ below or equal to one w.l.o.g. for all simulations.

As a first result we can confirm the existence of the different phases described in section 7.2. For low overall densities the particles move in random directions, as in the simulations without game interaction. The average over all orientations is zero in this state. This state is illustrated by figure 8.2a.

For increasing densities the species start to form cluster (patches of higher densities) that move through the system. When the overall density is high enough these patches combine and form bands of ordered particles that move in the direction of macroscopic order with a velocity of the order of magnitude of the particle velocity v_0. This wave consists of particles of both species. A snapshot of a typical wave is shown in figure 8.2b. In the high density wave band the particles of the two species are separated in stripes along the wave front. This phenomenon is due to the implementation of locality of the game interaction. See [38] for a detailed description of

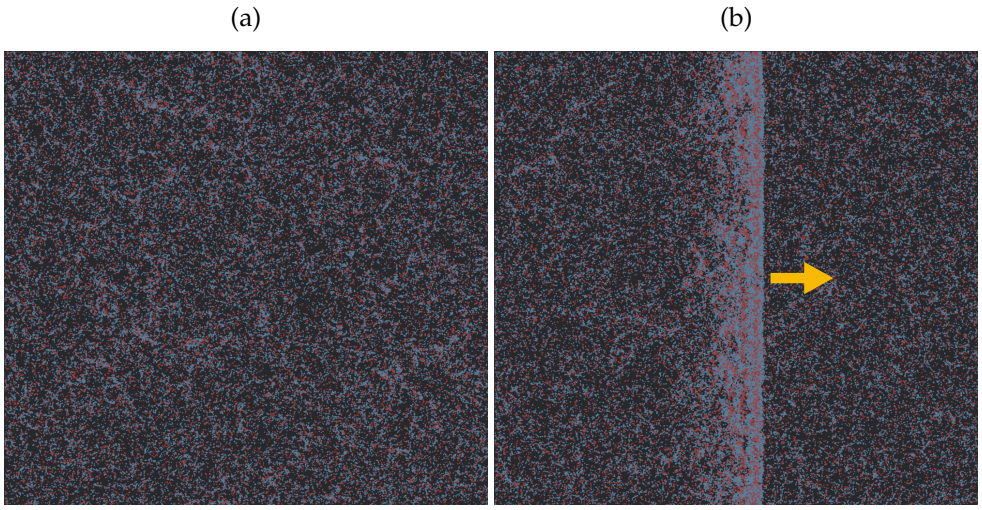

FIGURE 8.2: (a) Isotropic phase of the system. Blue dots are particles of species A, red dots particles of species B. Parameters are set to $\rho = N/L^2 = 0.3, \sigma = \sigma_0 = 0.5$, $\tau = 0.4$ and $\lambda = 0.5$. (b) For $\rho = 0.46$ particles of both species form a wave pattern, meaning a high density band of ordered particles. The wave front moves in the direction of macroscopic order (indicated by the yellow arrow).

this effect. Figure 8.3 shows the corresponding wave profile of the number of A- and B-particles, N_A and N_B, and a measure of the polar order fields w,u. The profiles of the distribution of particles in space were computed by splitting up the horizontal axes into small pieces dx and then counting all particles positioned in a slice $dx \times L$. For the polar order wave profiles the velocities of all particles in $dx \times L$ were added and divided by the number of particles in the particular slice. The figure shows the fraction of this value compared to the maximal possible order parameter $v_0\rho$. The wave profiles show the characteristic steep wave front and fall off less steep in the back. The background of the wave band is approximately isotropic as can be seen by the low and volatile values of w and u in the front and rear of the wave band in figure 8.3.

For $\lambda = 1$ the number of A-particles, N_A, equals the number of B-particles, N_B. In the analytic description the threshold density at the onset of order was twice the value of the threshold density for a one-species system. In the simulation the threshold density lies a little higher since the directional information is destroyed when a particle switches species. This acts as an additional noise in the system when a particle switches its species back and forth [38]. We observe solitonic waves as well as periodic solutions. For increasing densities the waves get broader as in the hydrodynamic description. There is a transition to a homogeneous state when the high density regions of the wave take up almost all of the system size.

If we turn off the game interaction but keep the ratios of A- and B-particles fixed at $\rho/2$, the species are no longer coupled to each other. We therefore observe independent traveling wave bands of both species that can move in arbitrary directions with an arbitrary offset respective to each other. All of these findings are in qualitative agreement with the hydrodynamic predictions.

For $\lambda < 1$ we found in the hydrodynamic description, that species A induces waves in species B for $\rho_{t,a} < \rho < \rho_{t,b}$. A simulation in the analogue parameter regime shows

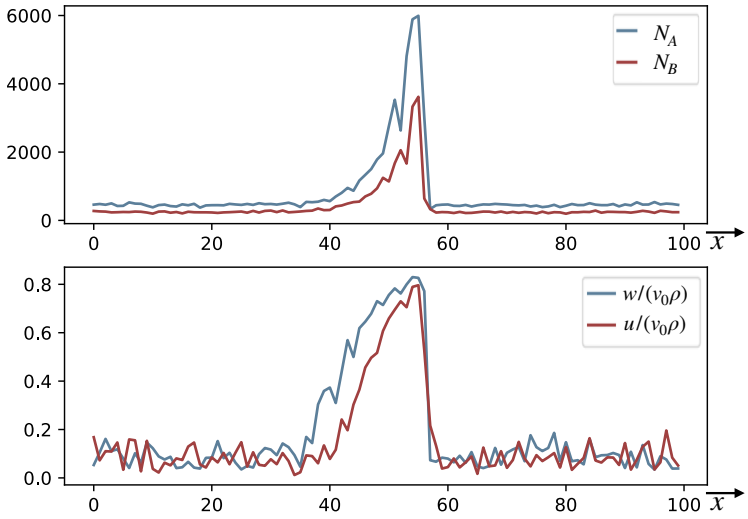

FIGURE 8.3: Wave profiles of different parameters in space. The system is in a wave state as shown in figure 8.2b. *Upper graph*: Wave profile of the number of particles of species A and B, N_A and N_B. *Lower Graph*: Fraction of the order fields w,u compared to the maximal value $v_0\rho$. The wave profiles have the characteristic steep wave front and fall off less steep in the back. The background of the wave band is approximately isotropic.

a wave pattern in A as well as in B that move simultaneous through the system. We can check that the wave in B is induced by the game interaction by comparing this result to a simulation without game interaction, but with the same ratios of A- and B-particles. Indeed, we find that B-particles are in an isotropic state in this case and only A-particles show a wave pattern. Hence, we can confirm the process of wave induction through game interaction and therefore the existence of the phase WP1.

Using this reasoning we can also confirm the induction of waves in A through species B, WP2, for densities high enough in certain parameter regimes. In between the two inhomogeneous states of the system we find a state with homogeneous order in A and random motion in B. The simulations also confirm the state of homogeneous order in both species for high density or low noise values.

We can thus in general confirm the existence of all of the five phases in qualitative agreement with hydrodynamic predictions. To find the different phases we used a noise sweep instead of increasing the value of the overall density ρ since it turned out to be the more convenient tool for the simulations.

The simulations do not confirm the density shift that the hydrodynamic treatment predicted. We do observe a small shift in the density of the stronger species to lower values (and a corresponding shift of the other species to higher values), but this shift is too small to match the hydrodynamic predictions. We suspect that it is due to a different mechanism, which we will briefly explain at the end of this section. Since this second mechanism is always present, it is difficult to find a measure of the density shift that is only due to the mechanism described in section 7.5 and we did not find a satisfying way to do so. It would be subject of further investigations to

find out whether it is nevertheless possible to measure the effect of a density shift in the agent-based simulation.

An other possibility for future investigations is to try different implementations of the game interaction in the simulation. The density shift in the hydrodynamic description is due to the non-linearity of the interaction term. This non-linearity is in the simulations so far only reflected in the calculations of the local densities. It is possible that a different game interaction rule between particles that has a stronger non-linear character might confirm the predictions of a density shift.

As mentioned above, we also find new effects of the game interaction in the agent-based simulation, that can not occur in continuous descriptions. In the equations, we assumed that game interactions depend on local densities. To transfer this assumption to agent-based models, we had to define a notion of "local" densities as relative numbers of particles that are not farther away than a game interaction radius d_{gt}. In order to get meaningful averages, d_{gt} has to be chosen sufficiently large (we chose $d_{gt} = 10 \cdot d_0$). In the Snowdrift game it is favourable for each particle to have as many particles of the other species in its game interaction range as possible. This results in the formation of patterns of the order of magnitude of the size of d_{gt}. This mechanism is also responsible for a shift in the densities, that makes it hard to measure the shift due to the mechanism described in section 7.5. We have developed a theory that can explain the formation of patterns and the pattern sizes using geometric reasoning. For an outline of this theory and detailed results of the pattern formation we refer to the Master thesis of Michael Obermüller [38].

Chapter 9

Summary

In this thesis we developed and analyzed the description of a system that combines the evolutionary dynamics of game theory with active motion. The system is characterized by the interplay between mobility in a spatially extended system and the locality of game theoretical interactions.

In the field of active matter one usually describes systems of particles that align according to collision rules and have a fixed number of particles [8, 40, 11]. An extension of this model to two species coupled through a game interaction that locally changes population numbers can change the properties of an active system and give rise to a range of new effects that are interesting from an active matter perspective.

To our knowledge there exist no studies about the influence of self-propelled motion on systems of interacting particle species. There is a number of systems in nature for which this interplay is relevant. Examples include different types of microorganisms [14, 12, 15, 16] that can exhibit collective motion and are in competition with other microbes, which can be understood in the language of game theory. Previous studies have shown that mobility, like diffusion, can change the outcome of cooperator-defector games in the sense that the population numbers are different to a well-mixed scenario [26, 37, 31]. It is therefore plausible that other types of mobility can also have an influence. In this thesis we asked the question of how the activity of particles changes the outcome of a Snowdrift scenario in a two-species system.

We defined a microscopic model system and used the framework of a kinetic Boltzmann approach to describe the system on a coarse-grained level. The Boltzmann equations for active matter are a well-established and robust tool [8, 7, 40] which we extended to include interactions between the two species. The interaction term is inspired from the replicator equations for the Snowdrift game scenario. It depends on local densities and lets particles switch species if it is advantageous. We coarse-grained the Boltzmann equations following a procedure developed by Bertin et al. [8] in which higher order correlations are truncated according to a scaling scheme. This coarse-graining led to four coupled hydrodynamic equations for the macroscopic quantities of the system: The densities and polar order fields of both species.

The coarse-grained hydrodynamic equations for our system have two main new features compared to the usual hydrodynamic equations of active matter. One new feature is that the individual densities are not conserved. They are coupled via a nonlinear game term that acts as a source- or sink-term depending on the local densities of both species. The conserved quantity of the system is the average of the overall density ρ, which plays the role of a control parameter. The second new property is that the momentum fields are not only coupled to their corresponding density field

but to the densities of both species. Fluctuations in one of the densities can therefore lead to an instability in the momentum fields of both species.

Besides the overall density ρ we identified the overall strength of the coupling between species, τ, and the relative strength of the two species, λ, as control parameters.

The results from linear stability analysis and numeric solutions of the hydrodynamic equations suggest that we can distinguish between up to five different phases, depending on the control parameters. There are (up to) three homogeneous phases (isotropic, homogeneous motion in the stronger species and homogeneous motion in both species) and two inhomogeneous phases. We find ordered bands of high density in both species in the inhomogeneous phases that travel simultaneously through the system on an isotropic background. Wave patterns at the onset of ordered motion are a typical feature of active matter systems [8]. The interesting new feature in our system is, that a wave pattern in one of the species gives rise to a non-linear feedback mechanism that induces a wave in the respective other species. An increase in the overall density first leads to an increase in wave amplitudes and then to a broadening of the wave patterns, while the low density background stays approximately unchanged. We have confirmed the existence of the five phases and the mechanism of wave induction through the game interaction in agent-based simulations.

The regimes of the different phases depend on all three control parameters. We find that the traveling wave phases typically exist in parameter regions wider than the linear instability domain of the homogeneous states. This result implies that there are regions in parameter space in which two stable solutions exist. In these regions the homogeneous solutions are sensitive to fluctuations. This subcritical nature of the bifurcation implies discontinuous transitions between the different phases.

The system exhibits all five distinct phases with discontinuous transitions between them only if one species is sufficiently stronger than the other one. For game parameters leading to more balanced ratios of densities, the two inhomogeneous phases merge and the transition between them becomes continuous. A third possibility realized in certain parameter regimes is that the stable branches of the inhomogeneous phases overlap, which leads to the existence of tristable states (one stable homogeneous solution and two stable inhomogeneous, traveling-wave solutions).

The fact that wave patterns in one species induce patterns in the other species leads to a couple of interesting effects. Since the waves travel through the system and the game interaction can only react within a time proportional to the inverse of the coupling of the game term, τ^{-1}, there is a time delay of the induced wave compared to the original wave. We measured this delay as a function of the game parameters and found that the delay is stronger, the smaller the relative and the total game strength is.

A second effect of the formation of waves is a feedback mechanism that reduces the average density of the inducing species (and increases the density of the other species accordingly) compared to a well-mixed system. In some parameter regimes this effect can even lead to an inversion of the game. We also found a state of the system in which the density shift leads to waves in both species that travel with different speeds. The faster wave passes the slower one periodically, which leads to an oscillatory behaviour of the average densities. For future studies it would be interesting to further explore the phenomenon of the density shift and its consequences like the emergence of new states of the system. An other task for the future is to try

to confirm the density shift with agent-based simulations, which we were not able to do so far.

We developed an analytic explanation for the mechanism of the density shift by studying the implications of the condition that average densities are constant in time when a stationary state is reached in the system. This condition only holds if the game interaction integrated over the whole system cancels out. We found that the density shift can be explained by the combination of the non-linearity of the game interaction and the asymmetric shape of the wave pattern.

We saw that the combination of an active matter system with an interaction inspired by game theory leads to a range of new and interesting phenomena. The implementation of the game interaction we chose for this thesis leads to a "pull" towards the game theoretical fixed point of the Snowdrift game at every point in space. It is therefore not suitable to describe phenomena like the formation of clusters consisting of only one species that have been reported for different spatially extended models of evolutionary game theory [26, 37, 31]. In future studies it could be interesting to develop and investigate other implementations of a game theoretical interaction in self-propelled systems.

Acknowledgements

Zunächst danke ich Prof. Frey, der mein Interesse für die statistische Physik bereits in seinen Vorlesungen weckte. Während meiner Masterarbeit konnte ich von seinem breiten physikalischen Wissen und klaren Blick für physikalisch interessante Fragestellungen profitieren und fühlte mich stets sehr wohl in unseren Gesprächen.

Vielen Dank auch an unsere Betreuer Lenz und Jonas, die immer ein offenes Ohr für uns und für jegliche Probleme während der Masterarbeit hatten. Eure lockere Art, die stets entspannte Atmosphäre und die Freiheit, die ihr uns in der Themenfindung gelassen habt, haben sehr zu der schönen Zeit am Lehrstuhl beigetragen. Ich bedanke mich auch für die Korrekturen und Verbesserungsvorschläge für diese Arbeit.

Mein spezieller Dank geht an Michi, mit dem ich zusammen an diesem Masterarbeitsprojekt gearbeitet habe. Danke für die vielen Diskussionen, deine Hilfe in allen physikalischen und technischen Problemen und vor allem auch für die moralische Unterstützung durch alle Hochs und Tiefs (und ein bisschen auch fürs Pflanzen gießen...).

Das Physikstudium wäre ohne die großartigen Freunde, die ich währenddessen kennengelernt habe, nie so schön gewesen. Mit euch waren sogar die langen Stunden in der Bib eine lustige und schöne Zeit. Danke für all die Kaffeepausen, Diskussionen, Suppenabende, Kastenläufe und alles andere.

Ich möchte auch all meinen anderen langjährigen, lieben Freunden und meinem Freund Simon danken. Vielen Dank fürs Zuhören, Motivieren und euer Freuen wenns was zu feiern gibt.

An meine tolle Familie: Danke für eure bedingungslose Unterstützung, Liebe und das Vertrauen, das ihr immer in mich hattet.

Bibliography

[1] R. Aditi Simha and Sriram Ramaswamy. "Hydrodynamic Fluctuations and Instabilities in Ordered Suspensions of Self-Propelled Particles". In: *Phys. Rev. Lett.* 89 (5 July 2002), p. 058101. DOI: 10.1103/PhysRevLett.89.058101.

[2] Igor S. Aranson and Lev S. Tsimring. "Pattern formation of microtubules and motors: Inelastic interaction of polar rods". In: *Phys. Rev. E* 71 (5 May 2005), p. 050901. DOI: 10.1103/PhysRevE.71.050901.

[3] Igor S. Aranson et al. "Model for dynamical coherence in thin films of self-propelled microorganisms". In: *Phys. Rev. E* 75 (4 Apr. 2007), p. 040901. DOI: 10.1103/PhysRevE.75.040901.

[4] R Axelrod and WD Hamilton. "The evolution of cooperation". In: *Science* 211.4489 (1981), pp. 1390–1396. ISSN: 0036-8075. DOI: 10.1126/science.7466396.

[5] Iztok Lebar Bajec and Frank H. Heppner. "Organized flight in birds". In: *Animal Behaviour* 78.4 (2009), pp. 777 –789. ISSN: 0003-3472. DOI: https://doi.org/10.1016/j.anbehav.2009.07.007.

[6] Aparna Baskaran and M. Cristina Marchetti. "Enhanced Diffusion and Ordering of Self-Propelled Rods". In: *Phys. Rev. Lett.* 101 (26 Dec. 2008), p. 268101. DOI: 10.1103/PhysRevLett.101.268101.

[7] Eric Bertin, Michel Droz, and Guillaume Grégoire. "Boltzmann and hydrodynamic description for self-propelled particles". In: 74.2 (Aug. 2006), p. 022101. DOI: 10.1103/PhysRevE.74.022101.

[8] Eric Bertin, Michel Droz, and Guillaume Grégoire. "Hydrodynamic equations for self-propelled particles: microscopic derivation and stability analysis". In: *Journal of Physics A Mathematical General* 42.44 (Nov. 2009), p. 445001. DOI: 10.1088/1751-8113/42/44/445001.

[9] T. Butt et al. "Myosin motors drive long range alignment of actin filaments." In: *The Journal of biological chemistry* 285 (7 2010), 4964–4974. DOI: 10.1074/jbc.M109.044792.

[10] H. Chaté et al. "Modeling collective motion: variations on the Vicsek model". In: *The European Physical Journal B* 64.3 (Aug. 2008), pp. 451–456. ISSN: 1434-6036. DOI: 10.1140/epjb/e2008-00275-9.

[11] Hugues Chaté et al. "Collective motion of self-propelled particles interacting without cohesion". In: *Phys. Rev. E* 77 (4 Apr. 2008), p. 046113. DOI: 10.1103/PhysRevE.77.046113.

[12] A. Czirók, M. Matsushita, and T. Vicsek. "Theory of periodic swarming of bacteria: Application to Proteus mirabilis". In: *Phys. Rev. E* 63 (3 2001), p. 031915. DOI: 10.1103/PhysRevE.63.031915.

[13] András Czirók, H Eugene Stanley, and Tamás Vicsek. "Spontaneously ordered motion of self-propelled particles". In: *Journal of Physics A: Mathematical and General* 30.5 (Mar. 1997), pp. 1375–1385. DOI: 10.1088/0305-4470/30/5/009.

[14] András Czirók et al. "Formation of complex bacterial colonies via self-generated vortices". In: *Phys. Rev. E* 54 (2 1996), pp. 1791–1801. DOI: 10.1103/PhysRevE.54.1791.

[15] Alma Dal Co, Simon van Vliet, and Martin Ackermann. "Emergent microscale gradients give rise to metabolic cross-feeding and antibiotic tolerance in clonal bacterial populations". In: *bioRxiv* (2019). DOI: 10.1101/534149.

[16] Alma Dal Co et al. "Short-range interactions govern cellular dynamics in microbial multi-genotype systems". In: *bioRxiv* (2019). DOI: 10.1101/530584.

[17] R M Dawes. "Social Dilemmas". In: *Annual Review of Psychology* 31.1 (1980), pp. 169–193. DOI: 10.1146/annurev.ps.31.020180.001125.

[18] Jonas Denk et al. "Active Curved Polymers Form Vortex Patterns on Membranes". In: *Phys. Rev. Lett.* 116 (17 Apr. 2016), p. 178301. DOI: 10.1103/PhysRevLett.116.178301.

[19] Julien Deseigne et al. "Vibrated polar disks: spontaneous motion, binary collisions, and collective dynamics". In: *Soft Matter* 8 (20 2012), pp. 5629–5639. DOI: 10.1039/C2SM25186H.

[20] Christopher Dombrowski et al. "Self-Concentration and Large-Scale Coherence in Bacterial Dynamics". In: *Phys. Rev. Lett.* 93 (9 Aug. 2004), p. 098103. DOI: 10.1103/PhysRevLett.93.098103.

[21] Stanley J. Farlow. *Partial Differential Equations for Scientists and Engineers*. Dover Publications, 1993.

[22] Erwin Frey and Tobias Reichenbach. "Bacterial Games". In: Feb. 2011, pp. 297–329. DOI: 10.1007/978-3-642-18137-5_13.

[23] W.D. Hamilton. "The genetical evolution of social behaviour. I". In: *Journal of Theoretical Biology* 7.1 (1964), pp. 1 –16. ISSN: 0022-5193. DOI: https://doi.org/10.1016/0022-5193(64)90038-4.

[24] John C. Harsanyi and Reinhard Selten. *A General Theory of Equilibrium Selection in Games*. 1st ed. Vol. 1. The MIT Press, 1988. DOI: 0262582384.

[25] Michael P. Hassell, Hugh N. Comins, and Robert M. May. "Species coexistence and self-organizing spatial dynamics". In: *Nature* 370 (July 1994), pp. 290–292. DOI: 10.1038/370290a0.

[26] Christoph Hauert and Michael Doebeli. "Spatial structure often inhibits the evolution of cooperation in the snowdrift game". In: *Nature* 428 (Apr. 2004), pp. 643–646. DOI: 10.1038/nature02360.

[27] Y. Hayakawa. "Spatiotemporal dynamics of skeins of wild geese". In: *EPL (Europhysics Letters)* 89.4 (2010), p. 48004. DOI: 10.1209/0295-5075/89/48004.

[28] Charlotte K. Hemelrijk and Hanspeter Kunz. "Density distribution and size sorting in fish schools: an individual-based model". In: *Behavioral Ecology* 16.1 (Feb. 2005), pp. 178–187. ISSN: 1045-2249. DOI: 10.1093/beheco/arh149.

[29] Josef Hofbauer and Karl Sigmund. *Evolutionary Games and Population Dynamics*. Cambridge University Press, 1998. DOI: 10.1017/CBO9781139173179.

[30] L. Huber et al. "Emergence of coexisting ordered states in active matter systems". In: *Science* 361.6399 (2018), pp. 255–258. ISSN: 0036-8075. DOI: 10.1126/science.aao5434.

[31] T. Killingback, M. Doebeli, and N. Knowlton. "Variable investment, the Continuous Prisoner's Dilemma, and the origin of cooperation". In: *Proceedings Biological sciences* 266 (1430 1999), 1723–1728. DOI: 10.1098/rspb.1999.0838.

[32] M. C. Marchetti et al. "Soft Active Matter". In: *arXiv e-prints*, arXiv:1207.2929 (July 2012).

[33] P. C. Martin, O. Parodi, and P. S. Pershan. "Unified Hydrodynamic Theory for Crystals, Liquid Crystals, and Normal Fluids". In: *Phys. Rev. A* 6 (6 Dec. 1972), pp. 2401–2420. DOI: 10.1103/PhysRevA.6.2401.

[34] Robert M. May. *Stability in ecosystems: some comments*. Springer Netherlands, 1975.

[35] Roger B. Myerson. "Nash Equilibrium and the History of Economic Theory". In: *Journal of Economic Literature* 37.3 (1999), pp. 1067–1082. DOI: 10.1257/jel.37.3.1067.

[36] John von Neumann and Oskar Morgenstern. *Theory of Games and Economic Behaviour*. 1944.

[37] Martin A. Nowak and Robert M. May. "Evolutionary games and spatial chaos". In: *Nature* 359 (Oct. 1992). DOI: 10.1038/359826a0.

[38] Michael Obermüller. "Game Theory and Active matter". In: *Master Thesis, Department of Statistical Physics at LMU Munich* (2019).

[39] Fernando Peruani et al. "Collective Motion and Nonequilibrium Cluster Formation in Colonies of Gliding Bacteria". In: *Phys. Rev. Lett.* 108 (9 Feb. 2012), p. 098102. DOI: 10.1103/PhysRevLett.108.098102.

[40] A. Peshkov et al. "Boltzmann-Ginzburg-Landau approach for continuous descriptions of generic Vicsek-like models". In: *The European Physical Journal Special Topics* 223.7 (June 2014), pp. 1315–1344. ISSN: 1951-6401. DOI: 10.1140/epjst/e2014-02193-y.

[41] Anton Peshkov et al. "Continuous Theory of Active Matter Systems with Metric-Free Interactions". In: *Phys. Rev. Lett.* 109 (9 Aug. 2012), p. 098101. DOI: 10.1103/PhysRevLett.109.098101.

[42] Anton Peshkov et al. "Nonlinear Field Equations for Aligning Self-Propelled Rods". In: *Phys. Rev. Lett.* 109 (26 Dec. 2012), p. 268701. DOI: 10.1103/PhysRevLett.109.268701.

[43] Sriram Ramaswamy. "The Mechanics and Statistics of Active Matter". In: *Annual Review of Condensed Matter Physics* 1.1 (2010), pp. 323–345. DOI: 10.1146/annurev-conmatphys-070909-104101.

[44] Tobias Reichenbach, Mauro Mobilia, and Erwin Frey. "Mobility promotes and jeopardizes biodiversity in rock–paper–scissors games". In: *Nature* 448 (Aug. 2007), 1046–1049. DOI: 10.1038/nature06095.

[45] Volker Schaller et al. "Polar pattern formation: hydrodynamic coupling of driven filaments". In: *Soft Matter* 7 (7 2011), pp. 3213–3218. DOI: 10.1039/C0SM01063D.

[46] Volker Schaller et al. "Polar patterns of driven filaments". In: *Nature* 467.73 (Sept. 2010).

[47] John Maynard Smith. *Evolution and the Theory of Games*. Cambridge University Press, 1982. DOI: 10.1017/CBO9780511806292.

[48] A. Snezhko et al. "Statistics of Active Transport in Xenopus Melanophores Cells". In: *Biophysical journal* 99 (10 2010), 3216–3223. DOI: 10.1016/j.bpj.2010.09.065.

[49] B. Szabó et al. "Phase transition in the collective migration of tissue cells: Experiment and model". In: *Phys. Rev. E* 74 (6 Dec. 2006), p. 061908. DOI: 10.1103/PhysRevE.74.061908.

[50] Florian Thüroff, Christoph A. Weber, and Erwin Frey. "Numerical Treatment of the Boltzmann Equation for Self-Propelled Particle Systems". In: *Phys. Rev. X* 4 (4 Nov. 2014), p. 041030. DOI: 10.1103/PhysRevX.4.041030.

[51] John Toner and Yuhai Tu. "Flocks, herds, and schools: A quantitative theory of flocking". In: *Phys. Rev. E* 58 (4 Oct. 1998), pp. 4828–4858. DOI: 10.1103/PhysRevE.58.4828.

[52] John Toner and Yuhai Tu. "Long-Range Order in a Two-Dimensional Dynamical XY Model: How Birds Fly Together". In: *Phys. Rev. Lett.* 75 (23 Dec. 1995), pp. 4326–4329. DOI: 10.1103/PhysRevLett.75.4326.

[53] John Toner, Yuhai Tu, and Sriram Ramaswamy. "Hydrodynamics and phases of flocks". In: *Annals of Physics - ANN PHYS N Y* 318 (July 2005), pp. 170–244. DOI: 10.1016/j.aop.2005.04.011.

[54] Tamás Vicsek et al. "Novel Type of Phase Transition in a System of Self-Driven Particles". In: *Phys. Rev. Lett.* 75 (6 Aug. 1995), pp. 1226–1229. DOI: 10.1103/PhysRevLett.75.1226.

[55] Tamás Vicsek and Anna Zafeiris. "Collective motion". In: *Physics Reports* 517.3 (2012), pp. 71 –140. ISSN: 0370-1573. DOI: https://doi.org/10.1016/j.physrep.2012.03.004.

[56] A. Ward et al. "Quorum decision-making facilitates information transfer in fish shoals". In: *Proceedings of the National Academy of Sciences of the United States of America* 105 (19 2008), 6948–6953. DOI: 10.1073/pnas.0710344105.

[57] Christoph A Weber, Florian Thüroff, and Erwin Frey. "Role of particle conservation in self-propelled particle systems". In: *New Journal of Physics* 15.4 (Apr. 2013), p. 045014. DOI: 10.1088/1367-2630/15/4/045014.

[58] H. P. Zhang et al. "Collective motion and density fluctuations in bacterial colonies". In: *Proceedings of the National Academy of Sciences* 107.31 (2010), pp. 13626–13630. ISSN: 0027-8424. DOI: 10.1073/pnas.1001651107.

Declaration of Authorship

Erklärung:

Hiermit erkläre ich, Johanna MAYER, die vorliegende Arbeit selbstständig verfasst zu haben und keine anderen als die in der Arbeit angegebenen Quellen und Hilfsmittel benutzt zu haben.

München, den 8. April 2021

Unterschrift:

_____